
Louisiana Transportation Research Center

Final Report 581

**Assessment of Continuous Deflection Measurement
Devices in Louisiana – Rolling Wheel Deflectometer**

by

Mostafa A. Elseifi, Ph.D., P.E.
Omar Elbagalati

LSU



4101 Gourrier Avenue | Baton Rouge, Louisiana 70808
(225) 767-9131 | (225) 767-9108 fax | www.ltrc.lsu.edu

1. Report No. FHWA/LA.17/581		2. Government Accession No.	3. Recipient's Catalog No.
4. Title and Subtitle Assessment of Continuous Deflection Measurement Devices in Louisiana – Rolling Wheel Deflectometer		5. Report Date September 2017	
		6. Performing Organization Code LTRC Project Number: 14-2P SIO Number: 30000144	
7. Author(s) Mostafa A. Elseifi and Omar Elbagalati		8. Performing Organization Report No.	
9. Performing Organization Name and Address Department of Civil and Environmental Engineering Louisiana State University Baton Rouge, LA 70803		10. Work Unit No.	
		11. Contract or Grant No.	
12. Sponsoring Agency Name and Address Louisiana Department of Transportation and Development P.O. Box 94245 Baton Rouge, LA 70804-9245		13. Type of Report and Period Covered Report 2013-2016	
		14. Sponsoring Agency Code LTRC	
15. Supplementary Notes Conducted in Cooperation with the U.S. Department of Transportation, Federal Highway Administration			
16. Abstract The use of the Rolling Wheel Deflectometer (RWD), which measures deflections at highway speeds, offers the potential to characterize the structural capacity of pavements without delays and in a cost-effective way. The objective of this study was twofold. First, this project evaluated pre-developed structural capacity indicators in predicting pavement structural deficiency based on RWD measurements. Based on this evaluation, the research team introduced modifications to improve prediction of pavement structural capacity. Second, a methodology was developed to integrate the most promising structural capacity indicator into the Louisiana Pavement Management System (PMS) decision matrix and the State overlay design procedure. Furthermore, this project assessed the cost-efficiency of RWD testing in identifying and repairing structurally-deficient sections prior to reaching very poor conditions, which may require complete reconstruction. Among the pre-developed structural capacity indicators, the SN_{RWD} was found to be the most promising model. Modifications were introduced to the SN_{RWD} model to improve its efficiency in identifying structurally-deficient pavements and to allow for predicting the Structural Number (SN) at a 0.1-mile interval. A model was developed to estimate the subgrade resilient modulus (M_r) based on the RWD data. To facilitate implementation of the results, a framework was developed to incorporate RWD testing results in Louisiana PMS and the State overlay design procedure. Results of the study found that RWD can result in significant savings to the Department if implemented in testing medium to high traffic volume roads with an Annual Average Daily Traffic (AADT) of 5,000 or more.			
17. Key Words Structural capacity, RWD, Continuous deflection		18. Distribution Statement Unrestricted. This document is available through the National Technical Information Service, Springfield, VA 21161.	
19. Security Classif. (of this report)	20. Security Classif. (of this page)	21. No. of Pages 147	22. Price

Project Review Committee

Each research project will have an advisory committee appointed by the LTRC Director. The Project Review Committee is responsible for assisting the LTRC Administrator or Manager in the development of acceptable research problem statements, requests for proposals, review of research proposals, oversight of approved research projects, and implementation of findings.

LTRC appreciates the dedication of the following Project Review Committee Members in guiding this research study to fruition.

LTRC Administrator

Kevin Gaspard, P.E.
Senior Pavement Research Engineer

Members

Simone Ardoin
Xingwei Chen
Christophe Fillastre
Amy Giddens
Hector Santiago
Don Weather

Directorate Implementation Sponsor

Janice P. Williams, P.E.
DOTD Chief Engineer

Assessment of Continuous Deflection Measurement Devices in Louisiana – Rolling Wheel Deflectometer

by

Mostafa A. Elseifi, Ph.D., P.E.

Associate Professor

Department of Civil and Environmental Engineering

Louisiana State University

3526c Patrick Taylor Hall

Baton Rouge, LA 70803

e-mail: elseifi@lsu.edu

and

Omar Elbagalati

Graduate Research Assistant

Department of Civil and Environmental Engineering

Louisiana State University

3526 Patrick Taylor Hall

Baton Rouge, LA 70803

e-mail: uelbag1@lsu.edu

LTRC Project No. 14-2P

State Project No. 736-99-1518

conducted for

Louisiana Department of Transportation and Development

Louisiana Transportation Research Center

The contents of this report reflect the views of the author/principal investigator who is responsible for the facts and the accuracy of the data presented herein. The contents do not necessarily reflect the views or policies of the Louisiana Department of Transportation and Development or the Louisiana Transportation Research Center. This report does not constitute a standard, specification, or regulation.

September 2017

ABSTRACT

The use of the Rolling Wheel Deflectometer (RWD), which measures deflections at highway speeds, offers the potential to characterize the structural capacity of the road network without major delays and in a cost-effective way. In 2009, the Louisiana Department of Transportation and Development (DOTD) conducted a comprehensive testing program of RWD in District 05. Measurements were used to assess the repeatability of RWD, the effect of truck speeds, and to study the relationship between RWD and Falling Weight Deflectometer (FWD) deflection measurements and pavement conditions. Based on the results of the experimental program, three structural capacity indicators were developed: the RWD index (RI), the RWD Structural Number (SN_{RWD}), and the Zone RWD Index (ZRI).

The objective of this study is twofold. First, this project evaluated the aforementioned structural capacity indicators in predicting pavement structural capacity based on RWD measurements. Based on this evaluation, the research team introduced modifications to improve prediction of pavement structural capacity and to estimate the subgrade resilient modulus (M_r) based on the RWD data. Second, in this study, a methodology was developed to integrate the most promising indicator into the Louisiana Pavement Management System (PMS) decision matrix and into the State overlay design procedure. Based on this analysis, this project assessed the cost-efficiency of RWD testing in identifying and repairing structurally-deficient sections prior to reaching very poor conditions, which may require excessive repair or reconstruction.

Among the pre-developed structural capacity indicators, the SN_{RWD} was found to be the most promising model. Modifications were introduced to the SN_{RWD} model to improve its capability in identifying structurally-deficient pavements and to allow for predicting the Structural Number (SN) at a 0.1-mile interval.

Based on the results of this study, it is recommended that structural capacity indicators be incorporated into the Louisiana PMS for treatments' selection as well as the State overlay design procedure. The effective pavement structural number is recommended to be considered in the overlay design procedure instead of the current practice of assuming 50% loss in the original structural capacity. Results of the study found that RWD can result in significant savings to the Department if implemented in testing medium to high traffic volume roads (e.g., Interstates, major arterials) with an Annual Average Daily Traffic (AADT) of 5,000 or more. The proposed modification to the overlay design procedure is implementation-ready and should be utilized by the Department to maximize savings to the state from using RWD.

ACKNOWLEDGMENTS

The authors recognize the efforts of Ashley Horne and Christophe Fillastre of DOTD, who cooperated with the research team during this project. This was critical for collecting and interpreting the Pavement Management System (PMS) data used in this study. The authors would also like to acknowledge the remarkable effort of Kevin Gaspard and Zhongjie "Doc" Zhang of the Louisiana Transportation Research Center (LTRC).

The U.S. Department of Transportation (USDOT), Federal Highway Administration (FHWA), and DOTD through LTRC financially supported this research project.

IMPLEMENTATION STATEMENT

Based on the findings and the results of this project, it is recommended to regularly test the road segments in the state trafficked with an AADT of 5,000 or more using RWD at a frequency of once every four years. In addition, continuous deflection data should be incorporated into the Louisiana PMS for treatments' selection as well as the state overlay design procedure. The effective pavement structural number is recommended to be used in the overlay design procedure instead of the current practice of assuming 50% loss in the original structural capacity. The proposed modifications to the overlay design procedure is implementation-ready and should be utilized by the Department to maximize savings to the state from using RWD.

TABLE OF CONTENTS

ABSTRACT	iii
ACKNOWLEDGMENTS	v
IMPLEMENTATION STATEMENT	vii
TABLE OF CONTENTS	ix
LIST OF TABLES	xiii
LIST OF FIGURES	xv
INTRODUCTION	1
Literature Review	1
Louisiana Pavement Management System	2
Overview of RWD Equipment	8
Incorporation of Structural Capacity in PMS	19
Artificial Neural Networks	27
OBJECTIVES	33
SCOPE	35
METHODOLOGY	37
Experimental Program	37
RWD Testing in Louisiana	37
FWD Testing in Louisiana	39
RWD Data Processing and Filtering	40
MnROAD Testing Program	40
Assess the Accuracy of the Developed Structural Capacity Indicators	42
RWD-Based Pavement Structural Capacity Indicators	42
Propose Modifications to the Most Promising Structural Capacity Indicator	43
Develop a Structural Index Based on Backcalculated Layer Moduli	44
Compare Rate of Deteriorations for Pavement Sections	44
Conduct an Overlay Design for the Selected Pavement Sections	45
Investigate the Feasibility of Predicting the Subgrade Modulus from RWD Data	45
Determine Cost Efficiency and Added Values of RWD Testing	46
Develop a One-Step Enhanced Decision Making Tool	46
DISCUSSION OF RESULTS	47
Accuracy of Structural Capacity Indicators	47
Statistical Analysis	47
Uniformity Index	48
Identification of Structurally Deficient Sections	50
Investigation of Cores	52

Selection of the Most Promising Indicator	54
Propose Modifications to the SN Model.....	54
Model Development.....	54
Sensitivity Analysis	56
Model Efficiency and Characteristics	57
Define $SN_{RWD0.1}$ Thresholds	60
Analysis of Structurally Deficient Sections	60
Summary of the Core Analysis	63
Develop a Structural Index Based on Backcalculated Moduli	64
FWD Testing.....	64
Backcalculation Analysis.....	65
Loss in Structural Capacity	66
Formulation of the Structural Health Index (SHI).....	67
Evaluation and Validation of the Structural Health Index.....	68
Comparison between SHI and the Pavement Condition Index (PCI).....	71
Compare Rates of Deteriorations for Pavement Sections.....	71
Functional Class.....	72
Structural Condition Index (SCI).....	72
Define SCI Intervals	73
Compare Structural Deterioration Rates	74
Overlay Design for Selected Pavement Sections.....	79
Current Overlay Design Procedure	79
Improved Overlay Design Procedure.....	81
Comparing Results of Both Procedures	82
Validation of the proposed approach	82
Investigate the Feasibility of Determining the Subgrade Modulus from RWD Data.	84
Correlation between the RWD and the Subgrade Resilient Modulus.....	84
ANN-Model Development.....	86
Model Prediction.....	88
Network Description	89
Forward Calculations	90
Model Evaluation and Analysis	90
Model Validation	92
Cost Efficiency and Added Values of RWD Testing	92
Approach 1: Modify the Treatment Selection Decision Matrix Procedure	93
Approach 2: Modify Treatment Selection and Overlay Design Procedure	96
Develop a One-Step Enhanced Decision Making Tool	103

Procedure Overview.....	104
Develop the Pattern Recognition System	105
Network Training and Performance.....	107
Forward Calculations	109
CONCLUSIONS.....	111
Structural Capacity Indicators.....	111
Modifications to the SN Model.....	111
Structural Health Index	112
Rates of Deterioration	112
Overlay Design	112
Subgrade Resilient Modulus	113
Cost Effectiveness Analysis of RWD Testing.....	113
Development of a One-Step Decision Making Tool.....	113
RECOMMENDATIONS	115
ACRONYMS, ABBREVIATIONS, AND SYMBOLS	117
REFERENCES	119
APPENDIX.....	125
Structurally Deficient Sections According to Each Indicator.....	125

LIST OF TABLES

Table 1 Louisiana highway network functional classification	2
Table 2 Louisiana PMS performance prediction models.....	7
Table 3 DOTD trigger values for rehabilitation strategies [10]	8
Table 4 Correlation between RWD measurements repeatability and pavement conditions..	11
Table 5 Pavement segments groups according to the AC layer thickness [17].....	15
Table 6 Temperature correction factors [24]	20
Table 7 Regression coefficients for the SSI model [24].....	21
Table 8 Trigger values for the SSI [24]	21
Table 9 Pavement condition categories [2]	23
Table 10 VDOT decision matrix for flexible pavement [2]	24
Table 11 Modified Structural Index (MSI) thresholds [2]	25
Table 12 Comparison between thresholds and FWD based measurements [26]	26
Table 13 Critical pavement response after overlay construction [26]	26
Table 14 Control sections classification according to AC thickness	47
Table 15 ANOVA results for thin sections.....	48
Table 16 ANOVA results for medium sections.....	48
Table 17 ANOVA results for thick sections	48
Table 18 Limiting thresholds for the three structural capacity indicators	50
Table 19 Averages performance indices for sections below 20% SN thresholds.....	51
Table 20 Averages performance Indices for sections above 20% RI thresholds.....	51
Table 21 Averages performance Indices for sections above 20% ZRI thresholds	52
Table 22 Sections classifications for core samples study	52
Table 23 Sensitivity analysis of SN model to variation in input values	57
Table 24 SN _{RWD01} results of the ANOVA analysis	59
Table 25 Functional class distribution	72
Table 26 Initial SCI intervals.....	74
Table 27 Linear fitting of deterioration rates for major collectors	79
Table 28 Linear fitting of deterioration rates for arterials	79
Table 29 Comparison between overlay design procedures using a mechanistic-empirical approach.....	83
Table 30 Correlation between RWD measurements and the FWD subgrade resilient modulus.....	85
Table 31 Modified decision matrix for arterials	94
Table 32 Modified decision matrix for collectors.....	95
Table 33 Change in treatment selection by applying proposed modification to decision matrix	96

Table 34 Change in projected cost of treatments based on modified decision matrix	96
Table 35 Transition matrix for the current and the enhanced trees procedure for the rural minor arterials	98
Table 36 Transition matrix for the current and the enhanced trees procedure for the rural major collectors.....	99
Table 37 Construction cost for each treatment strategy per mile	99
Table 38 Current and enhanced decision comparison for rural minor arterials.....	100
Table 39 Current and enhanced decision comparison for rural major collectors	100
Table 40 Current and enhanced decision comparison for urban minor arterials	100
Table 41 Current and enhanced decision comparison for rural locals.....	101
Table 42 Current and enhanced decision comparison for rural minor collectors	101
Table 43 Current and enhanced decision comparison at the control sections level.....	101
Table 44 Cost and productivity of RWD testing	102
Table 45 Forward calculations output form	110
Table 46 List of structural deficient section based on SN	125
Table 47 List of structural deficient section based on RI	126
Table 48 List of structural deficient section based on ZRI.....	127

LIST OF FIGURES

Figure 1 DOTD pavement network districts [9].....	3
Figure 2 Primary and secondary direction for collecting data [10]	3
Figure 3 ARAN vehicle used by LA PMS.....	4
Figure 4 Images by ARAN system for distress identification [10]	5
Figure 5 DOTD mainframe menu view [12]	5
Figure 6 General overview of the RWD system.....	9
Figure 7 RWD deflection measurement system	10
Figure 8 Variation of the RWD measurements with respect to the operational speed	12
Figure 9 Average RWD measurements vs average FWD measurements at the 16 research sites	13
Figure 10 RWD measurements vs. FWD measurements for (a) sites in very good conditions and (b) sites in poor and fair conditions [15]	14
Figure 11 ZRI CDF for group number 3 [17].....	15
Figure 12 Fuzzy functions for structurally sound and deficient groups	16
Figure 13 Example of feed-forward neural network structures	27
Figure 14 Back-Propagation algorithm.....	29
Figure 15 Logsig transfer function	30
Figure 16 Tansig transfer function.....	31
Figure 17 Hardlim transfer function	31
Figure 18 Locations of the 16 research sites in District 05 [14]	38
Figure 19 Coring test section Site 12 [14]	38
Figure 20 Core sample site 12 [14]	39
Figure 21 Illustration of the FWD test device used in the testing program [14]	39
Figure 22 Example of individual laser readings and deflections for Site 9 (315-02), LA 143 north of West Monroe (after ARA, Inc.).....	40
Figure 23 Overview of the MnROAD facility	41
Figure 24 MnROAD continuous deflection testing program [33]	42
Figure 25 Uniformity histogram for SN	49
Figure 26 Uniformity histogram for RI	49
Figure 27 Uniformity histogram for ZRI	50
Figure 28 ZRI cumulative distribution function for thin sections	51
Figure 29 Example of severe stripping in control section 161-08	52
Figure 30 Example of AC stripping in control section 831-06.....	53
Figure 31 Example of core sample in good structural conditions (Section 182-01)	53

Figure 32 $SN_{RWD0.1}$ model development.....	55
Figure 33 $SN_{RWD0.1}$ model validation	56
Figure 34 $SN_{RWD0.1}$ vs. SN_{FWD} longitudinal profile.....	56
Figure 35 Sensitivity analysis for the $SN_{RWD0.1}$ model	57
Figure 36 Average $SN_{RWD0.1}$ values for each PCI category ¹	58
Figure 37 Average $SN_{RWD0.1}$ values for each ALCR category ¹	59
Figure 38 Cores samples and its locations for structural deficient sections	63
Figure 39 (a) Cores observations summary (b) distribution according to PCI.....	64
Figure 40 Backcalculated layer moduli for sections with untreated base layer ¹	66
Figure 41 Backcalculated layer moduli for sections with cement-treated base layer.....	66
Figure 42 Relation between loss in structural number and the SHI	68
Figure 43 Stripped core samples from low SHI sections.....	69
Figure 44 Sections with high SHI core samples	70
Figure 45 Relation between SHI and pavement structural condition [38]	71
Figure 46 SCI histogram distribution	73
Figure 47 Alligator cracking deterioration for major collectors.....	75
Figure 48 Rutting deterioration for major collectors	75
Figure 49 Random cracking deterioration for major collectors.....	76
Figure 50 Roughness deterioration for major collectors.....	76
Figure 51 Alligator cracking deterioration for arterials.....	77
Figure 52 Rutting deterioration for arterials	77
Figure 53 Random cracking deterioration for arterials.....	78
Figure 54 Roughness deterioration for arterials.....	78
Figure 55 Type of errors in the current design procedure	80
Figure 56 Current and proposed overlay design procedures	81
Figure 57 Average overlay thicknesses using current and proposed design procedures.....	82
Figure 58 Comparison of $SN_{RWD0.1}$ and 50% structural capacity loss assumption to SN_{FWD}	84
Figure 59 Correlation between the subgrade resilient modulus and (a) D_1 and (b) D_0	86
Figure 60 Structure of the ANN model.....	87
Figure 61 ANN model performance	88
Figure 62 Regression plots of the developed ANN model for (a) the training data set (b) the validation data set (c) the testing data set and (d) All data.....	89
Figure 63 Bland and Altman Chart for the subgrade resilient modulus calculated based on FWD and RWD measurements	91
Figure 64 Model validation using data from the MnROAD testing program.....	92
Figure 65 General layout of the proposed implementation approaches	93

Figure 66 Correlation between the SCI and the SSCI	94
Figure 67 Enhanced decision tree for arterials	97
Figure 68 Enhanced decision tree for collectors	98
Figure 69 Monetary saving for each roadway functional class	102
Figure 70 Correlation between the saving amount and traffic volume	103
Figure 71 Pattern Recognition Confusion Matrix	104
Figure 72 Overview of the system developing procedure	105
Figure 73 The ANN-based pattern recognition model structure	107
Figure 74 Confusion matrices of the pattern recognition system for (a) the training data set (b) the validation data set (c) the testing data set (d) all data	109

INTRODUCTION

Pavement condition evaluation is considered the most important step in the selection of cost-effective maintenance and/or rehabilitation strategies. Commonly, non-structural factors such as surface distresses and ride quality have been used as the main indicators of in-service pavement conditions [1]. Yet, recent research found that there is a little statistical correlation between pavement structural and functional conditions [2]. Therefore, many agencies are working on implementing structural capacity indicators into their Pavement Management System (PMS) and decision-making processes. The Falling Weight Deflectometer (FWD) is widely used to assess the structural capacity of in-service pavements at the project level [3]. However, the stop and go process necessitates traffic control to ensure drivers and workers' safety, which limits the use of FWD at the network level [4]. The Rolling Wheel Deflectometer (RWD) has emerged in the last decade to measure pavement surface deflection while travelling at regular posted speed limits without causing users' delay [5]. The Danish Traffic Speed Deflectometer (TSD) has also been introduced to measure surface pavement deflection while travelling at traffic speed [6].

DOTD has established a comprehensive pavement management system through which the pavement network is surveyed once every two years [7]. The Automatic Road Analyzer (ARAN) vehicle is used to collect pavement surface condition data such as cracking, rutting, and roughness. However, no structural condition data are collected by the state to assist in the process of selecting a suitable treatment strategy, which may lead to two types of errors and loss of state funds because of the lack of consideration of structural conditions [8]: adding structure to a pavement that does not require it (Type I error – False Positive) and not adding structure to a pavement that requires it (Type II – False Negative). Examples of Type I errors include using treatments such as pavement reconstruction, medium overlays, and in some cases thin overlays on pavements that are not structurally-deficient and that only necessitate functional repairs. Type II error examples include using “functional” treatments such as micro-surfacing, surface treatment, and thin overlays on pavements that are structurally-deficient.

Literature Review

DOTD started to conduct windshield surveys in the early 1970s to establish a pavement distress data collection system, which evolved to videotaping in 1992, and to automatic collection in 1995 [9]. Currently, the Louisiana pavement network is surveyed every two years to collect and analyze pavement distress data. All nine districts in Louisiana are included in the PMS collection protocol.

The distresses data collected by DOTD PMS include International Roughness Index (IRI), cracking, rutting depth, patching, and faulting. The Louisiana PMS classifies longitudinal and transverse cracking as random cracks, which may be confusing and cause inadequate rehabilitation decisions, as each type of distresses has different causes and failure mechanisms [9]. The distress data for all pavements are based on a reference location system, which consists of control sections divided into log miles. The pavement distress data are collected and reported every 1/10th of a mile and pavement condition is reported based on an index scale from 0 to 100 in which 100 represents excellent conditions. In addition to distress data, DOTD PMS also collects vertical clearance measurements, traffic and advertising signs, geometric properties (horizontal curves, vertical curves, cross slope, edge drop offs, and clearance) and right of way images in all ramps [7].

Louisiana Pavement Management System

The pavement network in Louisiana is divided into nine districts as shown in Figure 1. The Louisiana highway network is the 32nd largest in the United States, which consists of more than 60,000 center lane miles and more than 13,000 bridges. The pavement network is categorized based on road function as Interstate Highways, Freeway and Expressway, Principal Arterials, Minor Arterials, Collectors, and Local Roads [9]. Yet, for the convenience of data analysis and budget allocation, PMS office has modified the concept originally developed by DOTD Task Force on Highway Project Identification and Prioritization and classified the pavement network in Louisiana into four categories as Interstate Highway System (IHS), National Highway System (NHS), State Highway System (SHS), and Regional Highway System (RHS), as presented in Table 1. The NHS includes interstate highways, some urban and rural arterial highways, and few urban and rural collector highways. The SHS complements the NHS and is comprised of the highways whose principal function is intercity, interregional, interstate and international transport of people and goods. The RHS consists of highways whose principal function is the local movement of people and goods.

Table 1
Louisiana highway network functional classification

Classification	Length (miles)	Percentage
IHS	893	5.4%
NHS	1,550	9.3%
SHS	7,043	42.2%
RHS	7,184	43.1%

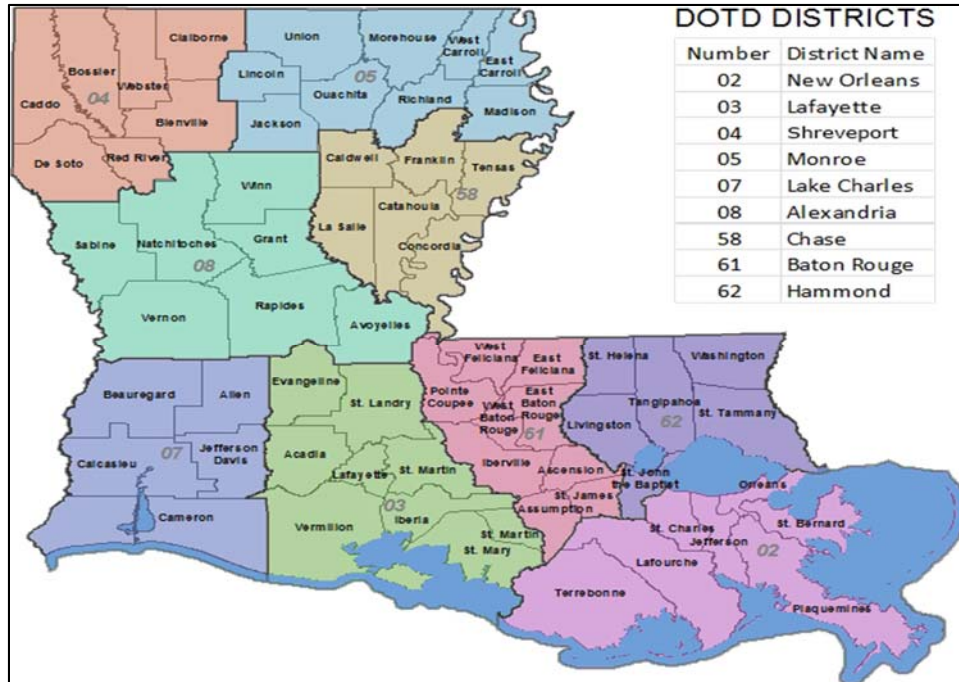


Figure 1
DOTD pavement network districts [9]

Louisiana PMS Data Collection. When collecting data, whether the images are right-of-way images or pavement surface images, the Department follows a general rule in relation to direction. The primary direction or Direction 1, in most cases, travels from south to north or from west to east. The opposite direction, also referred to as the secondary direction or Direction 2, travels north to south and from east to west as shown in Figure 2 [10].

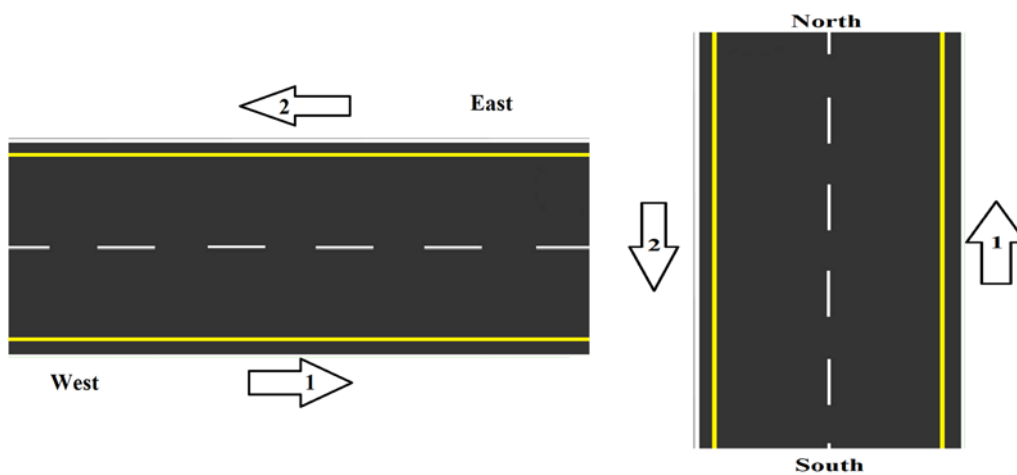
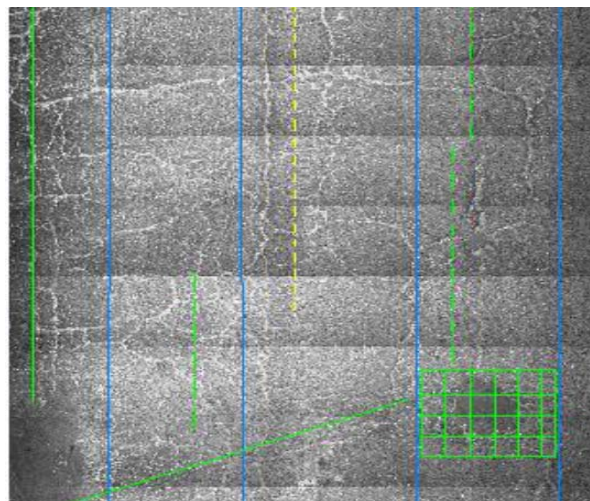


Figure 2
Primary and secondary direction for collecting data [10]




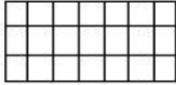
DOTD utilizes a special vehicle known as the Automatic Road Analyzer (ARAN) to survey the pavement network and collect pavement surface conditions data once every two years. This specific vehicle, shown in Figure 3, is equipped with cameras, lasers, sensors and computers to collect high-definition digital images of the pavement surface and right of way and electronic data of pavement distresses namely cracking, rutting, faulting, IRI, and macrotexture for both primary (i.e., South to North or West to East) and secondary (North to South or East to West) directions. While the ARAN is equipped with a GPS unit, the data are collected and reported for every $1/10^{\text{th}}$ of a mile of the road network [9]. The continuous digital images and distress data (VISIDATA) acquired by ARAN are utilized by each district, and the personnel has been trained to use the data [11]. When collecting pavement images, the various types of cracks are identified by distress category, rated in order of severity, measured, and recorded in the database; see Figure 4(a). Symbols indicate distress category and a three-color system is used to distinguish severity levels as shown in Figure 4(b) [10].



Figure 3
ARAN vehicle used by LA PMS



(a) Image by ARAN

Distress Symbols and Identification		Severity Level Color System	
Fatigue or Alligator Cracking	— — —	High	
Block Cracking	- - - - -	Medium	
Longitudinal Cracking		Low	
Transverse Cracking	—		
Patching			

(b) Distress Identification

Figure 4

Images by ARAN system for distress identification [10]

Louisiana Data Structure. The collected condition data are stored in the mainframe computer and are assigned a number according to the project. The project number consists of nine digits; the first five digits refer to the control section and the remaining four digits refer to the project number performed on the control section [9]. The material type and thickness information of asphalt, base, and subbase layers are located under Menu/Project/Roadway Xsec in Material Testing System (MATT) and the surface type, roadway geometry and traffic data are located in both MATT and under Menu/Summary Log in Highway Needs section [11]. The data collected by FWD and Ground Penetrating Radar (GPR) are not included in the PMS database. The mainframe system is a menu driven system, which allows DOTD users to access the data. The DOTD mainframe menu system is presented in Figure 5.

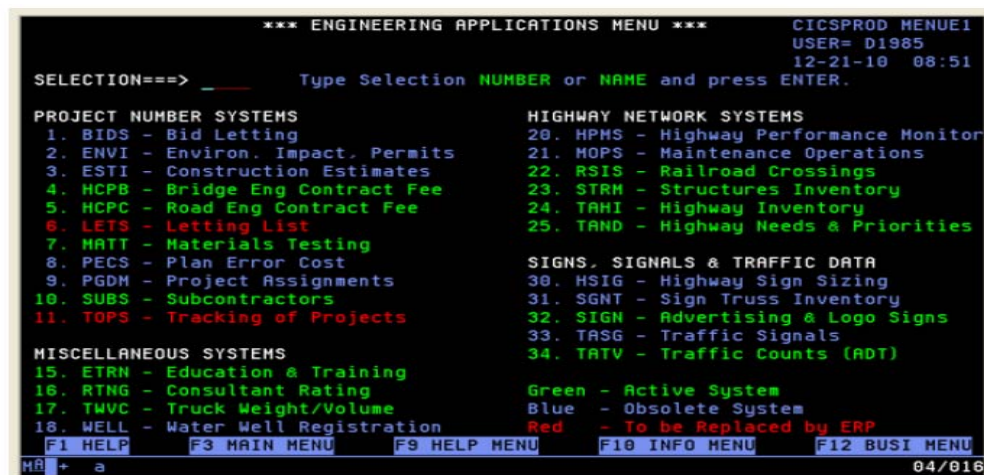


Figure 5

DOTD mainframe menu view [12]

The pavement data related to materials, traffic, and project are stored in separate databases and could be accessed and updated by authorized personnel in the different sections. In some cases, the data stored in different databases could be duplicate or may conflict [12]. All databases may be accessed through the mainframe menu system.

Louisiana PMS Data Storage. The collected condition data for the PMS are stored in a Structure Query Language (SQL) enterprise database used by Deighton Transportation Infrastructure Management System (DTIMS) and made available to end users through DOTD Pavement Management Intranet Web Portal, Visiweb, and IVision (Video Log view linked to pavement condition data).

Louisiana PMS Performance Prediction Models. Future pavement conditions can be predicted by performance models. Performance models can be utilized to determine the required maintenance and/or rehabilitation treatment as well as the deterioration rate and remaining service life (RSL) of the pavement. Performance models are functions of traffic loads, traffic volumes, material properties, weather data, and pavement type [7].

Empirical (Regression) models are used to predict pavement performance. The relation between performance index and age are plotted using performance curves for each pavement family. Pavement families are defined based on pavement type (composite, asphalt, jointed concrete, and continuously reinforced concrete pavements) and highway classification (i.e., IHS, NHS, SHS, and RHS) [9]. Distress index models currently used by DOTD are based on at least six years of data collected at two-year intervals. The models are primarily a function of “age” of the pavement. Table 2 presents the performance prediction models used by DOTD for flexible pavements in year 2010.

Louisiana PMS Data Analysis and Decision Matrix. Collected data are reported every 0.1 mile and are analyzed to calculate the Pavement Condition Index (PCI) on a scale from zero to 100. The PCI varies from 95 to 100, 85 to 94, 65 to 84, 50 to 64, and 49 or less for very good, good, fair, poor, and very poor roads, respectively. A number of threshold values are also used to trigger a specific course of maintenance and rehabilitation (M&R) actions [11]. For flexible pavements, the PCI is calculated as follows:

$$PCI = \text{MAX} (\text{MIN} (\text{RNDM}, \text{ALCR}, \text{PTCH}, \text{RUFF}, \text{RUT}), \{ \text{AVG} (\text{RNDM}, \text{ALCR}, \text{PTCH}, \text{RUFF}, \text{RUT}) - 0.85 \text{ STD} (\text{RNDM}, \text{ALCR}, \text{PTCH}, \text{RUFF}, \text{RUT}) \}) \quad (1)$$

where,

RNDM = random cracking index;

ALCR = alligator cracking index;

PTCH = patch index;
 RUFF = roughness index;
 RUT = rutting index;
 STD = standard deviation.

Table 2
Louisiana PMS performance prediction models

Category	Equation
Alligator Cracking Arterial	$100 - 0.7027 * AGE$
Alligator Cracking Collector	$100 - 0.6795 * AGE$
Alligator Cracking Interstate	$100 - 0.4172 * AGE$
Patching Arterial	$100 - 0.2130 * AGE$
Patching Collector	$100 - 0.2628 * AGE$
Patching Interstate	$100 - 0.2183 * AGE$
Random Cracking Arterial	$100 - 1.6102 * AGE$
Random Cracking Collector	$100 - 1.7534 * AGE$
Random Cracking Interstate	$100 - 1.6102 * AGE$
Roughness Arterial	$0.0003 * (AGE)^3 - 0.0391 * (AGE)^2 - 0.7983 * (AGE) + 100$
Roughness Collector	$0.0002 * (AGE)^3 - 0.0311 * (AGE)^2 - 0.5665 * (AGE) + 100$
Roughness Interstate	$0.0003 * (AGE)^3 - 0.0391 * (AGE)^2 - 0.7983 * (AGE) + 100$
Rutting Arterial	$100 * EXP(-0.0121 * AGE)$
Rutting Collector	$100 * EXP(-0.008 * AGE)$
Rutting Interstate	$100 * EXP(-0.0121 * AGE)$

The treatment decision matrix used by DOTD PMS mainly depends on the surface distress indices and the highway functional class (interstate, arterial, and collector). Table 3 presents the thresholds and trigger values, which are currently used by DOTD for treatment selection and decision making. As shown in this table, no structural capacity indicator is currently implemented into the State PMS and treatment selection process.

Table 3
DOTD trigger values for rehabilitation strategies [10]

Treatment type	Alligator cracks	Random	Patching	Rutting	Roughness
Micro-surfacing on interstate	≥98	≥98	≥98	≥80 <90	≥85
Thin overlay on interstate	≥90	≥85	≥90	<80	≥85 <90
Medium overlay on interstate	≥65 <90	<90	≥65 <90		<85
Structural overlay on interstate	<65		<65		
Micro-surfacing on arterial	≥95	≥95	≥95	≥65 <80	≥80
Thin overlay on arterial	≥90	≥80 <95	≥80	<65	≥70 <80
Medium overlay on arterial	≥50 <90	<80	≥60 <80		<70
Structural overlay on arterial	<50		<60		
Polymer surface treatment on collector	≥85 <95	≥80 <95	≥85	≥65	≥80
Micro-surfacing on collector	≥95	≥95	≥95	≥65 <80	≥80
Medium overlay on collector	≥60 <85	<80	≥65 <85	<65	≥60 <80
In place stabilization on collector	<60		<65		<60

Overview of RWD Equipment

The stationary nature of FWD limits its utilization at the network level; therefore, a number of moving deflection measurement devices were developed in the last decade. A SHRP2 study selected the RWD as one of the most promising moving deflection measurement devices [13].

The Rolling Wheel Deflectometer. The most recent version of the RWD was developed by Applied Research Associates (ARA, Inc.) in collaboration with FHWA Office of Asset Management. It consists of a 53-ft. long semitrailer applying a standard 18,000-lb. load on the pavement structure by means of a regular dual-tire assembly over the rear single axle [14]. A general view of the 53-ft. custom designed RWD trailer is shown in Figure 6.

The trailer is specifically designed to be long enough to separate the deflection basin, due to the 18-kip rear axle load, from the effect of the front axle load. In addition, the trailer is long-enough to accommodate the aluminum beam so that the laser range needed to tolerate any bouncing of the trailer during operation could be minimized.



Beam deflection system

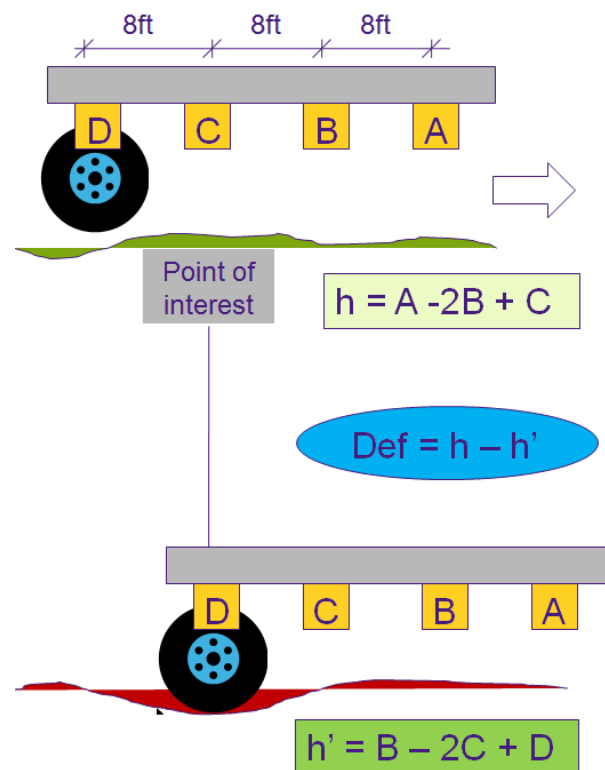


Cooling and loading system

Figure 6
General overview of the RWD system

The latest version of the RWD, introduced in 2003, can collect deflections at traffic speeds. Several modifications and upgrades were introduced to the RWD with respect to the laser sensors, data acquisition system, and software. The laser collection system was moved between the tires, and a new procedure was introduced for laser calibration. The laser sensors are set to collect a reading at a fixed interval of 0.6 in. at all truck speeds. Prior to the field testing program described in this study, a more accurate and stable deflection measurement system customized for pavement applications was installed. The upgraded system has a 4-in. measurement deflection range and has an accuracy of ± 0.001 in.

The whole deflection system of the beam and the laser sensors is housed in a thermal chamber to prevent external factors, such as wind and temperature fluctuation, from affecting the measurements during testing. The beam laser has four laser sensors that are used concurrently to measure the pavement surface deflection due to the rear axle based on optical trigonometry, as shown in Figure 7. The rear axle and wheels were designed and placed to prevent any conflict with laser paths. A two-person crew, driver, and operator is sufficient to perform the entire test as the RWD enables the operator to control the sensors, as well as to collect and store the data, through the use of a computer in the tractor. RWD is also equipped with a GPS for geo-referencing as well as an infrared thermometer for measuring surface pavement temperature.



In the figure, h and h' are the depth of the non-deflected and the deflected surface.

Figure 7
RWD deflection measurement system

RWD Studies in Louisiana. A comprehensive testing program was conducted by DOTD in District 05, Louisiana, 2009. The testing program aimed at assessing the capability of the RWD in evaluating pavements structural conditions, at the network-level. The RWD field testing program consisted of two phases. In the first phase, about 1,250 miles of the

asphalt road network in District 05 was tested using the RWD system based on ARA standard testing protocol. In the second phase, 16 road-sections (each 1.5 miles), referred to as research sites, were tested and were used for a detailed evaluation of RWD technology. The test plan consisted of conducting RWD and FWD measurements on the selected flexible pavement test sites. The FWD testing was conducted within 24 hours of the completion of RWD testing [15]. The testing program data were utilized by Elseifi and co-authors to assess the repeatability and characteristics of RWD measurements, the effect of the RWD operation speed, and to evaluate the relationship between RWD and FWD deflection measurements [16].

To assess the repeatability of the RWD measurements, three RWD runs were performed in each of the 16 research sites. The repeatability of the measurements was represented by the coefficient of variation (COV (%) = standard deviation x 100/ average). The repeatability of the RWD measurements was concluded to be acceptable with a COV (%) ranging from 7 to 22% and with an average of 15%. It was worth noting that the measurements uniformity and repeatability was improved in the sites that were in good conditions than in the sites that were in poor conditions as shown in Table 4 [16].

Table 4
Correlation between RWD measurements repeatability and pavement conditions

Site ID	Average (COV)%	Pavement Condition
1	15	Fair
2	16	Good
3	13	Very good
4	8	Very good
5	14	Very good
6	7	Very good
7	13	Very good
8	20	Fair
9	17	Very good
10	16	Poor
11	19	Poor
12	22	Fair
13	18	Good
14	19	Poor
15	15	Good
16	16	Poor

To assess the effect of the RWD operational speed on the deflection measurements, RWD runs were performed at each of the 16 research sites at speeds of 20, 30, 40, 50, and 60 mph

up to the posted speed limit on each section. The effect of the testing speed on the RWD measurements was minimal as shown in Figure 8. In addition, a statistical analysis was conducted between the RWD measurements at the different testing speeds (except the 60 mph speed as only one site was tested at this speed). According to the statistical analysis, the RWD measurements at the different testing speeds were found to be statistically equal at a 95% confidence level with a p-value of 0.355. This finding would allow comparing the RWD measurements conducted at different speeds and for different roadway functional classes [16].

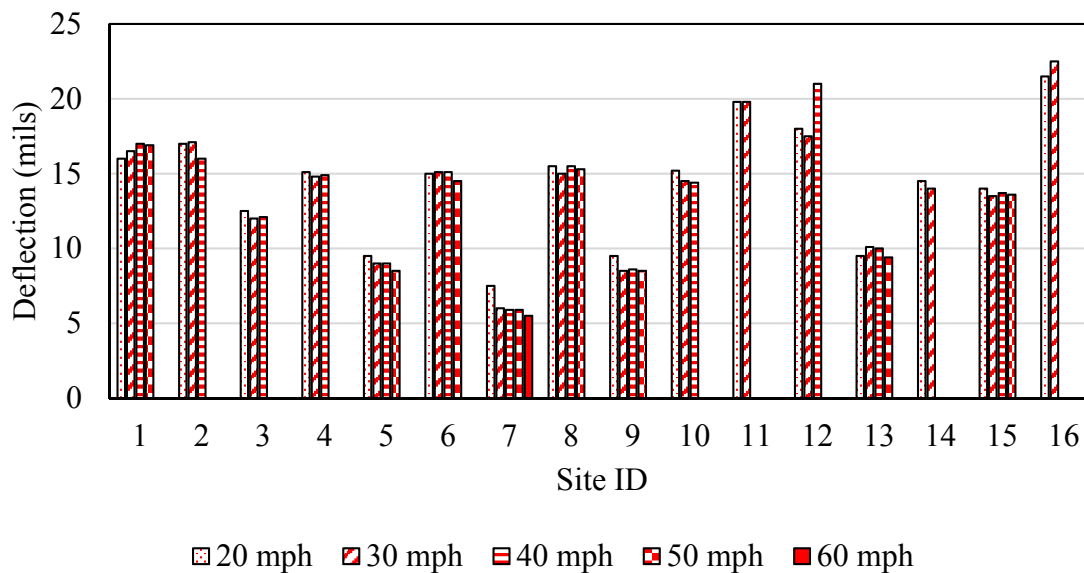


Figure 8
Variation of the RWD measurements with respect to the operational speed

RWD deflections were compared to the FWD maximum surface deflections at a load of 9,000 lbs., for the 16 research sites, as shown in Figure 9. It was noted that the scattering and uniformity of the FWD and RWD data correlated well with the conditions of the roadway, as shown in Figure 10. Both test methods reflected pavement conditions and structural integrity of the road network by providing for a greater average deflection and scattering for sites in poor conditions. RWD deflection measurements were in general agreement with FWD deflections measurements; however, the mean center deflections from RWD and FWD were statistically different for 15 of the 16 sites [15].

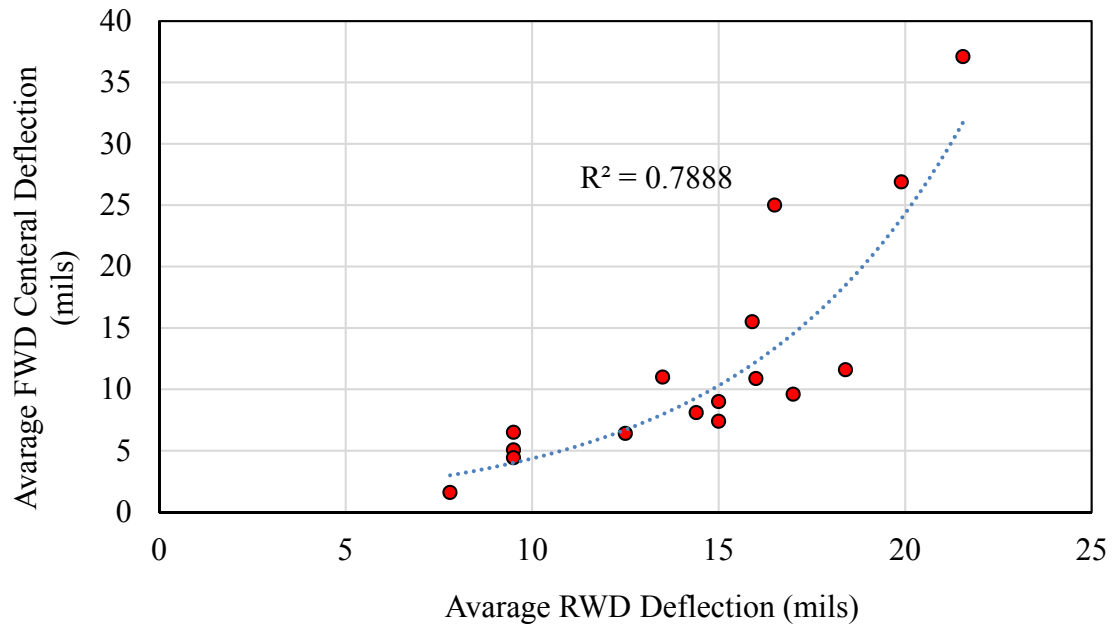
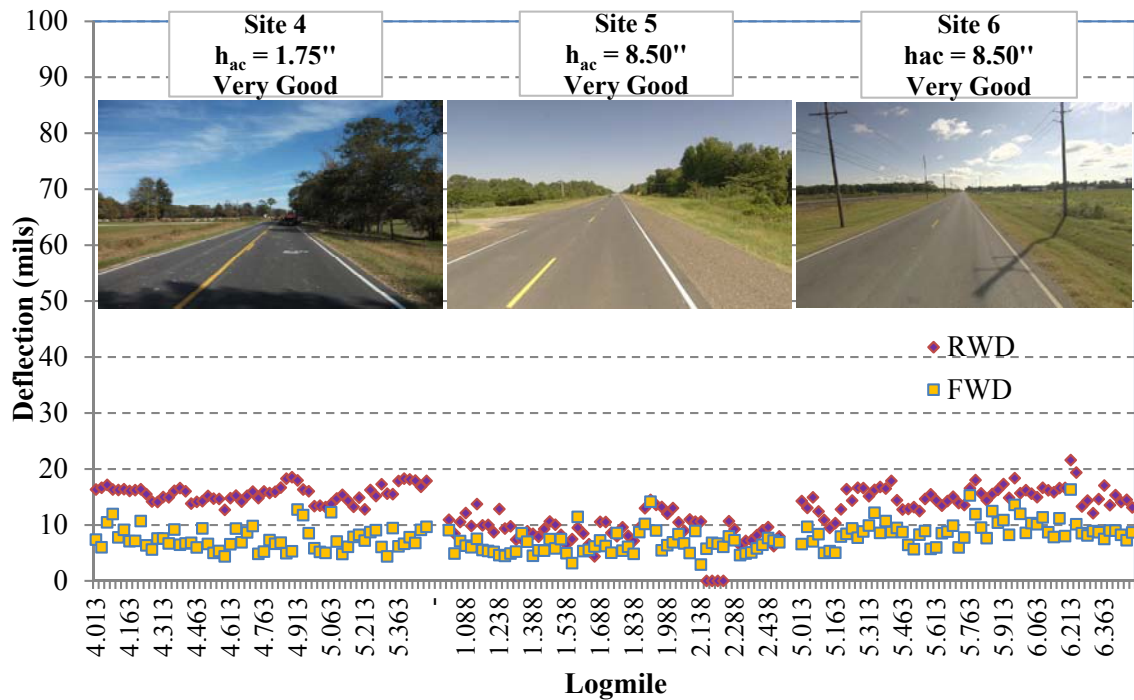


Figure 9
Average RWD measurements vs average FWD measurements at the 16 research sites



(a)

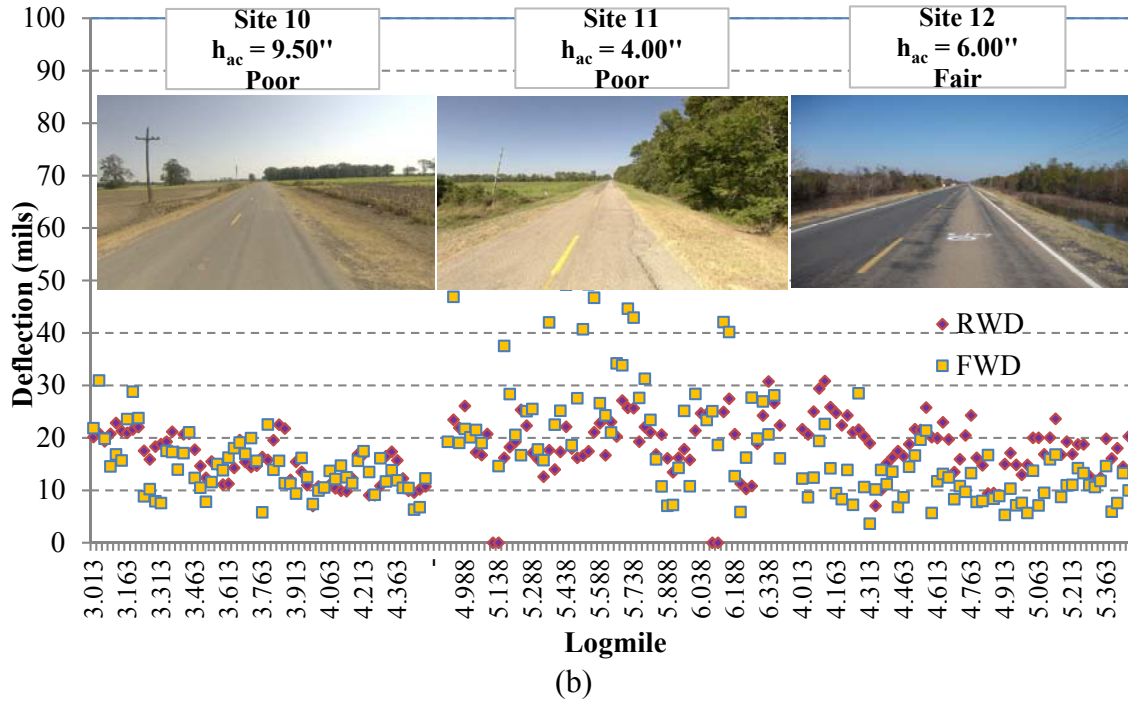


Figure 10
RWD measurements vs. FWD measurements for (a) sites in very good conditions and
(b) sites in poor and fair conditions [15]

Zhang and co-authors investigated the capability of the RWD technology in avoiding Type I and Type II errors when making treatment recommendations [17]. One example of Type I error is assigning a structural treatment (e.g., reconstruction or medium overlay) to a pavement section in good structural condition. On the other hand, an example of Type II error is to assign a functional treatment (e.g., microsurfacing or thin overlay) to a pavement section in poor structural condition. To achieve these objectives, an index calculated each 0.1 mile and based on the RWD data; namely, the Zone RWD Index (ZRI), was used [17].

All the elements of 0.1-mile pavement segments, tested with the RWD, were sorted based on the thickness of the Asphalt Concrete (AC) layer as shown in Table 5. Furthermore, for each AC layer thickness group, a Cumulative Distribution Function (CDF) was developed with respect to the ZRI. By assuming that 50 % of the RWD-tested pavement segments were in poor structural condition, ZRI thresholds were determined. According to the authors, a pavement segment with $ZRI > \text{the 50 percentile of ZRI CDF}$ would need structural rehabilitation. On the other hand, a pavement segment with $ZRI < \text{the 50 percentile of ZRI CDF}$ would need functional rehabilitation. Figure 11 presents an example of the ZRI CDF and the determination of the 50 percentile ZRI for group number 3 (3 to 4 in. AC layer thickness) [17].

Table 5
Pavement segments groups according to the AC layer thickness [17]

Group Number	AC layer Thickness Group (in.)	Number of 0.1-mile segments
1	0-2	878
2	2-3	1,366
3	3-4	1,690
4	4-5	1,575
5	5-6	969
6	6-7	675
7	7-8	645
8	8-9	649
9	9-10	440
10	10-11	305
11	11-12	252

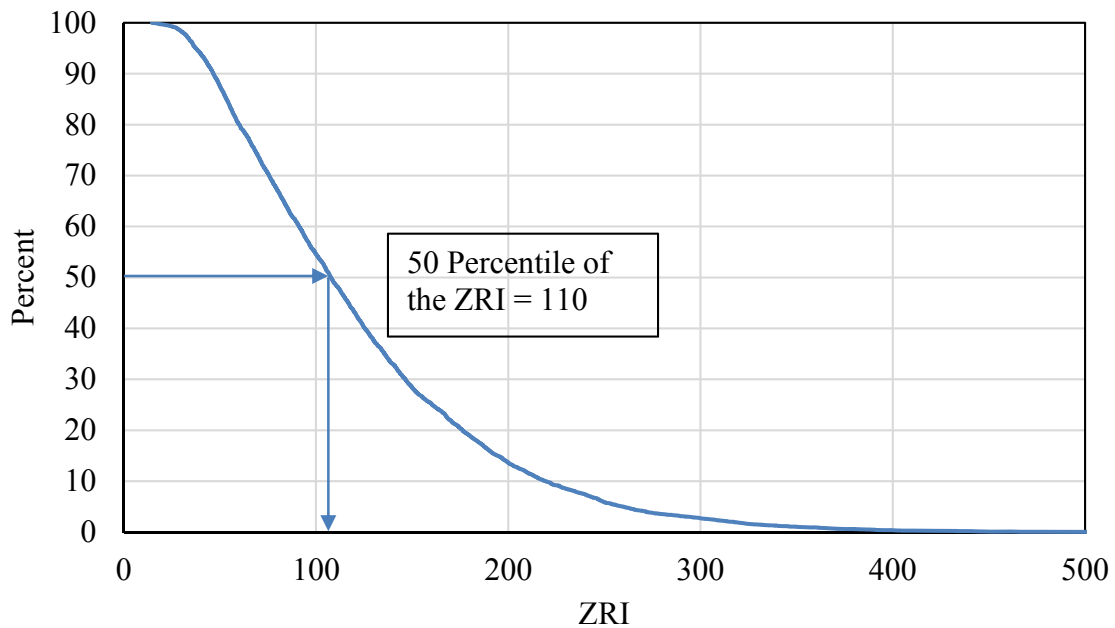


Figure 11
ZRI CDF for group number 3 [17]

By using the 50% ZRI CDF as a threshold for whether to assign structural treatments or functional treatments to the pavement sections, the percentages of Type I and Type II errors in the current DOTD practice were calculated. Results showed that current treatment selection practices have a Type I error percentage of 34% and a Type II error percentage of 39.5%. Based on these findings, the authors recommended future PMS to implement

structural indices in addition to the functional distress indices. Further, the RWD was identified as one of the most promising technology to be utilized for pavement structural evaluation purposes [17].

A study conducted by Gaspard and co-authors aimed at identifying RWD Index (RI) ranges for pavement treatment selection purposes. A set of theories were used to achieve the study objectives; namely, multivariate statistical methods, and fuzzy logic [18].

Statistical analysis revealed that the RI is not sufficient to assist in treatment selection practices used by DOTD. However, the RI was found to be a successful parameter to distinguish between structurally-sound and structurally-deficient pavement conditions. The authors recommended that structurally-sound pavements, based on the RI, not to receive a structural treatment or rehabilitation. On the other hand, the authors recommended further FWD testing to be conducted on pavements in structurally-deficient conditions, based on the RI, to determine the most appropriate treatment activity [18].

To minimize the effects of pavement thickness on RWD stiffness measurements, the data were stratified into thickness groups. Further, the authors employed a combination of fuzzy statistics, rank ordering, inductive reasoning, and engineering judgment from the scientific field of fuzzy logic to reveal function-theoretic relationships for structurally-sound and structurally-deficient pavements, their interaction, RI threshold ranges based upon pavement thickness groups, and algorithms to assess the structural conditions of large segments of roadways [18]. Figure 12 presents an example of the fuzzy RI thresholds for pavements with total thickness of 6 to 7 in. (thick group 6).

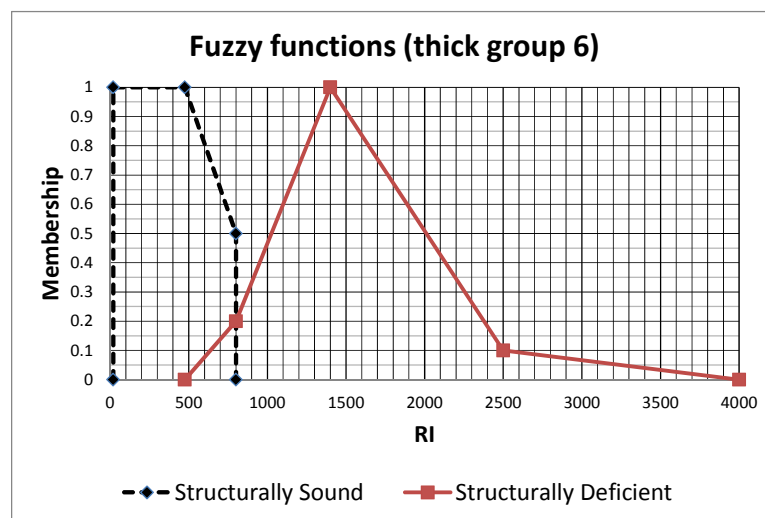


Figure 12
Fuzzy functions for structurally sound and deficient groups

Recent Studies on RWD. ARA, Inc. was contracted by the Pennsylvania Department of Transportation (PennDOT) to conduct a two-phase field testing program using the RWD in Pennsylvania. The first phase covered 288 miles of PennDOT road network in seven counties and was conducted in April 2013. In the second phase, a more detailed testing program was conducted on 16 road sections that were selected with different structural configurations and surface conditions [19].

The testing scheme consisted of conducting both RWD, coring, and FWD measurements on each of the selected sites in the second phase. FWD testing was conducted in the right wheel path at 200-ft intervals. Pavement temperature was recorded in conjunction with each test. Surface deflections were corrected for variation in pavement temperature by shifting the measurements to a standard temperature of 68°F (20°C) using the BELLS and the AASHTO 1993 methods. This method was also used to correct FWD deflection data [19]. The research team was able to calculate pavement remaining service life (RSL) using FWD or RWD data. Furthermore, the RWD device was found to be efficient since it allows for high-speed measurement of pavement deflections [20]. Based on these findings, the research team recommended using the RWD at the network level.

Gedafa and co-workers presented the results of a research effort aimed at estimating pavement structural number based on FWD and/or RWD measurements [21, 22]. The study divided the state road network in Kansas into 23 categories based on functional class, pavement type, traffic loading, and roadway width. For each roadway category, a regression model was developed to compute the SN from deflection data, traffic data, and surface condition indices. The study concluded that the structural condition of in-service flexible pavements could be assessed at the network level using the center deflection measured by either FWD or RWD. A model was also developed for the overall pavement network with a coefficient of determination (R^2) of 0.77:

$$\begin{aligned} \text{SN} = & 6.3763 - 0.3364 d_0 + 0.0062 d_0^2 - 0.0805 D + 0.01 D^2 - 0.0008 (d_0 * D) \\ & - 0.4115 \log (EAL) + 0.1438 (\log (EAL))^2 + 0.0836 \text{ETCR} - 0.0091 \text{EFCR} \\ & + 0.0004 \text{EFCR}^2 - 0.4061 \text{Rut} \end{aligned} \quad (2)$$

where,

SN= pavement structural number;

d_0 = center deflection (mils);

D= pavement depth (in.);

EAL = equivalent standard daily traffic;

EFCR/ETCR=equivalent fatigue/transverse cracking; and

Rut=rut depth (in.).

A study was conducted at the MnROAD facility to evaluate the accuracy of two traffic speed deflections devices (TSD and RWD) and to assess the use of the continuous deflectometers at the network level [23]. To assess the accuracy of the two continuous deflectometers, 20 sensors were embedded in the MnROAD facility (strain gauges, pressure cells, geophones, accelerometer, etc.). FWD was used to verify the performance of each sensor and to evaluate the correlation between RWD and FWD as well as the relation between the deflection velocity of the accelerometer and TSD. FWD measurements were found to have a strong correlation ($R^2=0.99$) with the installed deflection sensors, and the RWD measurements were found to have a good correlation ($R^2=0.86$) with the installed deflection sensors.

Researchers also used the installed geophones to calibrate the 3D Move software, which estimates pavement dynamic responses at any given point within the pavement structure using a continuum-based finite-layer approach. The software was then used in identifying the most promising indices from continuous deflectometers measurements that best describe the structural capacity of the pavement. Twelve structural capacity indicators were developed based on TSD and were recommended as the most promising indices to be used at the network level. The study concluded that both RWD and TSD are ready to be used at the network level and to develop models as structural capacity indicators.

The SHRP 2 project (R06F) aimed at assessing the applicability of current continuous deflection devices to be incorporated in the development of practical and cost-effective pavement rehabilitation strategies, and the ability of such devices to screen structurally-deficient pavement sections and scope their needs at the network level [13]. The research team selected the TSD along with the RWD as the most promising devices to achieve these goals. In order to evaluate the effectiveness of the TSD, various network-level sites were selected including different types of pavement sections. Each pavement type included subsections with good, fair, and poor functional conditions and reference FWD testing where possible.

The analysis of data indicated that both RWD and TSD provide adequate repeatability for network-level pavement management applications. Moreover, the TSD provides deflection measurements that are comparable to those collected using FWD; however, it was recommended to conduct further evaluation of the usefulness and cost-effectiveness of the TSD as well as the optimum method to interpret measurements from the device.

Incorporation of Structural Capacity in PMS

The effective structural number is typically calculated using the AASHTO 1993 pavement design guide procedure using FWD measurements. This approach assumes that the subgrade resilient modulus can be obtained by relating it to the surface deflection at a large distance from the load as shown in equation (3):

$$M_R = \frac{0.24 P}{d_r * r} \quad (3)$$

where,

M_R = backcalculated subgrade-resilient modulus (psi);

P = applied load (lbs.); and

d_r = deflection at a distance r from the center of the load (in.).

The effective modulus, which describes the strength of all pavement layers above the subgrade, can be computed from FWD deflection measured at the center of the load plate knowing the subgrade resilient modulus and the total thickness of the pavement structure. These properties can be related and used to calculate the effective modulus (E_p) using equation (4):

$$\frac{M_R d_0}{1.5qa} = \frac{1}{\sqrt{1 + \left(\frac{D}{a} * \sqrt[3]{\frac{E_p}{M_R}}\right)^2}} + \frac{\left[1 - \frac{1}{\sqrt{1 + \left(\frac{D}{a}\right)^2}}\right]}{\left(\frac{E_p}{M_R}\right)} \quad (4)$$

where,

E_p = effective modulus of all pavement layers above the subgrade (psi);

d_0 = deflection measured at the center of the load plate and adjusted to a standard temperature of 68°F (in.);

q = load plate pressure (psi);

a = load plate radius (in.);

D = total thickness of pavement layers above the subgrade (in.); and

M_R = subgrade-resilient modulus (psi).

Using the total thickness of the pavement layers and the effective pavement modulus calculated from equation (5), the effective structural number (SN_{eff}) can be computed using the following expression:

$$SN_{eff} = 0.00045 * D * E_p \quad (5)$$

where,

D = total thickness of the pavement layers (in); and

E_p = effective pavement modulus of all layers above the subgrade (psi).

Recent Studies on Implementing Structural Indicators in PMS. A study was conducted by Flora and co-workers that aimed at developing a structural condition based index scaled from zero to 100 and that could be implemented into the Indiana Department of Transportation (INDOT) PMS decision matrix. Data considered in the study were collected from more than 10,000 one-mile sections in Indiana and encompassed weather data, distress surveys, pavement type, and FWD measurements [24]. Pavement types were classified in this study into six families according to the type of pavement (Flexible/PCC) and the functional class (Interstate, National Highway System [NHS], and Non-NHS). The following model was developed to calculate the Structural Strength Index (SSI) knowing the FWD central deflection:

$$SSI_{jk} = 100 \left\{ 1 - \alpha e^{\frac{-\beta}{\sigma^\gamma}} \right\} \quad (6)$$

where,

j, k = indices identifying the pavement family;

α, β, γ = regression coefficients; and

σ = center surface deflection (mils.).

The measurements were corrected due to temperature variation as follows:

$$D_{corrected} = \alpha \sigma \quad (7)$$

where,

α: correction factor determined from Table 6.

Table 6
Temperature correction factors [24]

Pavement temp (°F)	41	50	59	68	77	86	95	104	113	122
Correction factor	0.74	0.81	0.9	1	1.11	1.22	1.34	1.46	1.59	1.72

The regression coefficients for equation (6) were determined for each pavement family as shown in Table 7.

Table 7
Regression coefficients for the SSI model [24]

Pavement Family	α	β	γ
Flexible interstate	1.0013	40.303	3.853
Flexible NHS	1.0035	66.811	3.106
Flexible Non NHS	1.0124	100.838	2.586
Rigid interstate	1.0345	14.301	3.056
Rigid NHS	1.0017	338.056	4.995
Rigid Non NHS	1.0717	23.600	1.999

To implement the SSI as a structural capacity indicator into INDOT PMS decision matrices, trigger values and ranges were established. Researchers set the thresholds for excellent, very good, good, fair, and poor conditions for the SSI based on the ranges shown in Table 8.

Table 8
Trigger values for the SSI [24]

Pavement Family	Excellent	Very good	Good	Fair	Poor
Flexible interstate	95-100	90-95	85-90	80-85	<80
Flexible NHS	90-100	85-90	80-85	75-80	<75
Flexible Non NHS	85-100	80-85	75-80	70-75	<70
Rigid interstate	95-100	90-95	85-90	80-85	<80
Rigid NHS	90-100	85-90	80-85	75-80	<75
Rigid Non NHS	85-100	80-85	75-80	70-75	<70

Texas. A research study was conducted by Zhang and co-workers and aimed at characterizing the structural conditions of in-service pavements to be used in PMS applications at the network level [8]. The researchers evaluated available structural capacity indicators and elected to use the pavement Structural Number (SN_{eff}) calculated based on FWD measurements, equation (5). To define the threshold values that would be implemented in PMS, the researchers collected FWD data from 13,522 roadway sections located in different climatic regions in Texas; the selected sections had varying soil moduli and traffic levels [25]. A Structural Condition Index (SCI) was calculated by dividing the SN_{eff} by the required SN for 20 years based on the following equation:

$$SCI = \frac{SN_{eff}}{SN_{req}} \quad (8)$$

where,

SCI= Structural Condition Index;

SN_{eff} = existing (estimated) Structural Number; and
 SN_{req} = required Structural Number.

A mechanical approach was used to validate the developed SCI; the vertical compressive strain at the top of the subgrade and the horizontal tensile strain at the bottom of the surface layer were determined at each FWD test point for the seven sections, using the WESLEA program. The Asphalt Institute (AI) rutting and fatigue equations were used in performance prediction [25]:

$$N_d = 1.365 \times 10^{-9} (\epsilon_c)^{-4.477} \quad (9)$$

where,

N_d = Number of repetitions for subgrade rutting failure; and

ϵ_c = Vertical compressive strain at the top of the subgrade.

$$N_f = 0.0796 \times 10^{-9} (\epsilon_t)^{-3.291} (E)^{-0.854} \quad (10)$$

where,

N_f = Number of repetitions for fatigue failure;

ϵ_t = Horizontal tensile strain at the bottom of the AC layer; and

E = Surface layer modulus.

The numbers of repetitions for failure for both fatigue and rutting were then used to calculate the fatigue remaining life ratio and the rutting remaining life ratio, respectively:

$$\text{Fatigue Remaining Life Ratio} = \frac{N_f}{\text{Estimated Number of ESALs in 20 Years}} \quad (11)$$

$$\text{Rutting Remaining Life Ratio} = \frac{N_d}{\text{Estimated Number of ESALs in 20 Years}} \quad (12)$$

The rutting/fatigue remaining life ratios were computed for each of the FWD test points and were then compared to the SCI value for the same point. The coefficient of determination (R^2) was used in the comparison. Both rutting and fatigue remaining life ratios for asphalt pavements showed good correlation with the SCI with R^2 of 0.98 and 0.92, respectively.

Results also showed that the SCI was sensitive to pavement deterioration. This conclusion was based on sensitivity analysis conducted between the TxDOT PMS data for years 2000, 2001, and 2002 and the matching deflection data. Based on this analysis, the authors

recommended that the SCI be used as a screening tool at the network level for PMS applications.

A research project was conducted by Bryce and co-workers and aimed at developing a structural-based index and implementing it in the VDOT network-level pavement evaluation and rehabilitation process [2]. The research effort was divided into three main tasks (1) Develop a structural condition index at the network-level; (2) Find a methodology to implement this index into the VDOT pavement evaluation process; and (3) Identify pavement management applications and situations to use the structural index.

The researchers conducted a comprehensive study on the VDOT PMS evaluation process, decision matrices, and enhanced decision trees. It was found that VDOT divides the pavement distress indices into two categories; load related distresses (LDR) and non-load related distresses (NDR); the lowest value of both indices is then called the critical condition index (CCI). The CCI has a scale from 1 to 100 and the value of 100 describes excellent conditions. The categories of pavement conditions according to the CCI are shown in Table 9.

Table 9
Pavement condition categories [2]

Index Scale (CCI)	Pavement Condition
≥ 90	Excellent
70-89	Good
60-69	Fair
50-59	Poor
≤ 49	Very poor

The authors found that the decision process is divided into three steps; the first step is a decision matrix that has the pavement distresses as the inputs and decisions as outputs as shown in Table 10. The second step is a filter in which the CCI is implemented. The final step is an enhanced decision tree where traffic data, pavement age, and structural efficiency are implemented. The enhanced decision tree was the best candidate to implement a structural capacity indicator into the decision process.

Table 10
VDOT decision matrix for flexible pavement [2]

			Alligator cracking								
Frequency			Rare			Occasional			Frequent		
Severity			Low	Medium	High	Low	Medium	High	Low	Medium	High
Rutting	< 10%	None	DN	DN	CM	DN	CM	CM	PM	CM	RM
		< 0.5in	DN	DN	CM	DN	CM	CM	PM	CM	RM
		> 0.5in	CM ¹	CM	CM	CM	RM	RM	CM	RM	RM
	10% ^	None	DN	DN	CM	DN	CM	CM	PM	CM	RM
		< 0.5in	CM	CM	CM	CM	CM	CM	CM	RM	RM
		> 0.5in	RM	RM	RM	RM	RM	RM	RM	RC	RC

¹ CM= Corrective Maintenance; DN= Do Nothing; PM= Preventive Maintenance; RC= Rehabilitation/Reconstruction; and RM= Restorative Maintenance

The critical condition index filter is a strategy to compare the decision from the decision matrix with thresholds values of the CCI. For example, the following criteria are used for Interstate:

- For CCI values above 89, the treatment category is always DN.
- For CCI values above 84, the treatment category is always DN or PM.
- For CCI values below 60 the treatment category is at least CM, i.e., CM, RM or RC.
- For CCI values below 49 the treatment category is at least RM, i.e., RM or RC.
- For CCI values below 37 the treatment category is always RC.

Several structural capacity indices were studied by the authors to select the most promising one to be implemented in the enhanced decision tree. The Structural Condition Index (SCI), which was developed by Texas Department of Transportation, was selected to be modified and implemented into the VDOT enhanced decision tree. The SCI is calculated from FWD measurements after being normalized to 9,000 lb. load as follows:

$$SCI = \frac{SN_{Eff}}{SN_{Req}} \quad (13)$$

where,

$$SN_{Eff} = k_1 * SIP^{k_2} * H_p^{k_3},$$

$$k_1 = 0.4728;$$

$$k_2 = -0.4810;$$

$$k_3 = 0.7581;$$

SIP= $D_0 - D_{1.5HP}$; and

D_0 = peak deflection under the 9,000 lb. load, and $D_{1.5HP}$ = the deflection at a distance of 1.5 times the pavement depth.

The SCI was modified by the authors and was renamed as the Modified Structural Index (MSI) as shown in the following equation:

$$MSI = \frac{0.4728 * (D_0 - D_{1.5HP})^{-0.481} * H_p^{0.7581}}{0.05716 * (\log(ESAL) - 2.32 * \log(M_r) + 9.07605)^{2.36777}} \quad (14)$$

where,

D_0 = FWD central deflection (thousandth of an inch [mils.]);

$D_{1.5HP}$ = FWD deflection at a distance 1.5 x total pavement thickness (mils.);

H_p = Pavement thickness (in.); ESAL = Equivalent single axle load; and

M_r = Subgrade resilient modulus (ksi).

An analysis was conducted to calculate the MSI from FWD measurements along Interstate I-81, which had a length of 325 miles. Thresholds were then defined for the MSI and were implemented into the enhanced decision tree taking into consideration the pavement age as shown in Table 11.

Table 11
Modified Structural Index (MSI) thresholds [2]

Initial decision		DN		PM		CM		RM		RC	
Pavement age (years)		≤ 6	> 6	≤ 6	> 6	≤ 6	> 6	≤ 6	> 6	≤ 6	> 6
MSI	≥ 1	DN	PM	PM	PM	CM	CM	RM	RM	RC	RC
	< 1 and ≥ 0.9	CM	RM	CM	RM	RM	RM	RC	RC	RC	RC
	< 0.9	RM	RM	RM	RM	RC	RC	RC	RC	RC	RC

A study conducted by Tutumluer and Sarker to evaluate the use of Non-Destructive Testing (NDT) in evaluating pavement structural conditions as well as the use of NDT measurements in the design of asphalt overlays [26]. Testing was conducted by using FWD in five pavement sections located in two different counties in Illinois. The Illinois Department of Transportation (IDOT) Dynatest FWD machine was used in the testing program with geophones spaced at 0, 12, 24, 36, 48, 60, and 72 in. from the center of the load. Sections with high degrees of deterioration and that had been selected for rehabilitation were selected

for FWD testing. Every section was tested at intervals of 200 ft.; however, some stations were eliminated from the study as non-decreasing deflection bowls were detected.

Upon completion of FWD testing, the deflection basin measurements were used to conduct backcalculation analysis of the pavement layers' moduli [26]. A software based on Artificial Neural Network (ANN-Pro) was used in the backcalculation analysis. A finite element-based software (ILLI-PAVE FE) was then used to determine the tensile strain at the bottom of the asphalt layer ϵ_t . Thresholds for both ϵ_t and the surface deflection δ_v were then calculated based on the following equations:

$$N_f = \frac{8.78 \cdot 10^{-8}}{\epsilon_t^{3.5}} \quad (15)$$

$$N_f = \frac{5.73 \cdot 10^{10}}{\delta_v^4} \quad (16)$$

where,

N_f = number of ESALs to failure.

By comparing threshold values calculated from equations (15) and (16) with the pavement response due to FWD loading, the need for an overlay was assessed as shown in Table 12. In addition, by conducting the FWD testing after the construction of the overlay and calculating the new ϵ_t and δ_v , the predicted life of the constructed overlay was estimated as shown in Table 13.

Table 12
Comparison between thresholds and FWD based measurements [26]

Section Number	Design ESALs	ϵ_t threshold	δ_v (mil) threshold	ϵ_t FWD	δ_v (mil) FWD	Overlay required?
1	13,524	6.36E-4	45.36	6.13E-4	46.33	Yes
2	13,524	6.36E-4	45.36	6.06E-4	52.21	Yes
3	13,524	6.36E-4	45.36	4.52E-4	48.47	Yes
4	13,524	6.36E-4	45.36	5.32E-4	47.88	Yes

Table 13
Critical pavement response after overlay construction [26]

Section Number	ϵ_t FWD	δ_v (mil) FWD	Capacity > Demand (Design period= 20 years)
1	4.33E-4	33.42	Yes
2	4.44E-4	38.50	Yes
3	4.24E-4	34.22	Yes
4	4.56E-4	37.22	Yes

Artificial Neural Networks

In this study, artificial neural network (ANN) was utilized for two purposes. First, ANN was used to estimate the subgrade resilient modulus (M_r) based on RWD measurements. Second, ANN was used to develop a one-step decision making tool, that takes into consideration both structural and functional conditions of the pavement structure. ANNs have commonly been used for solving complex engineering problems in the last three decades [27]. ANNs are parallel computing schemes that imitate biological neural networks [28]. They are effective and accurate tools for solving complex nonlinear problems as they provide robust models that can continuously be updated as new data become available. In addition, they can be used in databases with either large or relatively small amount of data [29].

The Feed-Forward ANN. The most commonly used ANN structure for both regression analysis and supervised classification is the feed-forward model. This model topology consists of an input layer (i) in which the input independent variables are implemented, one or more processing (hidden) layers (j), and a target (output) layer (k) in which the depended variables are implemented [30]. The network topology is simulating the biological human brain. Each layer consists of processing units called “neurons,” and every neuron in a layer is connected with all neurons in the previous layer [31]. Each of these connections is assigned a “weight”, and each neuron is assigned a “bias.” An example of a feedforward network with one hidden layer is shown in Figure 13.

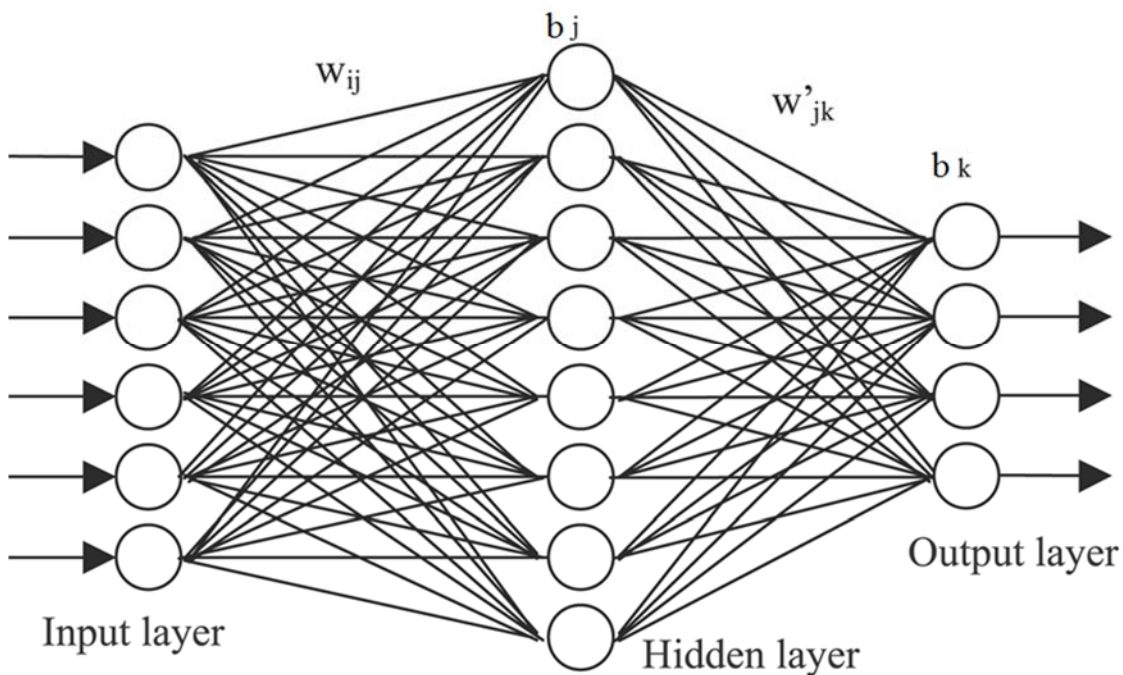


Figure 13
Example of feed-forward neural network structures

ANN Back-Propagation Training Algorithm. The process of calculating the weights and biases of the ANN is called the learning process or the training process. The most common used training procedure is the back-propagation error optimization algorithm. In this procedure, random values for weights and biases are assigned to the network connections and neurons, respectively. The network output (y) is then calculated based on the randomly assigned weights and biases and compared with the target value (t) to calculate the error. A squared loss function is used to calculate the error as shown in the following equation:

$$E = \frac{1}{2} (t - y)^2 = \frac{1}{2} [t - f(w, b, x)]^2 \quad (17)$$

where,

E= error function;

w= network weights;

b= network biases; and

x= in depended variables.

Equation (17) is then used as an objective function that needs to be minimized in a regular optimization problem. This optimization problem is solved using the Stochastic Gradient Descent (SGD). In the SGD method, the weight parameters are iteratively updated in the direction of the error loss function until a minimum is reached. The process of updating the weight parameters to minimize the error is called backpropagation. Figure 14 illustrates the concept of the backpropagation algorithm.

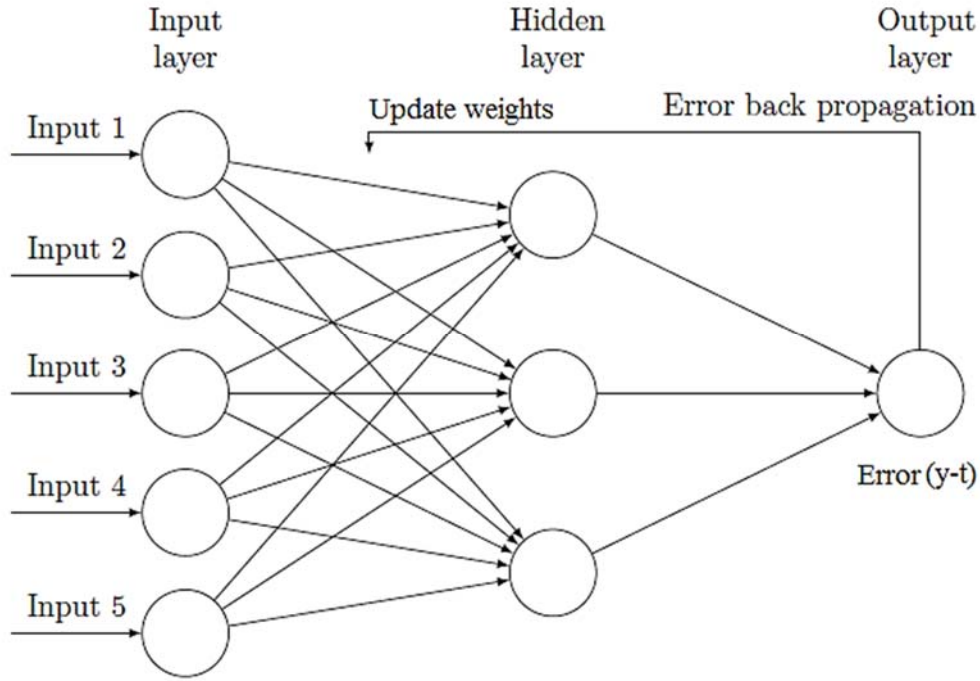


Figure 14
Back propagation algorithm

ANN Forward Calculations. After the network is trained, proper weights and biases are assigned to the network connections and neurons, respectively. These weights and biases are then used by the network to conduct forward-calculation on new data. First, the inputs to the hidden layer (j) are calculated by multiplying the input vector by the weight matrix (W_{ij}) and adding the hidden bias vector (b_j), see Figure 13. Second, an activation function is used to calculate the outputs of the hidden layer (j). The output vector is then calculated by multiplying the hidden vector by the weight vector (W'_{jk}) and adding the bias values (b_k), see Figure 13. The general equation of a backpropagation algorithm-based neural network with one hidden layer, one output variable, and a tan-sigmoid (tansig) transfer function can be described as follows [32]:

$$y = (b_k + \sum_1^{n_j} \text{tansig}(b_j + \sum_1^{n_i} a_i W_{ij}) W'_{jk}) \quad (18)$$

where,

k = the model output at layer k ;

n_j = number of neurons in the hidden layer;

n_i = number of neurons in the input layer; and

a_i = the input variables.

ANN Transfer Functions. The ANN transfer function, also known as activation functions, are differentiable non-linear functions, applied to the weighted input of the neuron to produce the neuron output. By using transfer functions, ANNs acquire their non-linearity. On other words, without activation functions, a neural network could not learn non-linear relationships. The most commonly used ANN transfer functions for regression analysis purposes are the logistic sigmoidal function (logsig), which produces outputs between “0” and “+1” as shown in Figure 15, and the tan sigmoidal function (tansig), which produces outputs between “-1” and “+1” as shown in Figure 16. For classification or decision problems, the step function ‘hardlim’ is the most commonly used. The hardlim function forces the neuron to produce an output of “0” or “1,” which allows the network to do classifications or make decisions. Equations (19) and (20) defines the logsig and tansig transfer functions, respectively.

$$\text{logsig}(x) = \frac{1}{1+e^{-x}} \quad (19)$$

$$\text{tansig}(x) = \frac{e^x - e^{-x}}{e^x + e^{-x}} \quad (20)$$

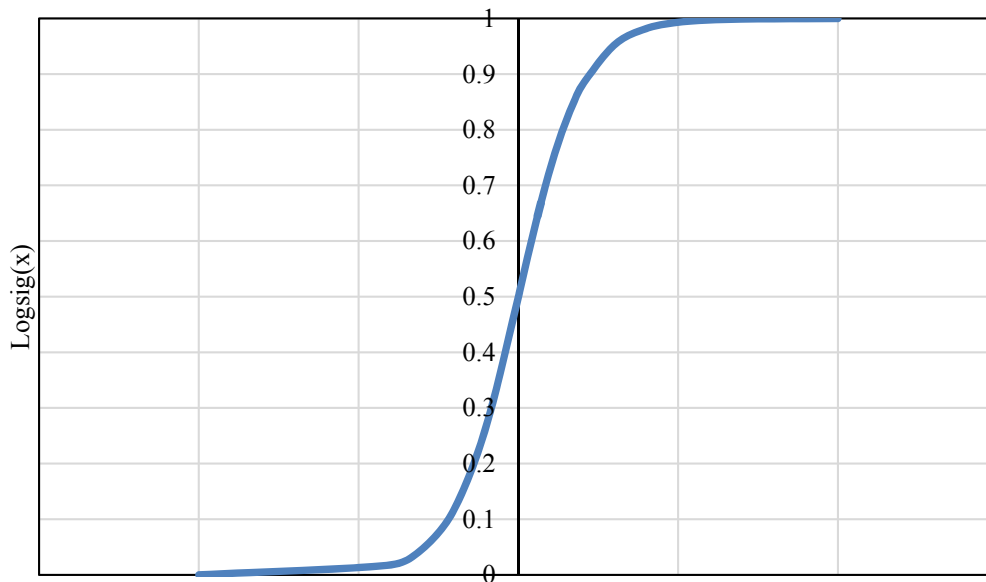


Figure 15
Logsig transfer function

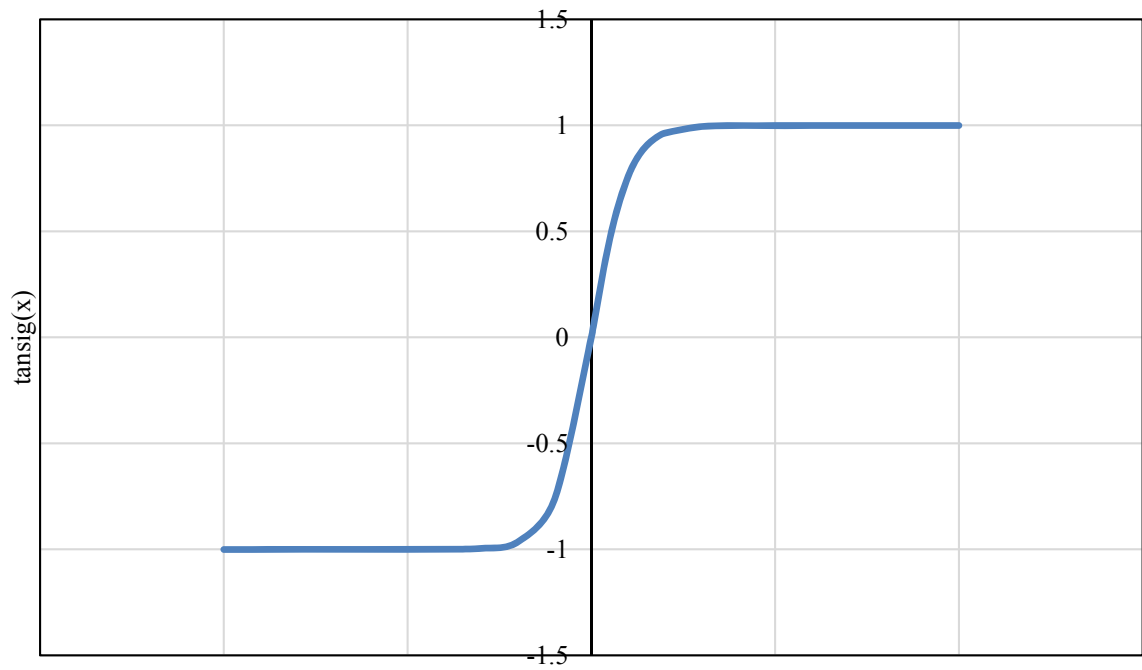


Figure 16
Tansig transfer function

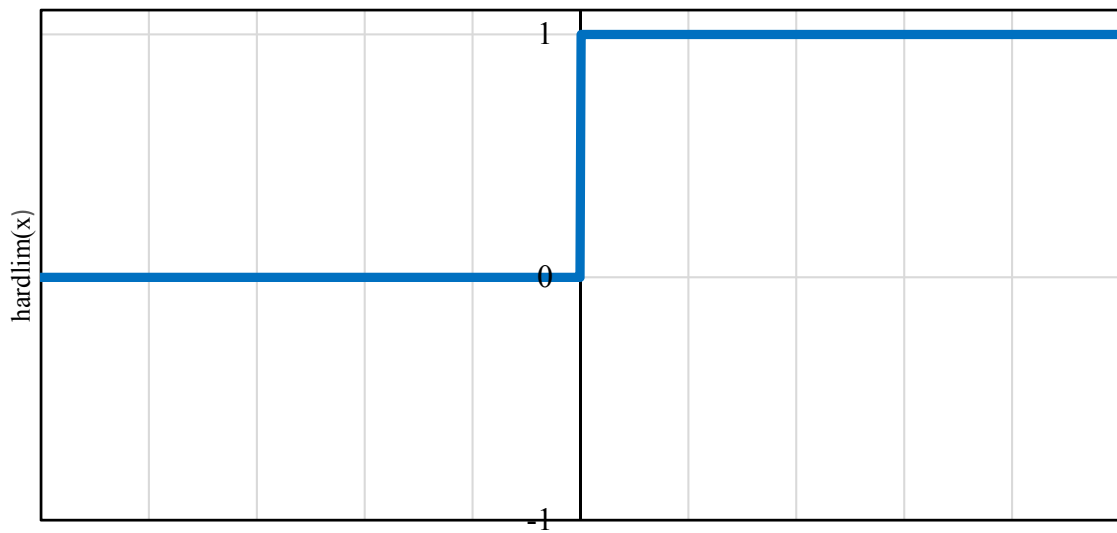


Figure 17
Hardlim transfer function

OBJECTIVES

The objective of this study was twofold. First, this project evaluated structural capacity indicators previously developed in 09-1P and their effectiveness in predicting pavement structural conditions based on RWD measurements. Based on this evaluation, the research team introduced modifications to improve prediction of pavement structural conditions and to allow for screening and identifying structurally-deficient locations in pavements based on a 0.1-mile test interval. Second, a methodology was developed to integrate the most promising structural capacity indicator into the Louisiana Pavement Management System (PMS) decision matrix and into overlay design. This project also assessed the cost-efficiency of RWD testing in identifying and repairing structurally-deficient sections prior to reaching very poor conditions.

SCOPE

Measurements from the comprehensive testing program of the RWD conducted by DOTD in 2009, in District 05, were analyzed. Furthermore, the research team analyzed PMS data collected in District 05 from 2005 to 2013 to determine the rate of structural and functional deteriorations for pavements that are structurally deficient and those that are structurally sound. Current practices for selecting pavement maintenance and rehabilitation strategies were modified such that both structural and functional pavement conditions are considered in treatment selections and to improve the accuracy of the overlay design procedure in the state.

METHODOLOGY

To achieve the study objectives, the research activities were divided into two phases. In the first phase, a comprehensive review of Louisiana PMS and recent studies dealing with continuous deflection testing was conducted. In addition, a critical evaluation of the structural capacity indicators developed for RWD was performed based on the original RWD and FWD data sets collected in 2009 and the new PMS data collected in 2011 and 2013. Based on this evaluation, modifications were suggested for the most promising structural capacity indicator in order to improve identification of structurally-deficient sections. In the second phase, a methodology was developed to incorporate the most accurate structural capacity indicator into Louisiana PMS and overlay design. Further, the cost-efficiency and added values of RWD testing in identifying and repairing structurally-deficient sections were evaluated.

Experimental Program

RWD Testing in Louisiana

The complete field testing program requested by DOTD consisted of two phases. In the first phase, the asphalt road network (about 1,250 miles) in District 05, referred to as network sites, was tested using the RWD deflection system based on ARA, Inc. standard testing protocol. LTRC also selected 58 sections to be tested using FWD. In the second phase, 16 road-sections (1.5 miles each), referred to as research sites, were selected and used for a detailed evaluation of the RWD technology as shown in Figure 18 [14].

In addition to RWD testing, the test plan in Phase II included conducting FWD testing on selected flexible and surface treatment pavement test sites. The testing plan specified that FWD testing should be conducted within 24 hours following completion of RWD testing on the selected sites in order to maintain the same testing conditions. The field testing program for RWD and FWD was conducted successfully in December 2009 with no major problems during the course of the experiment [14].

To assess repeatability of the measurements and the effects of truck speed, triplicate runs were performed at different speeds of 20, 30, 40, 50, and 60 mph. However, the test speed was restricted by the posted speed limits on a number of sites. Only Site 7 was selected on the Interstate Highway System (I-20), which permitted testing at 60 mph. However, testing at 50 mph was conducted on 8 of the 16 sites. Road segments were also selected to represent different pavement conditions as described by the PCI, with varying HMA thicknesses and base types. Traffic volume widely varied in the selected sections from an Annual Average Daily Traffic (AADT) of 244 to 29,357; these traffic volumes range from low to heavy.

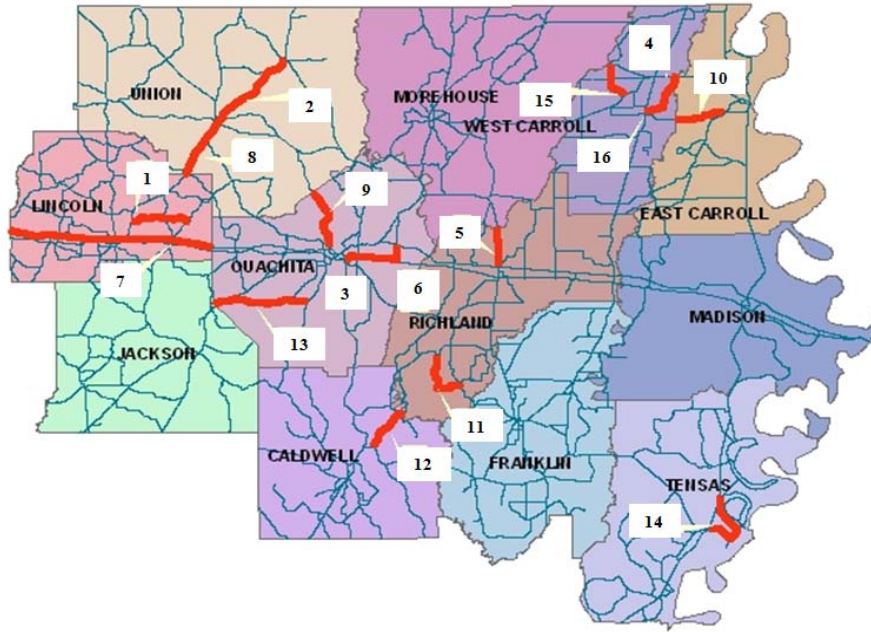


Figure 18
Locations of the 16 research sites in District 05 [14]

Pavement temperature was recorded in conjunction with each test. The pavement surface temperature ranged from 29.3 to 69.8°F (-1.5 to 21°C) with an average temperature of 48.2°F (9°C) during the testing process. To assist in the analysis, pavement design of the selected sites was obtained using cores and construction documents. Figure 19 shows the coring location for research Site 12, while Figure 20 shows the core sample for the same location, which provided accurate information about layer types and thicknesses. In addition, the test plan included supportive measurements, such as roughness, pavement temperature, and distress survey for the selected sites.



Figure 19
Coring test section Site 12 [14]



Figure 20
Core sample Site 12 [14]

FWD Testing in Louisiana

Nondestructive FWD deflection testing was conducted to measure the load response characteristics of the pavement layers and subgrade. Deflection testing was performed in accordance with ASTM D 4694, “Standard Test Method for Deflections with a Falling Weight-Type Impulse Load Device” and D 4695, “Standard Guide for General Pavement Deflection Measurements.” The FWD device shown in Figure 21 was configured to have a 9-sensor array, with sensors spaced at 0, 8, 12, 18, 24, 36, 48, 60, and 72 in. from the load plate. Three load levels of 9,000, 12,000, and 15,000 lb. were used in the FWD deflection-testing program. The FWD testing was conducted at a frequency of 0.1 mile with the testing location selected in the middle of the interval used in RWD testing. As previously noted, FWD tests were conducted within 24 hours of RWD testing on the outer wheel path [14].



Figure 21
Illustration of the FWD test device used in the testing program [14]

RWD Data Processing and Filtering

During RWD testing, laser deflection readings are measured at 0.6-in. intervals. Irrelevant data such as measurements collected on top of a bridge, sharp horizontal and vertical curves, and at traffic signals were removed. Erroneous data may also be obtained if the pavement surface is wet or in areas with severe cracking at the pavement surface. Valid deflection measurements were then averaged for two primary reasons: (a) minimizing the truck bouncing and vibration effects on the measured deflections and (b) decreasing the data to a manageable file size. After the averaging process is complete, deflections are normalized to a standard temperature of 68°F for sound comparison between data collected at different times of the day. Figure 22 presents the raw data collected on Site 9 by the four laser sensors [14].

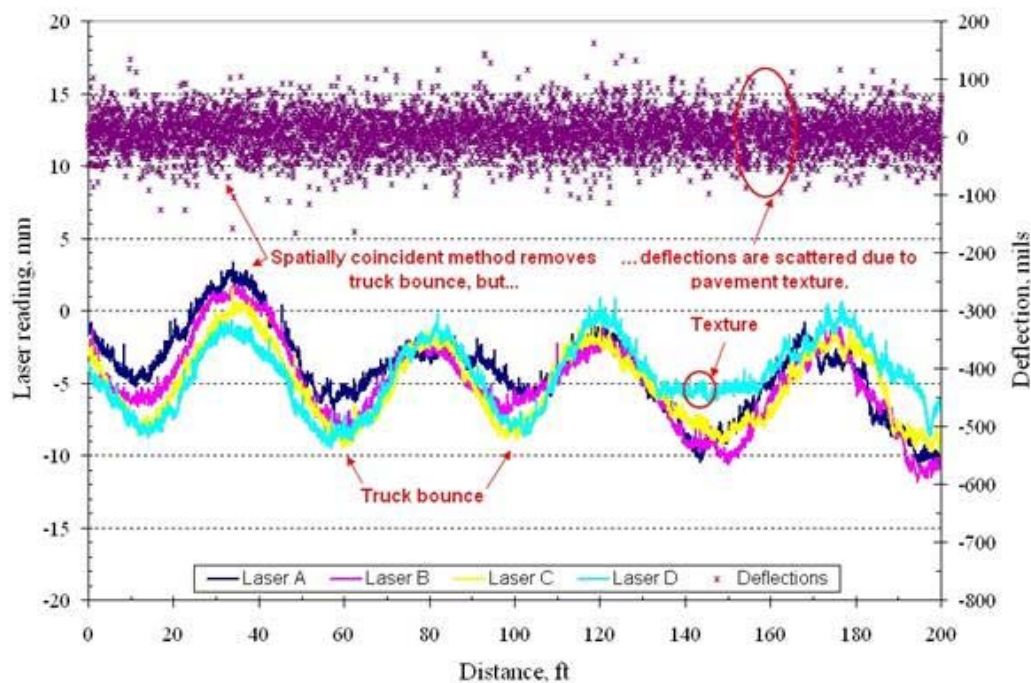


Figure 22

Example of individual laser readings and deflections for Site 9 (315-02), LA 143 north of West Monroe (after ARA, Inc.)

MnROAD Testing Program

The present study made use of RWD data collected on the MnROAD testing facility for validation of the subgrade modulus of resilience model based on independently-collected data. The data were collected in 2013 during a comprehensive pavement deflection testing program conducted at the MnROAD facility in Minnesota [33]. The surveyed road network

consists of a 3.5-mile mainline roadway (ML) with 45 sections and with “live traffic” as part of Interstate 94 near Albertville, Minnesota. In addition, a 2.5-mile closed-loop low volume roadway (LVR) consisting of 28 sections was also surveyed; the section lengths were typically about 500 ft. In addition to the test sections along the mainline and low volume road of the MnROAD, an 18-mile segment in Wright County was also tested. The segment is located about 20 miles from the MnROAD facility and was divided into nine sections. An overview of the facility is shown in Figure 23.



Figure 23
Overview of the MnROAD facility

Testing was conducted using the Traffic-Speed Deflectometer (TSD), RWD, and the Euroconsult Curvimeter; see Figure 24 [33]. FWD was used as a reference for comparison and evaluation purposes. Tested sections varied between flexible pavements, rigid pavements, and composite pavement sections. Yet, the present study focused on RWD measurements; therefore, only RWD and FWD data collected on flexible pavements were considered. The flexible pavement test segments at which both FWD and RWD measurements were conducted consisted of 16 sections; six in the main line and 10 in the low volume roadway.



Figure 24
MnROAD continuous deflection testing program [33]

Assess the Accuracy of the Developed Structural Capacity Indicators

The objective of this task was to analyze and evaluate the accuracy of the structural capacity indicators previously developed as part of Project 09-1P based on RWD testing. To achieve this objective, the research team evaluated the structural deterioration of the sections that were predicted to be structurally-deficient based on the structural capacity indicators by analyzing the core samples and FWD measurements. In addition, the research team compared the PMS data collected in 2013 in terms of structural distresses including cracking (e.g., fatigue) and rutting to the PMS data collected in 2009 to assess the levels of structural deterioration in these sections and whether identified sections were truly structurally-deficient. Further, an analysis of variance (ANOVA) was conducted between the structural indicators and the surface performance indices in order to assess which indicators are mostly dependent on pavement surface conditions. Based on this analysis, the research team assessed the prediction accuracy of the structural capacity indicators originally developed based on RWD testing.

RWD-Based Pavement Structural Capacity Indicators

During the original study, the research team observed that RWD describes the deterioration of the pavement structure through both an increase in the magnitude of the deflection and an increase in the scattering and variability of the deflection measurements. Elseifi and co-authors introduced a parameter known as the RWD Index (RI) based on the average RWD deflection and the standard deviation for a 1.5-mile test interval [18]:

$$RI = \text{Avg. RWD deflection} * \text{Std. Dev. of RWD deflection} \quad (21)$$

where,

RI = RWD Index (mm² or mils²);

Avg. RWD deflection = average deflection (mm or mils) measured on a road segment with a length of 1.5 miles; and

Std. Dev. of RWD deflection = standard deviation (mm or mils) of average RWD deflections in 1.5-mile test interval.

The RI index correlated reasonably well with the effective pavement structural number (SN_{eff}) determined from FWD. Since RWD measurements are based on 0.1 mile of pavement segment, the zone RWD Index (ZRI) was introduced with a new definition of a structural index based on RWD data, which was defined as follows:

$$ZRI = \text{average RWD deflection} * \text{fourth root of variance} \quad (22)$$

where,

ZRI is in $mm^{3/2}$ or $mils^{3/2}$ and the average of deflection and variance are based on the 0.1-mile pavement segment.

Based on the RI index and various expressions evaluated during the course of the original study (09-1P), the following relationship between SN- and RWD-measured parameters was introduced:

$$SN_{RWD} = -6.37 - \frac{150.69 * RI^{-.81}}{RI + 19.04} + 23.52 RWD^{-.24} - 1.39 \ln(SD) \quad (23)$$

where,

RI = RWD Index ($mils^2$) = Avg. RWD deflection * SD of RWD deflection;

SD = standard deviation of RWD deflection on a road segment (mils);

RWD = Avg. RWD deflection measured on a road segment (mils); and

SN_{RWD} = Pavement Structural Number based on RWD measurements.

Propose Modifications to the Most Promising Structural Capacity Indicator

Based on the results of the previous task, the most promising structural capacity indicator was selected to detect structurally-deficient pavements based on RWD testing. In this task, RWD measurements were analyzed further to improve prediction and to ensure that the maximum accuracy would be achieved through these measurements. To achieve this objective, the research team evaluated the assumptions made in the development of equations (21) to (23) and modified the original model to improve prediction accuracy and to allow for assessing pavement structural conditions every 0.1 mile. In this analysis, pavements were categorized based on thickness, type of base layer, and traffic volume during service. The

main outcome of this task was an updated structural capacity indicator that can be used to identify structurally deficient pavements based on RWD testing and at a 0.1-mile test interval.

Develop a Structural Index Based on Backcalculated Layer Moduli

The objective of this task was to develop a structural index (from 0 to 100) that describes the structural integrity of pavement sections based on the backcalculated AC layer moduli of in-service pavements as predicted from FWD testing. To achieve this objective, FWD-collected data were used in a backcalculation process; the backcalculation software, ELMOD 6, was used based on the equivalent thickness method. The backcalculated moduli were correlated and categorized statistically to establish a structural index that ranges from 0 to 100 in which 100 describes perfect structural conditions and 0 describes a totally damaged pavement structure. The developed index may be incorporated into Louisiana PMS to describe pavement structural conditions based on FWD measurements and to guide in the selection of appropriate treatment strategies.

Falling weight deflectometer measurements from 52 in-service pavement sections with a total length of approximately 320 miles were used to develop the structural index. Furthermore, Ground Penetrating Radar (GPR) data were used in this task for pavement thickness information. In addition to GPR testing, core samples were used to detect any materials deterioration underneath the pavement surface. At least one core sample was available from each homogenous control section. Core samples were also used to determine the type of base layer used in the pavement structure; this was beneficial to ensure the accuracy of the backcalculation process in case of the presence of a cement-treated base layer.

Compare Rate of Deteriorations for Pavement Sections

In this task, the research team analyzed PMS data collected in District 05 from 2005 to 2013 to determine the rate of structural and functional deteriorations for pavements that are structurally deficient and those that are structurally sound. Based on this analysis, the research team determined whether the rates of deterioration are significantly different for pavements that are structurally deficient and those that are structurally sound. Results of this analysis were used in the subsequent tasks to assess cost-efficiency of RWD testing and the added values of identifying structurally deficient pavements to the State PMS. In light of this analysis, the research team assessed whether the identification of structurally deficient pavements at an early stage of deterioration may save state funds by addressing this deterioration early in the pavement service life.

To compare pavement levels of deterioration, the research team categorized the tested road segments into five categories based on structural conditions (e.g., excellent, good, fair...etc.). The categorization process was based on thresholds obtained from the developed structural capacity indicators. For each category, the PMS data at years from 2005 to 2013 were evaluated. Segments, which showed an increase in one or more of the performance indices during the analysis period, were eliminated since it indicates that a treatment has been applied on these segments. In addition, to offset the traffic volumes effect on the level of deterioration; segments were divided according to their functional class (e.g., arterials, collectors, etc.), then each class was studied separately.

Conduct an Overlay Design for the Selected Pavement Sections

Based on the data collected in previous tasks, and in the RWD testing program, the research team conducted an overlay design of selected pavement sections. These sections included structurally-deficient and structurally-sound pavement sections in District 05. The objective of these overlay designs, which were based on RWD measured deflections, was to quantify the difference in overlay thickness if RWD measurements are considered in the design process.

The overlay design was conducted according to DOTD current design practices and based on the assumptions of a 10-years design life and 2-in. milling. The proposed design procedure considered the actual pavement structural capacity based on RWD measurements and compared the obtained designs with current practices adopted by DOTD office of design, which assumes 50% loss in structural capacity.

Investigate the Feasibility of Predicting the Subgrade Modulus from RWD Data

In this task, the two RWD deflection measurements (D_0 and D_{18}) were used to develop an artificial neural network (ANN) model to predict the subgrade modulus. The correlation between the proposed ANN model and the AASHTO 1993 FWD-based model were evaluated:

$$M_r = \frac{0.24 \cdot P}{d_r \cdot r} \quad (24)$$

where,

M_r = backcalculated subgrade-resilient modulus (psi);

P = applied load (pounds); and

d_r = deflection at a distance r (in) from the center of the load (in).

Determine Cost Efficiency and Added Values of RWD Testing

The objective of this task was to evaluate the cost-efficiency of using RWD measurements in PMS activities at the network level and the benefits that may be obtained by adopting this test method in Louisiana. To achieve this objective, monetary savings obtained by providing for the most cost effective rehabilitation treatment methods were compared against the cost of collecting and analyzing RWD deflection data. Data needed in the cost-analysis were obtained from the analysis conducted in the previous tasks and by querying existing databases in the Louisiana PMS. Current state of practice was compared to an improved treatment selection strategy developed based on RWD measurements and existing PMS indices.

Develop a One-Step Enhanced Decision Making Tool

The objective of this task was to develop a one-step enhanced decision-making tool that considers both structural and functional pavement conditions in treatment selection at the network level. To achieve this objective, an artificial neural network-based pattern recognition system was trained and validated using pavement condition data and RWD measurements-based SN to arrive at the most optimum maintenance and rehabilitation (M&R) decisions. The developed tool needed to be time-efficient and easy to use since it will be adopted by PMS engineers to determine the final enhanced M&R decisions (which requires several analysis steps) based on RWD measurements and the modified overlay design procedure.

DISCUSSION OF RESULTS

Accuracy of Structural Capacity Indicators

Pavement structural capacity was predicted based on RWD measurements using the indicators presented in equations (21) to (23). RWD data from 188 control sections in District 05 were considered in this analysis with a total length of 1,066 miles. The center deflection (D_0) was the main input used from RWD measurements. Performance indices were also extracted from PMS, namely, the Alligator Cracking Index (ALCR), the Rutting Index (RUT), the Roughness Index (RUFF), the Random Cracking Index (RNDM), the Patching Index (PTCH), and the overall Pavement Condition Index (PCI).

To assess whether the structural capacity indicators are affected by pavement surface conditions; data from the 188 control sections were categorized into three groups according to the AC layer thickness: thin, which includes pavements with AC thickness less than 3 in., medium with AC thickness from 3 to 6 in., and thick sections with AC thickness more than 6 in. as shown in Table 14.

Table 14
Control sections classification according to AC thickness

Pavement Characteristics	Group 1	Group 2	Group 3
Pavement Class	Thin	Medium	Thick
AC Thickness range (in.)	<3	From 3 to 6	>6
Number of control sections	34	77	77
Total length (miles)	194	548	324

Statistical Analysis

An Analysis of Variance (ANOVA) was conducted on the aforementioned road categories to assess the influence of each pavement performance index on the structural capacity indicators. Results of the analysis are presented in Tables 15 to 17. Statistical analysis was conducted at a 95% confidence level such that a P-value less than 0.05 indicates significant correlation. As shown in these tables, the ZRI was the structural capacity indicator that correlated the most with pavement performance surface indices. On the other hand, the SN did not correlate with most pavement performance surface indices. A low correlation is desirable as it indicates that a structural capacity indicator provides useful information, which is not already available from the existing pavement performance surface indices.

Table 15
ANOVA results for thin sections

Indicator	Performance Indices					
	R _{uff}	ALCR	RUT	PCI	RNDM	PTCH
SN	0.1524	0.4618	0.6286	0.6440	0.4223	0.0195
RI	0.3534	0.5348	0.5771	0.9250	0.0628	0.0528
ZRI	<.0001	0.02	<.0001	0.30	<.0001	<.0001

Table 16
ANOVA results for medium sections

Indicator	Performance Indices					
	R _{uff}	ALCR	RUT	PCI	RNDM	PTCH
SN	<.0001	0.7	0.2	0.01	0.6	0.01
RI	<.0001	0.03	0.02	0.001	0.3	<.0001
ZRI	<.0001	0.70	0.07	0.052	0.0022	<.0001

Table 17
ANOVA results for thick sections

Indicator	Performance Indices					
	R _{uff}	ALCR	RUT	PCI	RNDM	PTCH
SN	0.1190	0.1029	0.5050	0.5206	0.8393	0.0711
RI	0.0002	0.1810	0.3475	0.5157	0.8428	0.6018
ZRI	<.0001	0.3145	0.0182	0.0008	<.0001	<.0001

Uniformity Index

To evaluate the uniformity of each structural capacity indicator, the Uniformity Index (UI) was calculated for each control section for the ZRI, SN, and RI according to equation (25). The average uniformity coefficient was calculated to be 82% for the SN model, 69% for the RI, and 62% for the ZRI. The uniformity distributions are shown in Figures 25 to 27 for the three structural capacity indicators.

$$UI\% = \left[1 - \left(\frac{SD}{AVG} \right) \right] * 100 \quad (25)$$

where,

SD = standard deviation of the indicator for every control section; and

AVG = Mean value of the indicator for every control section.

Since the road network in Louisiana PMS is divided into control sections such that each section has similar characteristics (i.e., traffic volume, pavement structure, and subgrade

type), variation of the structural conditions within the same control section is expected to be negligible. Therefore, a suitable structural capacity indicator is expected to have a high uniformity index within the same control section. As shown in Figures 25 to 27, the SN model had the most uniform prediction within the evaluated control sections, followed by the RI, and finally the ZRI.

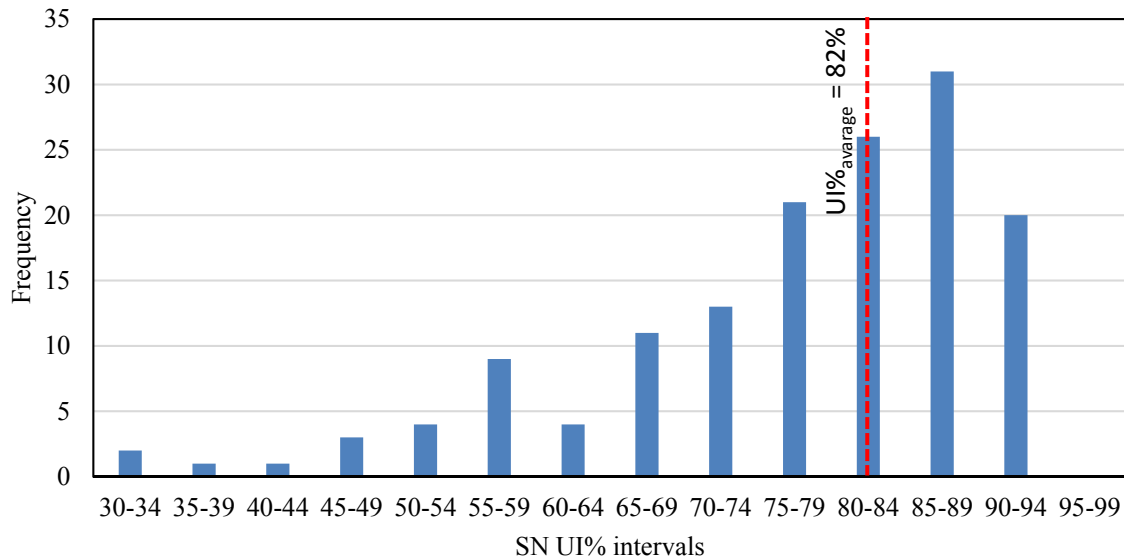


Figure 25
Uniformity histogram for SN

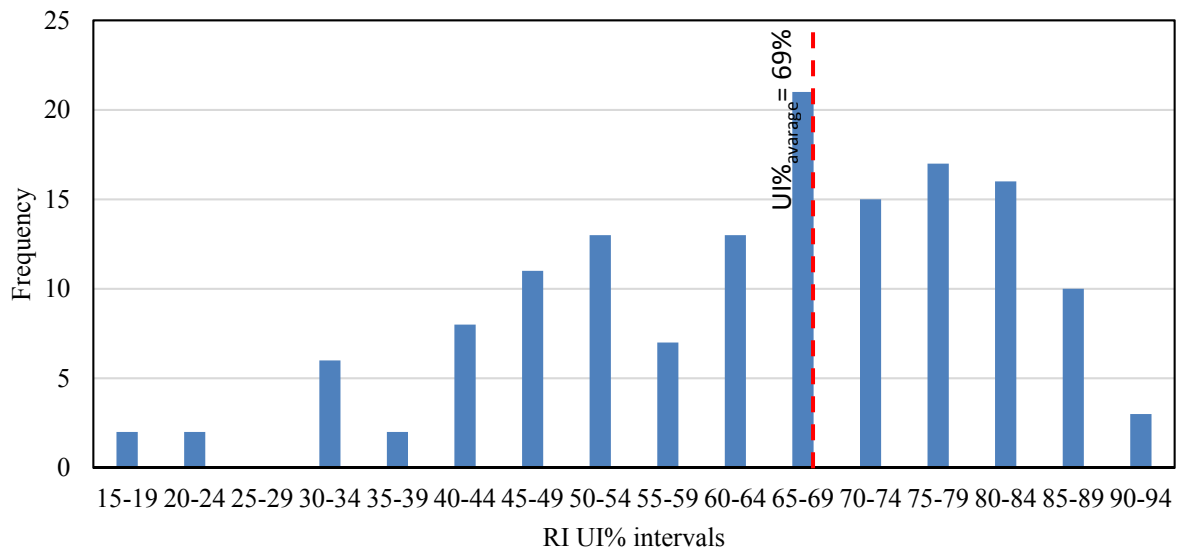


Figure 26
Uniformity histogram for RI

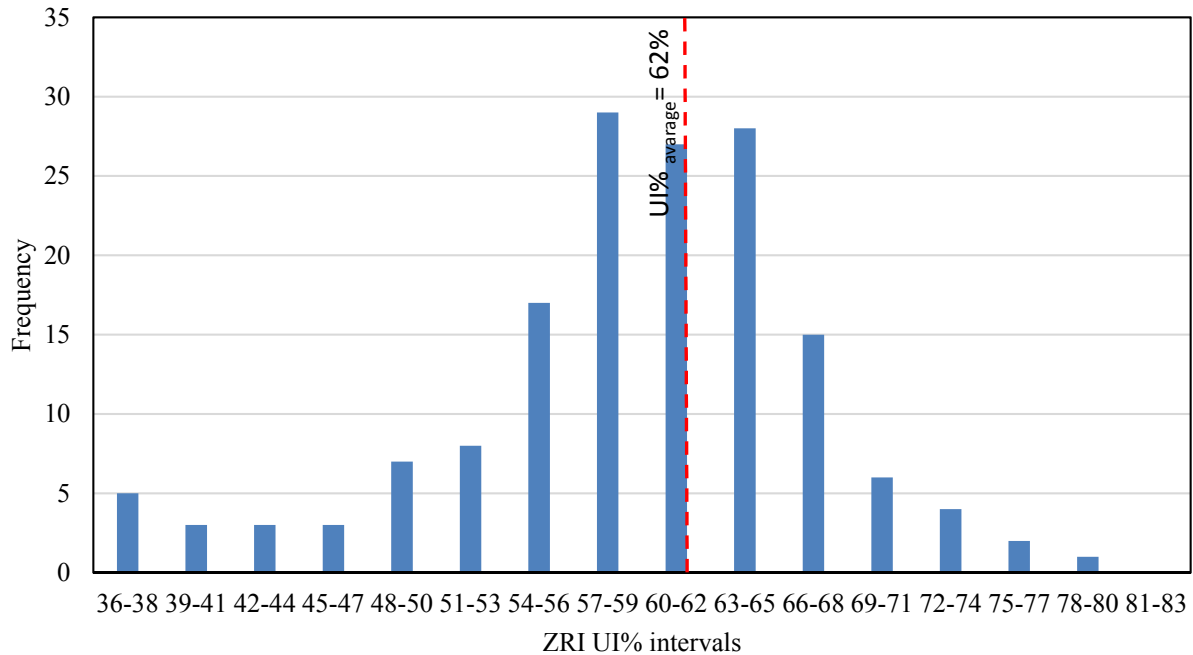


Figure 27
Uniformity histogram for ZRI

Identification of Structurally Deficient Sections

To assess the relationship between the structural capacity indicators and in-situ pavement structural conditions, core samples and pavement condition data were analyzed for the lowest-ranked sections according to each approach. These sections were the 20% control sections that have the lowest SN, the 20% sections that have the largest RI, and the 20% control sections that have the largest ZRI. The thresholds for structural deficiency were estimated from the cumulative distribution functions for each structural capacity indicator. Table 18 presents the calculated thresholds for each indicator. An example of determining the ZRI threshold for thin sections is presented in Figure 28.

Table 18
Limiting thresholds for the three structural capacity indicators

Category	SN	RI	ZRI
Thin	2.40	125.7	196
Medium	2.74	110.5	176
Thick	3.10	87.5	150

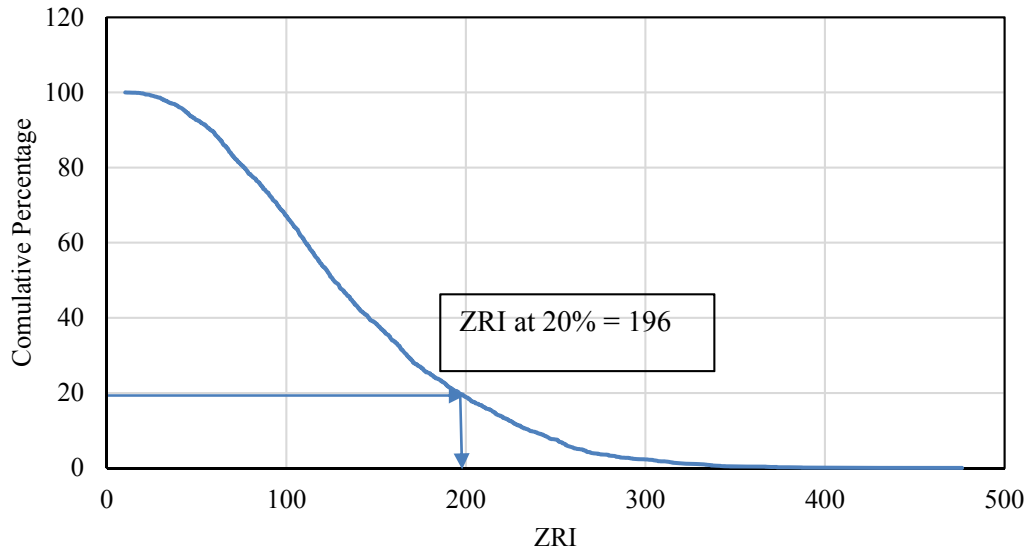


Figure 28
ZRI cumulative distribution function for thin sections

Using the thresholds presented in Table 18, the average values of the functional surface indicators for sections considered structurally-deficient were calculated and are shown in Tables 19 to 21. As shown in these tables, structurally deficient sections were in some cases in pavements with good surface conditions. These results support the need to implement a pavement structural condition indicator into PMS in addition to the current functional indices. A list of identified pavement sections is presented in Appendix A. It is worth noting that the sections considered deficient according to SN were almost the same as the sections considered deficient according to RI.

Table 19
Averages performance indices for sections below 20% SN thresholds

	ALCR	RUT	RUFF	RNDM	PTCH	PCI
Thin	83.70	90.95	62.60	87.88	79.76	68.54
Medium	79.36	92.64	69.28	84.62	79.41	69.75
Thick	89.68	85.83	76.11	90.76	90.53	77.40

Table 20
Averages performance Indices for sections above 20% RI thresholds

	ALCR	RUT	RUFF	RNDM	PTCH	PCI
Thin	83.73	90.94	62.63	87.88	79.76	68.53
Medium	82.25	92.77	70.87	85.77	81.51	71.90
Thick	89.68	85.84	76.11	90.76	90.53	77.40

Table 21
Averages performance Indices for sections above 20% ZRI thresholds

	ALCR	RUT	RUFF	RNDM	PTCH	PCI
Thin	75.23	91.48	66.26	82.85	74.74	65.73
Medium	80.46	95.57	77.02	84.97	94.47	76.50
Thick	92.16	85.60	77.83	94.40	98.44	81.06

Investigation of Cores

Table 22 categorizes structurally-deficient sections into three groups. Group 1 includes sections that were classified as deficient based on the three structural capacity prediction approaches (i.e., SN, RI, and ZRI). Group 2 includes sections that were classified as deficient by only the SN and RI approaches, and Group 3 includes sections that were classified as deficient by only the ZRI. Cores' conditions were correlated to the three groups to assess whether a section is either structurally deficient or structurally-sound.

Table 22
Sections classifications for core samples study

Group ID	SN	RI	ZRI
1	Deficient	Deficient	Deficient
2	Deficient	Deficient	Sound
3	Sound	Sound	Deficient

Group 1. This group includes sections that were classified as structurally deficient based on the three indicators. Investigation of core samples indicated that 85% of the sections in this group suffered from major to medium stripping in one or more of the AC layers, as shown in Figure 29.



Figure 29
Example of severe stripping in control section 161-08

Group 2. This group includes sections that were determined to be structurally deficient based on the SN and the RI approaches but not by the ZRI. Investigation of core samples showed that 60% of the sections in this group suffered from major to medium stripping in one or more of the AC layers as shown in Figure 30. This indicates that the SN and RI approaches successfully identified these sections as structurally-deficient.



Figure 30
Example of AC stripping in control section 831-06

Group 3. This group includes sections that were classified as structurally deficient based on the ZRI approach only. Investigation of core samples showed that only 18% of the sections in this group suffered from medium stripping in the AC layers; however, the majority of the sections were in good conditions as shown in Figure 31. These results indicated that the ZRI approach did not successfully identify structurally deficient sections.



Figure 31
Example of core sample in good structural conditions (Section 182-01)

Selection of the Most Promising Indicator

According to the ANOVA results, the ZRI was found to be significantly affected by pavement surface conditions. In addition, the uniformity index analysis indicated that the ZRI was the indicator with the lowest uniformity (62%). Furthermore, investigation of the core samples showed that the ZRI did not successfully identify pavement structural deficiency in some of the sections. Therefore, the ZRI was not considered in the rest of the analysis.

Investigation of the core samples indicated that the RI and the SN were the most promising indicators to detect pavement structural deficiency; yet, sections considered deficient according to the SN thresholds were found to be the same sections as those considered deficient according to the RI thresholds. Therefore, either one of these two indicators would be acceptable. Since the in-service SN is a key input in the AASHTO 1993 overlay design approach, it was considered as the most promising indicator, and was, therefore, selected for further modifications.

Propose Modifications to the SN Model

The SN model showed an acceptable accuracy in identifying pavement structural deficiency; however, the main shortcoming of the model is that it predicts the SN at 1.5-mile intervals. Obtaining an average SN value every 1.5-mile prevented identifying structurally deficient locations in shorter pavement segments. Additionally, the model was found to over-estimate SN in thin sections. The main objective of this task was to develop an improved statistical model to predict pavement SN every 0.1 mile based on RWD measurements.

Model Development

A new model was developed based on RWD and FWD measurements obtained from 12 different road segments distributed equally on the predefined three thickness categories, Table 14 (thick, medium, and thin). The AC layer(s) thickness and the Annual Average Daily Traffic (AADT) were found to have significant effects on the pavement SN with P-values of 0.0039 and less than 0.0001, respectively. Therefore, both factors were included in the new model. It is noted that the total pavement thickness was considered in the model but it was not found to improve prediction accuracy. The SAS 9.4 software was used in fitting the new model, which was defined as follows [34]:

$$SN_{RWD0.1} = -14.72 + 27.55 * \left(\frac{AC_{th}}{D_0} \right)^{0.04695} - 2.426 * \ln SD + 0.29 * \ln ADTPLN \quad (26)$$

where,

AC_{th} = Asphalt concrete layer(s) thickness of the pavement structure (in.);
 D_0 = Avg. RWD deflection measured each 0.1 mile (mils.);
 SD = Standard deviation of the RWD deflection each 0.1 mile (mils.);
 ADT_{PLN} = Average Annual Daily Traffic per lane (Vehicle/day); and
 $SN_{RWD0.1}$ = Structural Number based on RWD measurements for 0.1 mile interval.

Figure 32 presents the fitting of the model during the development phase. As previously noted, the main advantage of the modified model is that it allows the estimation of the pavement structural number at 0.1-mile interval of the road segment ($SN_{RWD0.1}$). The $SN_{RWD0.1}$ was validated based on 25 road sections, which were not used in the development phase with a total length of 45.5 miles. As shown in Figure 33, the modified model demonstrated a reasonable accuracy with a Root Mean Square Error (RMSE) of 0.8 and a coefficient of determination (R^2) of 0.76 in the validation phase. Figure 34 compares the SN predicted from FWD based on the 1993 AASHTO method to the SN predicted from RWD measurements based on the new model, equation (26). As shown in this figure, there was a relatively good agreement between the two approaches indicating that the modified model can be effectively used to predict SN at an interval of 0.1-mile [34].

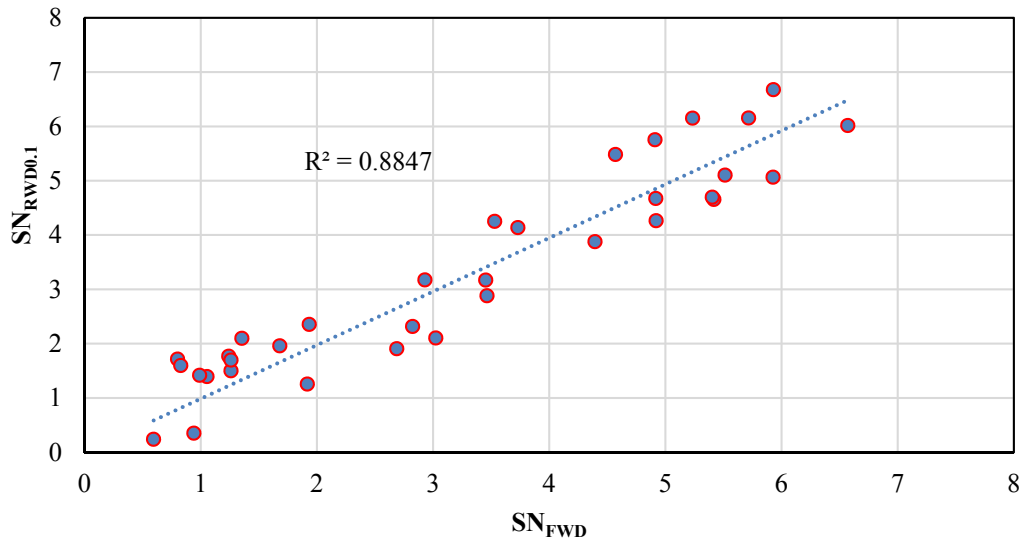


Figure 32
 $SN_{RWD0.1}$ model development

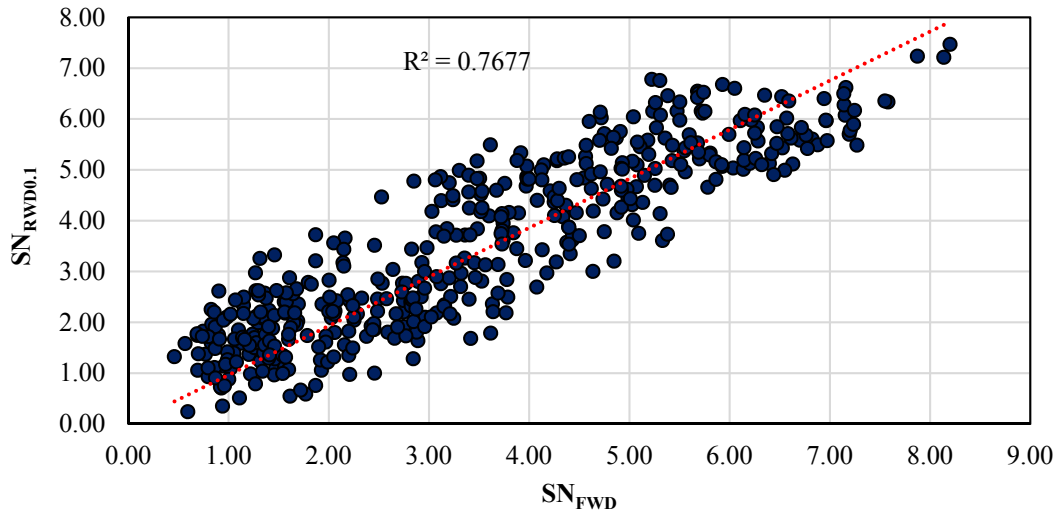


Figure 33
 $SN_{RWD0.1}$ model validation

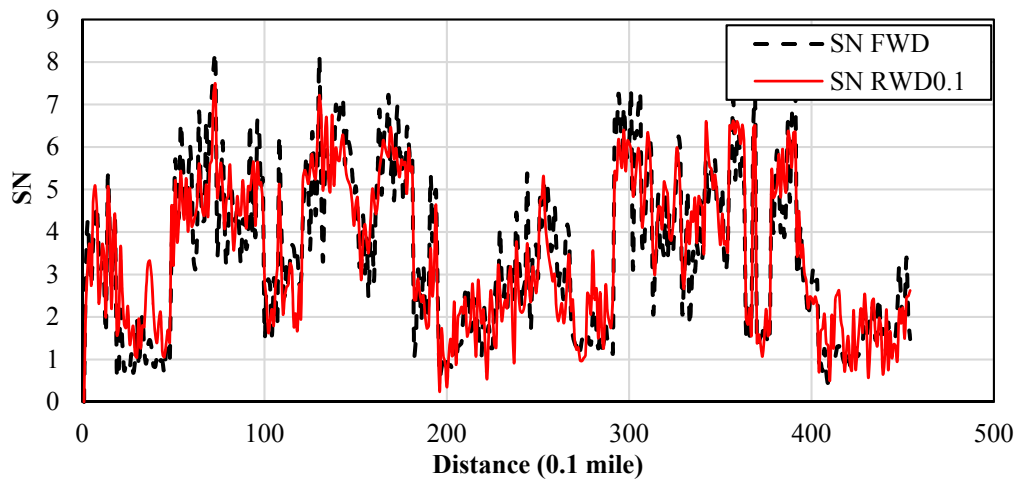


Figure 34
 $SN_{RWD0.1}$ vs. SN_{FWD} longitudinal profile

Sensitivity Analysis

The sensitivity of the modified model to the various input parameters was evaluated. In this analysis, each of the input parameters was varied, and the change in the predicted $SN_{RWD0.1}$ was calculated. The average value for each parameter in the model was used as a baseline, and each parameter was varied between the minimum and maximum values as shown in Table 23.

Table 23
Sensitivity analysis of SN model to variation in input values

Parameter	AC _{th} (in.)	D ₀ (mils)	SD (mils)	ADT veh/day
Baseline	5.6	16.5	65	970
Max. value	2.0	50	20	5050
Min. value	12.0	1	140	50

Figure 35 presents the change in SN associated with a change in the different input parameters from the minimum to the maximum values. Results of the sensitivity analysis indicated that the $SN_{RWD0.1}$ was the most sensitive to D_0 (RWD Deflection) and the deflection standard deviation (SD), and was the least sensitive to traffic daily volume (ADT) and AC thickness (AC_{th}).

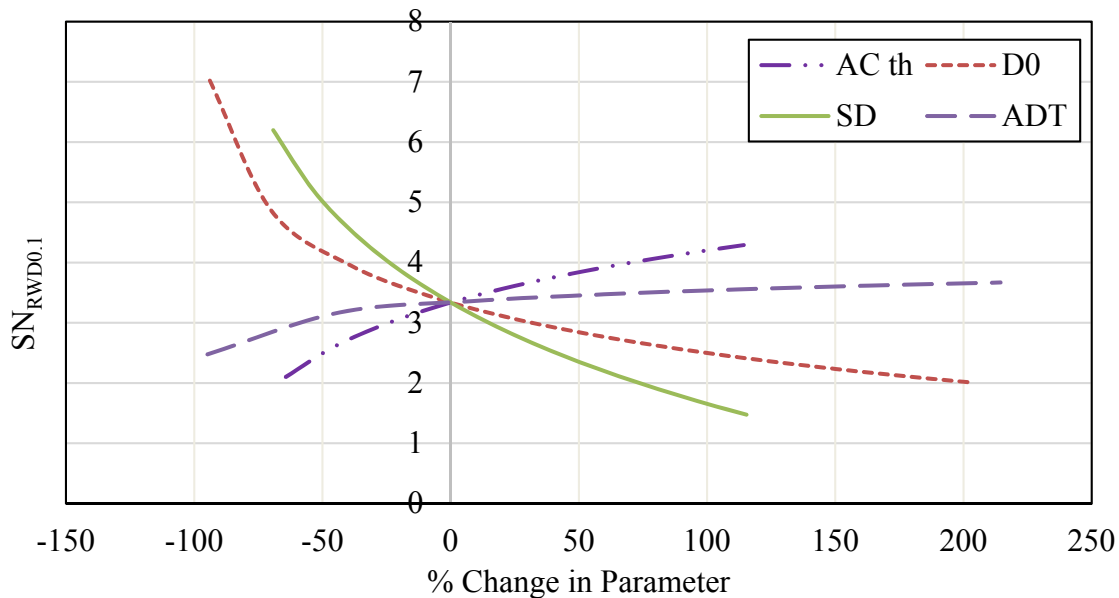


Figure 35
Sensitivity analysis for the $SN_{RWD0.1}$ model

Model Efficiency and Characteristics

While the accuracy of the model has been demonstrated through the previous analysis, it was unclear whether the model is able to identify structurally deficient pavements as opposed to functionally deficient pavements, which could already be identified using conventional functional indices in the State PMS. In this part of the study, the model's ability to identify structurally-deficient pavements was investigated. Surveyed road sections were used to study the efficiency of the $SN_{RWD0.1}$ model in identifying structurally deficient pavements.

Road sections were divided into six categories according to the AC layer(s) thickness and to the type of base layer (treated or untreated). The treated category mostly included sections that were cement-treated as this technique is widely used to address poor soil conditions in the State. Road segments were also classified into three categories based on the Pavement Condition Index (PCI). Road sections with an average PCI less than 65 were considered in the poor category; the fair category included road sections with an average PCI greater than 65 and less than 85, and sections with an average PCI greater than or equal to 85 were considered in the good category.

Variation with ALCR and PCI. The $SN_{RWD0.1}$ was calculated for each 0.1-mile interval for the 153 road sections; the average value along the section was then calculated for each road segment. The average $SN_{RWD0.1}$ for each road category was calculated to study its variation from one road category to another. Figure 36 shows that the average $SN_{RWD0.1}$ for the sections in the “Poor” category was not consistently lower than the average $SN_{RWD0.1}$ for sections in the “Fair” category. Similarly, sections in the “Good” category commonly had $SN_{RWD0.1}$ average values higher than those in the “Fair” and the “Poor” categories; however, this was not applicable to all road segments indicating that the trend between structurally-deficient and functionally-deficient is not definitive. A similar observation was detected for the ALCR categories as shown in Figure 37. The trends presented in this analysis indicate that $SN_{RWD0.1}$ is not fully correlated to the functional conditions of the roadway surface. It is noted that there were no thick treated sections in poor conditions in the PCI analysis as shown in Figure 36. In addition, there were no thick treated sections in poor or fair conditions in the ALCR analysis as shown in Figure 37.

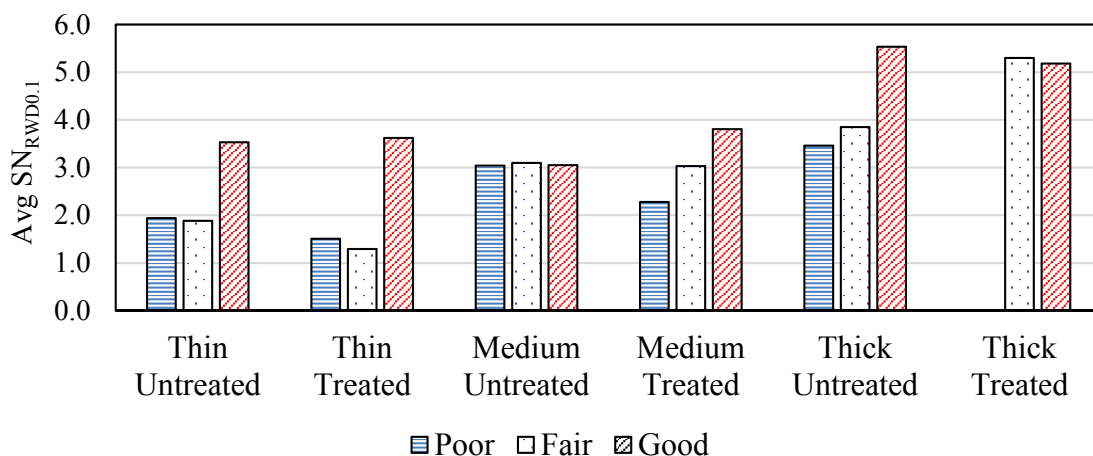


Figure 36
Average $SN_{RWD0.1}$ values for each PCI category¹

¹ no thick-treated sections in the poor category.

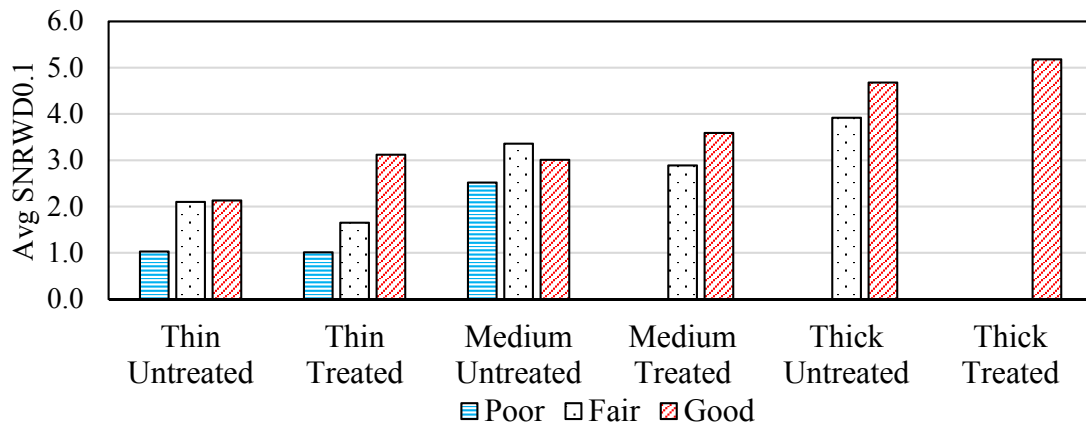


Figure 37
Average $SN_{RWD0.1}$ values for each ALCR category¹

¹ No medium-treated, thick-untreated, and thick-treated sections in the poor category and no thick-treated sections in the fair category.

ANOVA. An Analysis of Variance was conducted on the aforementioned road categories to assess the effect of each of the pavement performance indicators (RNDM, ALCR, PTCH, RUFF, RUT, and PCI) on the $SN_{RWD0.1}$. As shown in Table 24, the ANOVA analysis indicated that in three out of the six categories, the $SN_{RWD0.1}$ had significant correlation with the PCI, while in the other three categories, it was not correlated to the PCI. Therefore, one may assume that considering a structurally-based index such as $SN_{RWD0.1}$ would allow for the identification of additional road segments that are in need of repair and/or maintenance and that are not currently identified by the functional indices. This assumption was further investigated by analyzing surveyed road segments and the extracted cores from these sections.

Table 24
 $SN_{RWD0.1}$ results of the ANOVA analysis

Category Indices	No of points	Pr > t					
		RNDM	ALCR	PTCH	RUFF	RUT	PCI
Thin (untreated)	2640	0.7272	0.0454	0.0673	0.0749	0.0289	0.0318
Thin (treated)	1860	0.5913	0.5603	0.0557	0.3088	0.5214	0.1172
Medium (untreated)	3750	0.4504	0.9082	0.7949	0.2556	0.3758	0.5168
Medium (treated)	3750	0.1964	0.0660	0.0084	0.0057	0.0563	0.0131
Thick (untreated)	3490	0.0151	0.3883	0.0254	0.0050	0.0253	0.0349
Thick (treated)	1710	0.2001	0.6144	0.2955	0.4027	0.1841	0.2489

Define $SN_{RWD0.1}$ Thresholds

In order to identify structurally deficient sections for different pavement layers' thicknesses, the original (design) SN was calculated for each road segment using equation (27). Road segments that exhibited a drop of 50% or more from the design SN were considered structurally-deficient and were selected for more detailed analysis.

$$SN = a_1 * D_1 + a_2 * m_2 * D_2 + a_3 * m_3 * D_3 \quad (27)$$

where,

a_1 , a_2 , and a_3 = structural layer coefficients for the asphalt layer, base layer, and subbase layer, respectively as defined by the design office in DOTD;

D_1 , D_2 , and D_3 = layer thicknesses (in.) for the asphalt layer, the base layer, and the subbase layer, respectively; and

m_2 and m_3 = drainage coefficients for the base layer and the subbase layer, respectively.

The a_1 value was set to be 0.42, the a_2 values were set to be 0.14 for treated base and 0.07 for untreated base. The a_3 values were set to be 0.11 for cement-treated subbase, and 0.04 for untreated subbase. These values are consistent with DOTD pavement design procedure. The m_2 and m_3 coefficients were considered to be equal to 1.0 in all cases.

Analysis of Structurally Deficient Sections

Twenty-three sections were observed to have a drop of 50% or more from the design SN (i.e., $SN_{RWD0.1} \leq 50\%$ of the design SN) and were selected for a comprehensive core examination. In the following, one road segment from each category of the predefined six categories is presented; a summarized analysis is then presented for all road sections.

Control Section 333-01 (LA 582). This road section is located in West Carroll Parish and was constructed in 1982; it has an AADT of 450. The section had a length of 5.8 miles and the pavement structure consisted of four AC layers with a total thickness of 7 in. and a 12 in. treated sandy clay base layer on top of a clay subgrade. A chip seal maintenance was conducted in 2005. At the location of the core, the PCI was 87 and the average PCI along the section was 91.4. At the location of the core, $SN_{RWD0.1}$ was 1.64 and the average $SN_{RWD0.1}$ along the section was 1.48. Given a reduction of 70% in structural capacity, this section was considered to be structurally-deficient. Upon examination of the core, stripping in the AC layer was detected in the two bottom AC layers; see Figure 38(a). While this section was categorized by the PCI as in very good conditions, this road is structurally deficient as identified by the SN calculated from RWD.

Control Section 818-08 (LA 881). This road section is located in East Carroll Parish and was constructed in 1981 with an AADT of 340. The section had a length of 5.7 miles, and the pavement structure consisted of 6.75 in. AC layer and 11 in. crushed gravel with sand base layer on top of a clay subgrade. Two cores were extracted at two different locations. At the first location, the PCI was 68 and the $SN_{RWD0.1}$ was 1.9, and at the second location, the PCI was 74.5 and the $SN_{RWD0.1}$ was 1.8. The average PCI for the entire section was 61.4 and the average $SN_{RWD0.1}$ was 1.88. Given a reduction of 58% in structural capacity, this section was considered to be structurally-deficient. Upon examination of the core, severe stripping in the AC layer was detected as only 2 in. out of 6 in. were recovered, see Figure 38(b). This road was structurally and functionally-deficient as identified by the SN calculated from RWD and the PCI.

Control Section 834-12 (LA 134). This road section is located in Morehouse Parish and has an AADT of 400. The section had a length of 9.6 miles and the pavement structure consisted of 5 in. of AC and a 12 in. treated granular base layer on top of a clay subgrade. A chip-seal was applied in 2007 and was the last treatment applied on the section. At the location of the core, the PCI was 94 and the average PCI along the section was 91.6. At the location of the core, $SN_{RWD0.1}$ was 1.1 and the average $SN_{RWD0.1}$ along the section was 2.2. Given a reduction of 52% in structural capacity, this section was considered to be structurally-deficient. Upon examination of the core, severe stripping in the AC layer was detected as only 1.2 in. was recovered out of the 5 in. layer, see Figure 38(c). While this section was categorized by the PCI as in very good conditions, this road is structurally-deficient as identified by the SN calculated from RWD.

Control Section 164-02 (LA 577). This road section is located in Madison Parish and was constructed in 1985 with an AADT of 290. The section had a length of 15.6 miles and the pavement structure consisted of two AC layers with a total thickness of 5 in. and a 14 in. treated granular base layer on top of a clay subgrade. An overlay was applied in 2002. At the location of the core, the PCI was 72 and the average PCI along the section was 71. At the location of the core, the $SN_{RWD0.1}$ was 1.84 and the average $SN_{RWD0.1}$ along the section was 1.86. Given a reduction of 53% in structural capacity, this section was considered to be structurally-deficient. Upon examination of the core, severe stripping in the AC layer and failure in the base layer were detected; see Figure 38(d). While this section was categorized by the PCI as in a fair condition, this road is structurally-deficient as identified by the SN calculated from RWD.

Control Section 831-04 (LA 822). This road section is located in Lincoln Parish and was constructed in 1959 with an AADT of 144. The section had a length of 6.6 miles and the pavement structure consisted of two AC layers with a total thickness of 2 in. and a 14 in. granular base layer on top of a sand subgrade. At the location of the core, the PCI was 51 and the average PCI along the section was 60. At the location of the core, the $SN_{RWD0.1}$ was 0.63 and the average $SN_{RWD0.1}$ along the section was also 0.63. Given a reduction of 78% in structural capacity, this section was considered to be structurally-deficient. Upon examination of the core, stripping in the AC layer was detected, see Figure 38(e). This road is structurally and functionally-deficient as identified by the SN calculated from RWD and the PCI.

Control Section 308-04 (LA 507). This road section is located in Lincoln Parish and with an AADT of 1,200. The section had a length of 7.8 mi. and the pavement structure consisted of 3 in. AC and a 9 in. treated granular base layer on top of a sandy clay subgrade. A chip seal was applied in 2006. At the location of the core, the PCI was 89 and the average PCI along the section was 77. At the location of the core, $SN_{RWD0.1}$ was 1.55 and the average $SN_{RWD0.1}$ along the section was 1.56. Given a reduction of 63% in structural capacity, this section was considered to be structurally-deficient. Upon examination of the core, stripping in the AC layer and debonding between the asphalt layer and the base layer were detected; see Figure 38(f). While this section was categorized by the PCI as in a fair condition, this road is structurally-deficient as identified by the SN calculated from RWD



(a) Route LA 582



(b) Route LA 881





(c) Route LA 134



(d) Route LA 577



(e) Route LA 822



(f) Route LA 507



Figure 38
Cores samples and its locations for structural deficient sections

Summary of the Core Analysis

A total of 23 road sections were found to have more than 50% loss in structural capacity. As shown in Figure 39(a), AC stripping was the most common distress in the sections with a noticeable drop in SN ($SN_{RWD0.1} \leq 50\%$ of the design SN). As shown in Figure 39(b), only 26% of those sections were in the “Poor” category according to the PCI indicating that considering a structural-based index would allow identifying these sections as structurally-deficient. Currently, structurally-deficient sections that are classified in the “Fair” or “Good” categories by the PCI are not identified as in need of maintenance and/or rehabilitation.

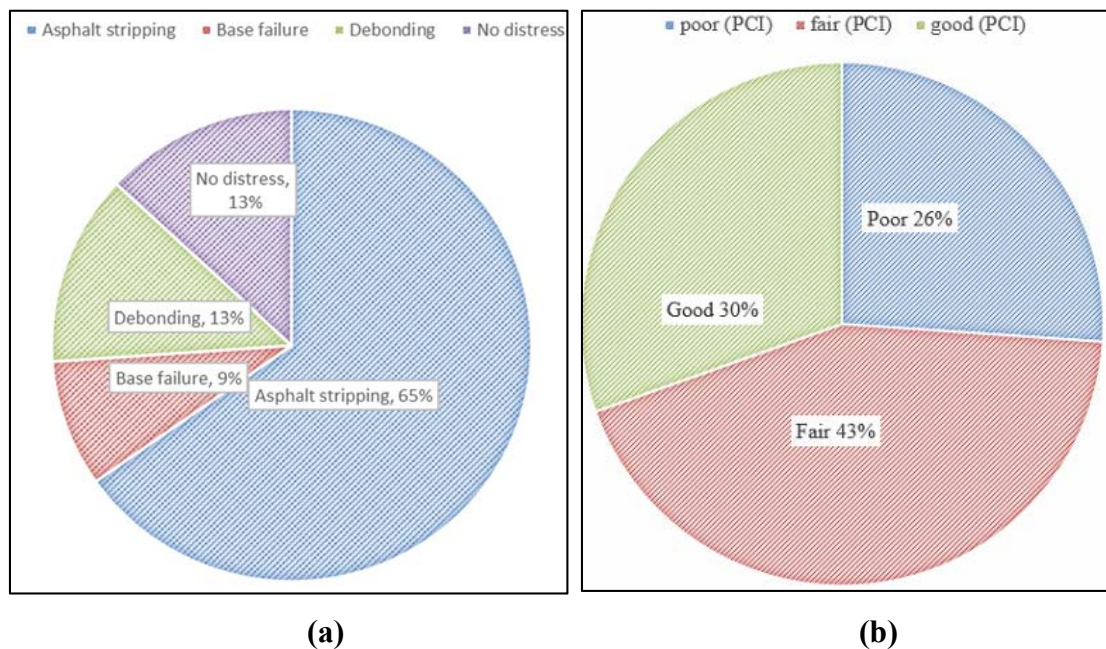


Figure 39
(a) Cores observations summary (b) distribution according to PCI

Develop a Structural Index Based on Backcalculated Moduli

The objective of this task was to develop a structural condition index, known as the Structural Health Index (SHI), on a scale from zero to 100 that describes the structural integrity of in-service pavements based on the backcalculated layer moduli as predicted from FWD testing. To achieve this objective, FWD-collected data were used in a backcalculation process; the backcalculation software, ELMOD 6, was used based on the deflection basin method. The backcalculated moduli were then correlated and categorized statistically to establish a structural index that ranges from zero to 100 in which 100 describes perfect structural conditions of the pavement structure. The developed index may be incorporated into Louisiana PMS to describe pavement structural conditions based on FWD measurements and to guide in the selection of appropriate treatment strategies.

FWD Testing

Fifty-two in-service pavement sections with a total length of approximately 320 mi. located in District 05 of Louisiana were tested [18]. Nondestructive FWD deflection testing was conducted to measure the structural capacity of in-service pavements and to backcalculate the elastic moduli of the pavement layers and subgrade. Deflection testing was performed in

accordance with ASTM D 4694, “Standard Test Method for Deflections with a Falling Weight-Type Impulse Load Device” and D 4695, “Standard Guide for General Deflection Measurements.” The FWD device was configured to have 9-sensor-array with sensors spaced at 0, 8.0, 12.0, 18.0, 24.0, 36.0, 48.0, 60.0, and 72.0 in. from the center of the load plate [35]. FWD testing was conducted at an interval of 0.1 mi. in the right wheel path and was not conducted on top of the cracked areas resulting in 1,107 test locations. Three load levels of 9,000, 12,000, and 15,000 lbs. were used in the FWD deflection-testing program. Pavement temperature was recorded in conjunction with each test.

Backcalculation Analysis

The first step toward developing a pavement structural index was to conduct the backcalculation analysis using FWD data collected on the aforementioned test sections. The Dynatest software ELMOD 6 was used in this study to perform the backcalculation analysis. The ELMOD 6 program provides three methods to conduct the backcalculation of layer moduli (radius of curvature, deflection basin fit, and finite element based method). For this study, the deflection basin method was used in the backcalculation analysis. The backcalculation analysis was conducted until a RMSE of 2% or less was achieved. The BELLS2 model was used for correcting the AC moduli for temperature [36, 37]; the reference temperature was set at 25°C. This method requires the infrared (IR) surface temperature at the time of FWD measurements and the average of the previous day’s minimum and maximum air temperatures.

Fifty-two in-service road sections were analyzed to backcalculate the layer moduli. Road segments were divided into two categories: (1) untreated base sections, representing sections with regular granular base layer or with no base; and (2) sections with cement-treated base layer [38]. The results of the backcalculated layer moduli for a sample of the road segments are presented in Figures 40 and 41. As shown in Figure 40, there were five road sections that were constructed with the asphalt layer directly on top of the subgrade with no base layer in between.

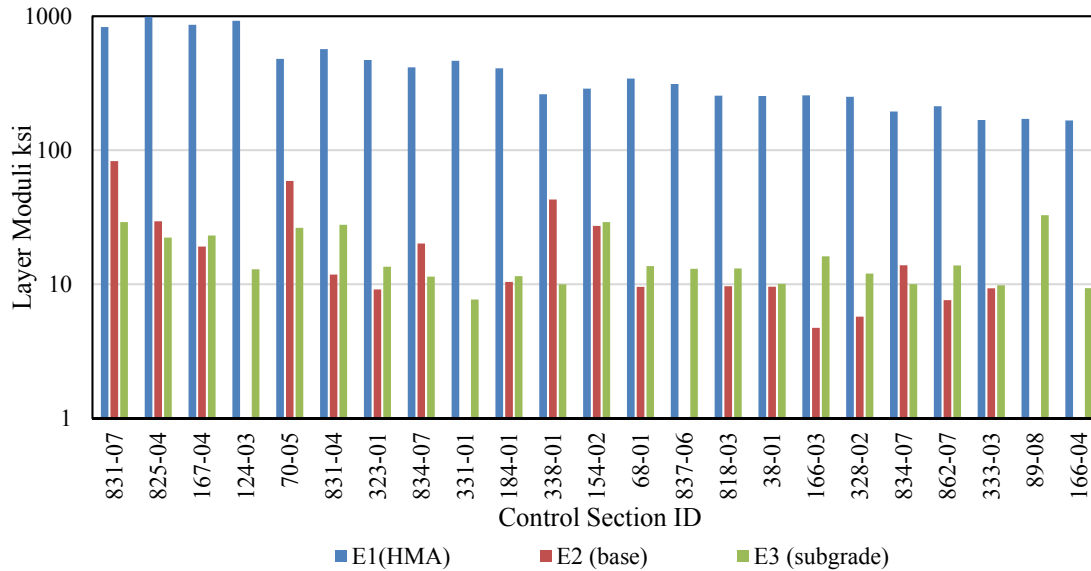


Figure 40
Backcalculated layer moduli for sections with untreated base layer¹

¹ No base layer in sections 124-03, 331-01, 837-06, 89-08, and 166-04.

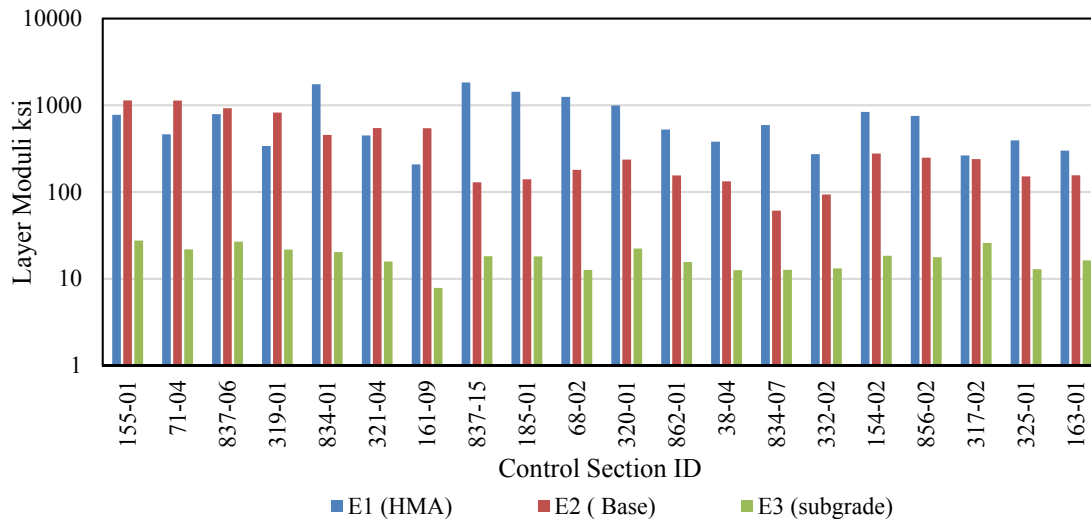


Figure 41
Backcalculated layer moduli for sections with cement-treated base layer

Loss in Structural Capacity

After conducting the backcalculation analysis, the next step in the development of the structural index was to determine the effects of layer moduli on the structural capacity of the pavement. Change in SN is an indicator of the change in the pavement structural capacity.

The loss of structural capacity was quantified as the difference between the pavement SN at the time of construction and at the time of FWD testing. To calculate the pavement SN at the time of construction, equation (27) was used.

The same equation was used to determine the SN of the pavement at the time of FWD testing; however, due to pavement deterioration from both traffic and environmental loading, the values of a_1 and a_2 would be less than the original typical design values. The following equations were used to estimate the values of a_1 and a_2 from the backcalculated layer moduli based on the AASHTO 1986 design guide [39, 40]:

$$a_1 = a + b \cdot \log(E_1) + c \cdot (\log(E_1))^2 \quad (28)$$

where,

$a = -9.904$, $b = 2.958$, $c = -0.224$, and E_1 = AC backcalculated layer modulus (ksi).

$$a_2 = 0.249 \log(E_2) - 0.977 \quad (29)$$

where,

E_2 = base layer backcalculated modulus (ksi).

Formulation of the Structural Health Index (SHI)

The Structural Health Index (SHI) was defined based on the loss in SN such that it was scaled logistically from zero to 100. A sigmodal function was selected to represent the correlation between the loss in SN % and the SHI as presented in equation (30). Constant parameters in the function were optimized such that sections with a loss in SN ≥ 50 % would have SHI values near zero, and sections with minimal or no loss in SN would have SHI values near 100 [38].

$$SHI = \frac{100}{1 + e^{0.15 (SN \text{ loss } \% - 30)}} \quad (30)$$

Based on equation (30), the correlation between the SHI and the loss in SN% for the 52 road sections is presented in Figure 42.

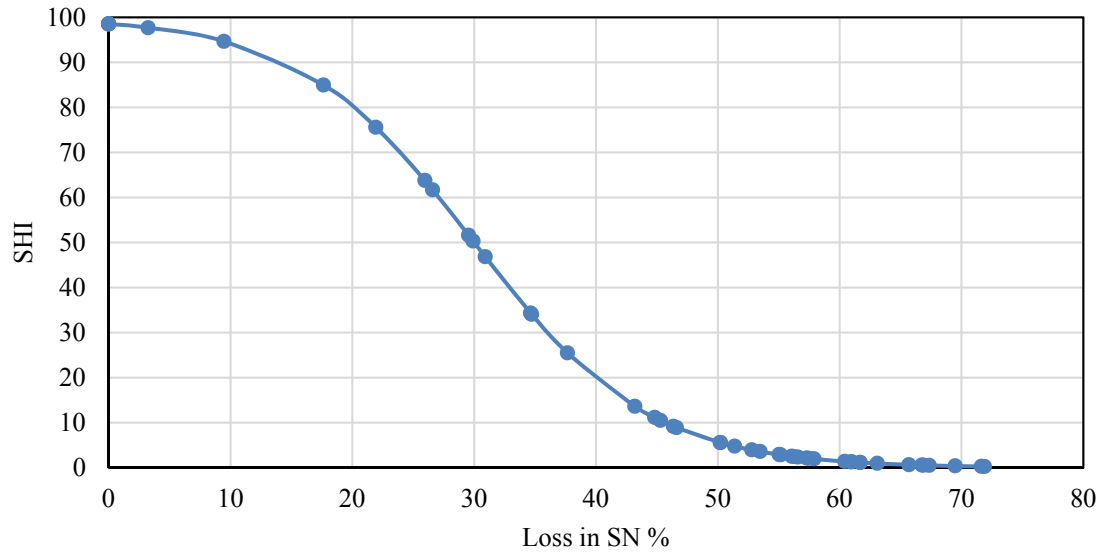


Figure 42
Relation between loss in structural number and the SHI

Evaluation and Validation of the Structural Health Index

After developing the SHI, a comprehensive evaluation of the extracted cores was conducted. The road sections were classified into two categories according to the core conditions. Sections with core samples with no visible asphalt stripping or material deterioration were categorized as “Good.” Sections with asphalt stripping and/or material deterioration were categorized as “Poor.” For the 52 road sections, 25 cores were found to be under the “Poor” category and the remaining 27 were classified under the “Good” category. The average SHI for the Poor sections was equal to 9 and the average PCI was equal to 77. The average SHI for the Good sections was equal to 60 and the average PCI was equal to 87. Figure 43 shows two examples of cores extracted from sections with low SHI values: Control Section 163-01 (route LA 133), which had an SHI of 10 and control section 834-07 (route LA 835), which had an SHI value of 6. In addition, examples of cores extracted at sections with high SHI value are shown in Figure 44 for control sections 155-01 (route LA 143) and 319-01 (route LA 155), which have an SHI value of 98.5 and 82, respectively [38].



(a) Control Section 834-07



(b) Control Section 163-01

Figure 43
Stripped core samples from low SHI sections



(a) Control Section 155-01



(b) Control Section 319-01

Figure 44
Sections with high SHI core samples

Figure 45 presents the percentage of “Poor” and “Good” sections for the different ranges of SHI. As shown in this figure, for section with SHI values greater than 70, 100% of the sections were in good conditions. In contrast, for sections with SHI values less than 20, 100% of the sections were in poor conditions. These trends support the successful description of pavement structural conditions through the SHI.

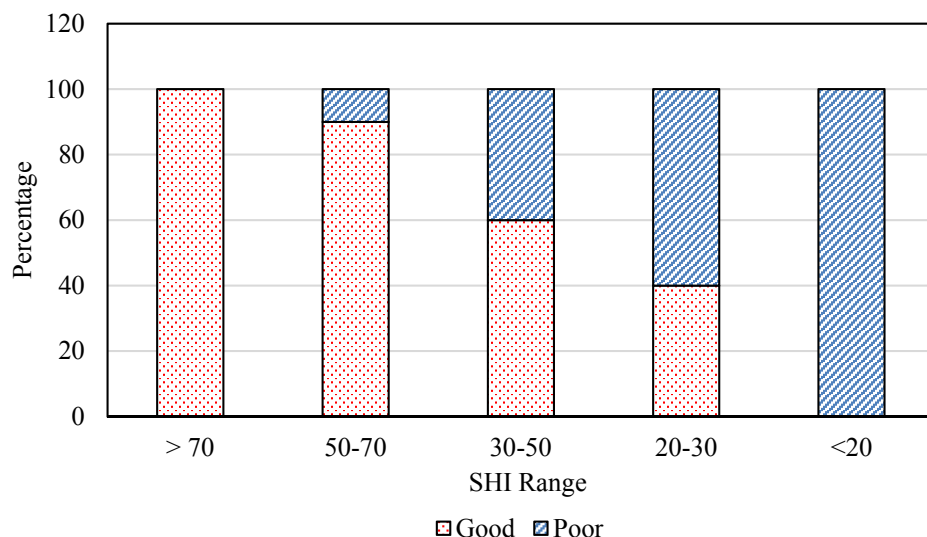


Figure 45
Relation between SHI and pavement structural condition [38]

Comparison between SHI and the Pavement Condition Index (PCI)

To ensure that the use of SHI effectively contributes to the current decision matrix used in Louisiana and adds values to the functional indices currently used by the state, a statistical t-test analysis was conducted between SHI and PCI. Results of the t-test showed that there is a significant difference between the PCI and the SHI with a P-value less than 0.001. Further, the Pearson correlation index between PCI and SHI was equal to 0.41, which indicates a poor correlation between the two indices. These results indicate the use of the SHI would provide additional performance information not currently available in the State PMS.

Compare Rates of Deteriorations for Pavement Sections

Pavements in poor structural conditions are expected to have a faster rate of deterioration than pavements in good structural conditions [8]. In this task, the research team analyzed PMS data collected in District 05 from 2005 to 2013 to determine the rate of structural and functional deteriorations for pavements that are structurally-deficient and those that are structurally-sound. Based on this analysis, the research team assessed whether the rates of deterioration are significantly different for pavements that are structurally-deficient and those that are structurally sound.

Functional Class

As traffic volume is the main factor that affects the rate of pavement deterioration, sections were classified according to their functional class. As shown in Table 25, rural major collectors, rural minor arterials, and urban minor arterials had the highest traffic volumes in the available data set. It is noted from Table 25 that only 6.9 miles of urban collectors were tested, which provided insufficient amount of data for further analysis of this functional class. Calculations were performed in this analysis at 0.1-mile intervals to match the DOTD PMS practice in averaging data and assigning decisions based on 0.1-mile interval.

Table 25
Functional class distribution

Functional Class	Total (Length miles)	Average AADT (Vehicle /day)
Rural Major Collector	449.2	1,800
Rural Minor Collector	321.5	898
Rural Local	152.2	598
Rural Minor Arterial	71.2	4,800
Urban Minor Arterial	56.3	6,400
Urban Collector	6.9	3000

Segments that received treatment during the monitoring period were removed from the analysis to avoid misleading results. Two procedures were followed in the elimination process. First, any segment that had a maintenance project recorded in the PMS database between 2005 and 2013 was removed. Second, any segment that showed an increase in one or more of the performance indices values during the analysis period was eliminated. For example, if a road had an ALCR value of 80 in year 2005 and an ALCR value of 90 in year 2007, it would be eliminated from the analysis since repair activities would have taken place on this segment.

Structural Condition Index (SCI)

To describe in-service pavement structural conditions, a new parameter termed the Structural Condition Index (SCI), was introduced. The SCI is calculated as the ratio between the in-service structural number ($SN_{RWD0.1}$) and the AASHTO SN required for a design life of 10 years (SN_{req10}) as follows:

$$SCI = \frac{SN_{RWD0.1}}{SN_{req10}} \quad (31)$$

The AASHTO 1993 design equation was used to calculate required SN for a design period of 10 years (SN_{req10}) as shown below:

$$\log(W_{18}) = Z_R S_0 + 9.36 \log_{10}(SN + 1) - 0.2 + \frac{\log\left[\frac{\Delta PSI}{4.2} - 1.5\right]}{0.4 + \frac{1094}{(SN+1)^{5.19}}} + 2.32 \log MR - 8.07 \quad (32)$$

where,

W_{18} = equivalent single axle load for the design period (ESALS);

Z_R = Standard normal deviation for selected reliability;

S_0 = Standard deviation;

ΔPSI = Design Serviceability loss;

M_R = Resilient Modulus of Subgrade (psi); and

SN = AASHTO structural number.

According to DOTD office of design, the reliability level was considered 90% ($Z_R = -1.282$), ΔPSI was considered 1.7, and the S_0 was considered 0.49. The subgrade modulus values were determined from DOTD parish resilient modulus map. Traffic ESALs were obtained from the Highway Needs File.

Define SCI Intervals

The SCI was calculated for each 0.1 mile-segment of the road sections; it was noticed to follow a normally-distributed function around a mean of 1.4 as shown in Figure 46. Based on the trends observed in this figure, initial SCI intervals were defined and are provided in Table 26.

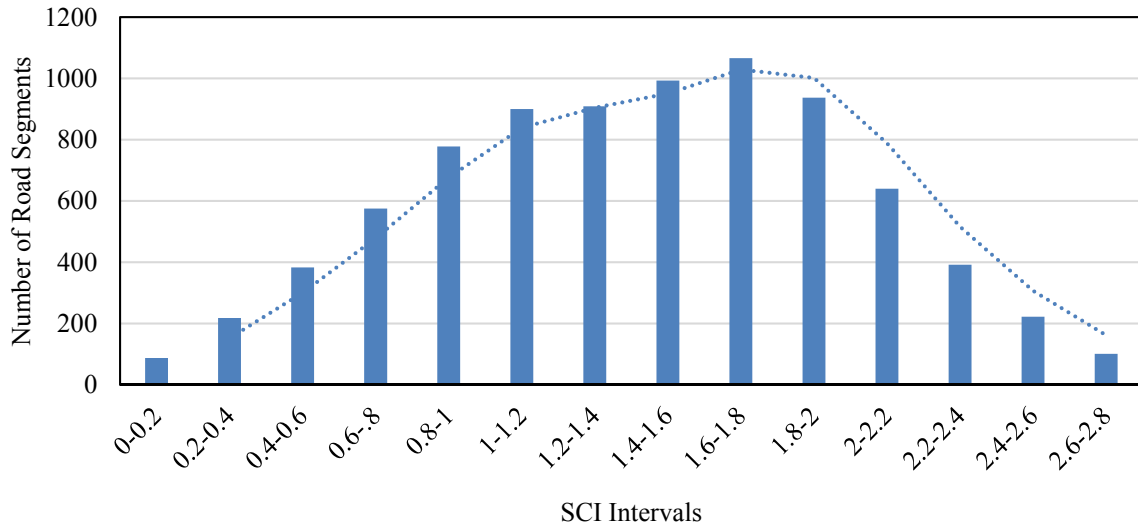


Figure 46
SCI histogram distribution

Table 26
Initial SCI intervals

SCI Range	Structural Capacity
SCI<0.6	Very low
1>SCI≥0.6	Low
1.5>SCI≥1	Low to Medium
2>SCI≥1.5	Medium
SCI≥2	high

Compare Structural Deterioration Rates

For each SCI interval, PMS data were collected for the collection cycles from 2005 to 2013. However, the number of sections that did not receive treatment for that relatively long period of time were found to be too small to definitively assess the deterioration trends. Hence, the criterion was changed to include all sections that did not received treatment from 2009 to 2013 such that all pavement sections selected had three data points. Figures 47 to 54 present the deterioration trends of the performance indices for each predefined SCI interval. By fitting these trends linearly, the slope of each line is an indicator of the deterioration rates, which are presented in Tables 27 and 28.

As shown in Tables 27 and 28, there is a correlation between the SCI category and the rate of deterioration. For example, sections in the very low and the low categories are deteriorating faster than sections in the high and the medium categories. It is worth noting that the rates of deterioration were independent of the initial values of the performance indices for the collectors, except for roughness. However, for the arterials, the rate of deterioration was affected by both the SCI value and the initial values of the performance indices.

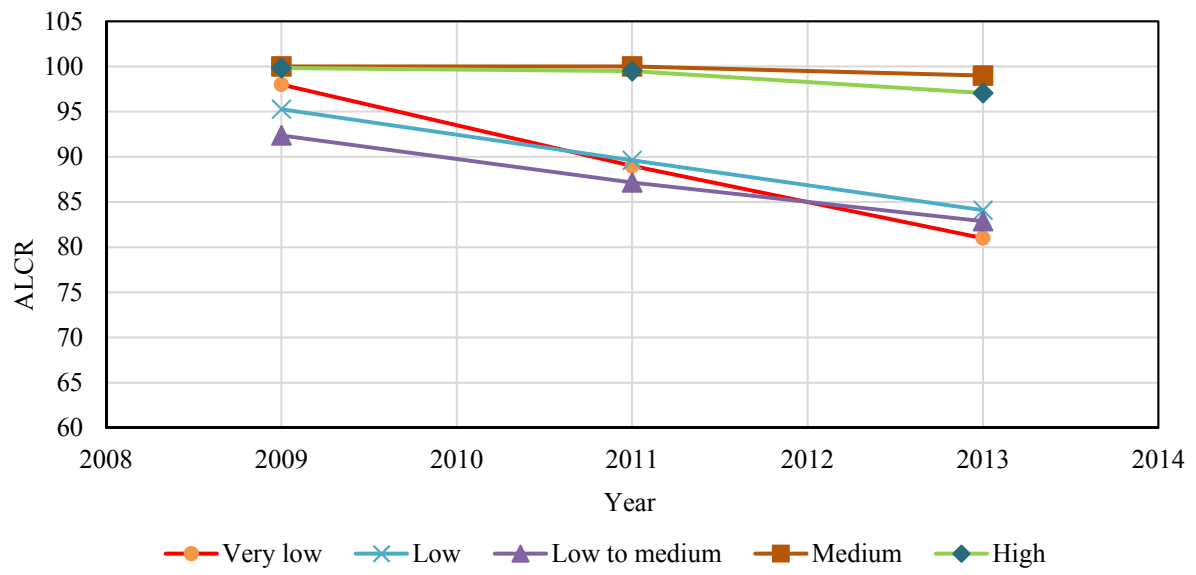


Figure 47
Alligator cracking deterioration for major collectors

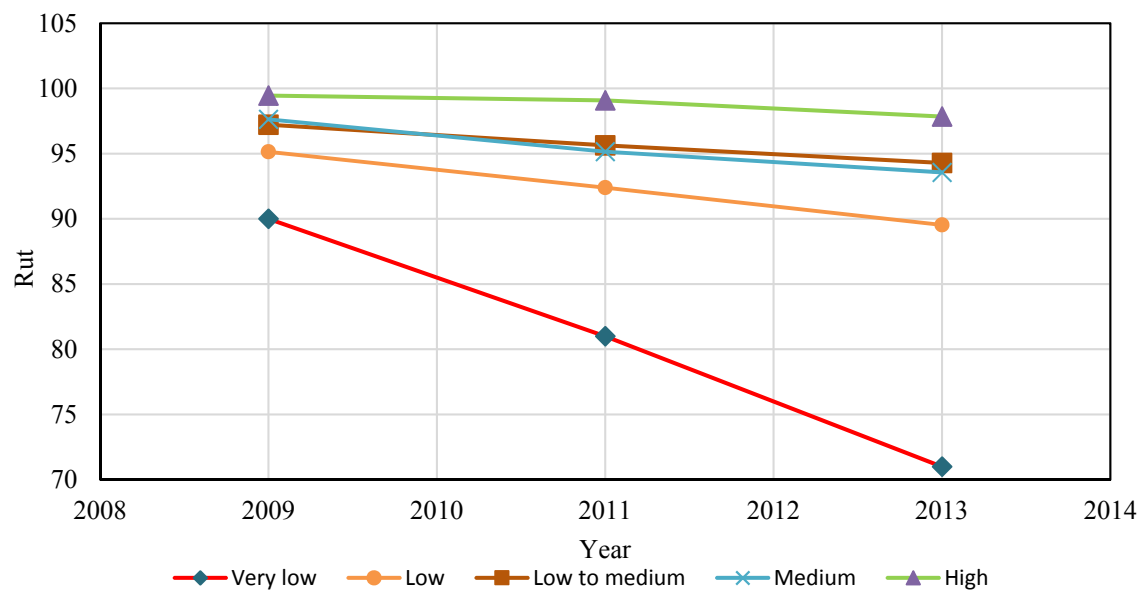


Figure 48
Rutting deterioration for major collectors

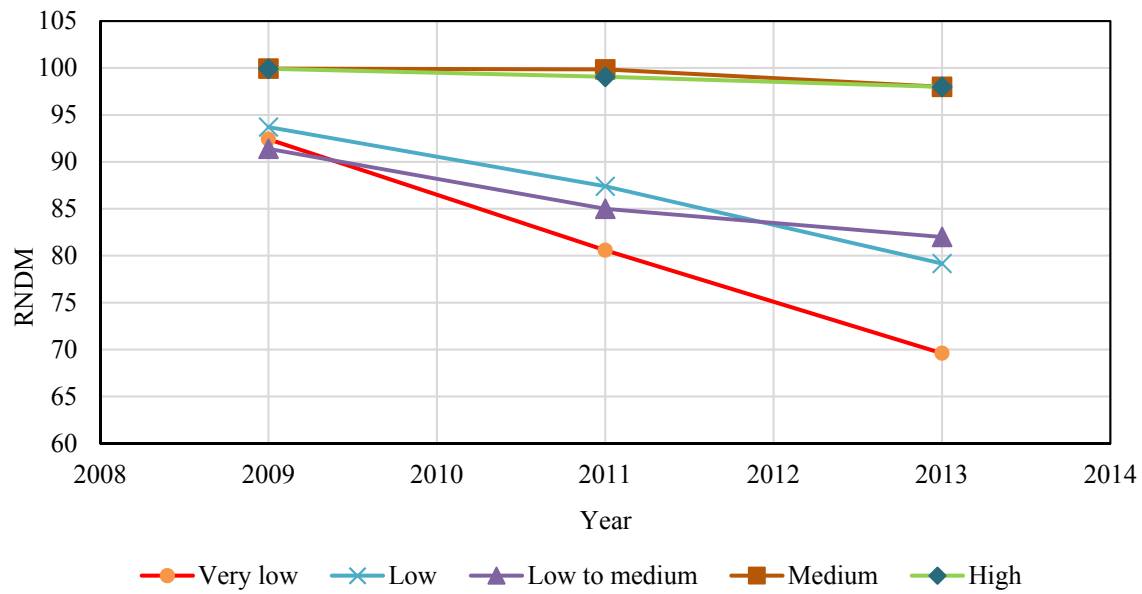


Figure 49
Random cracking deterioration for major collectors

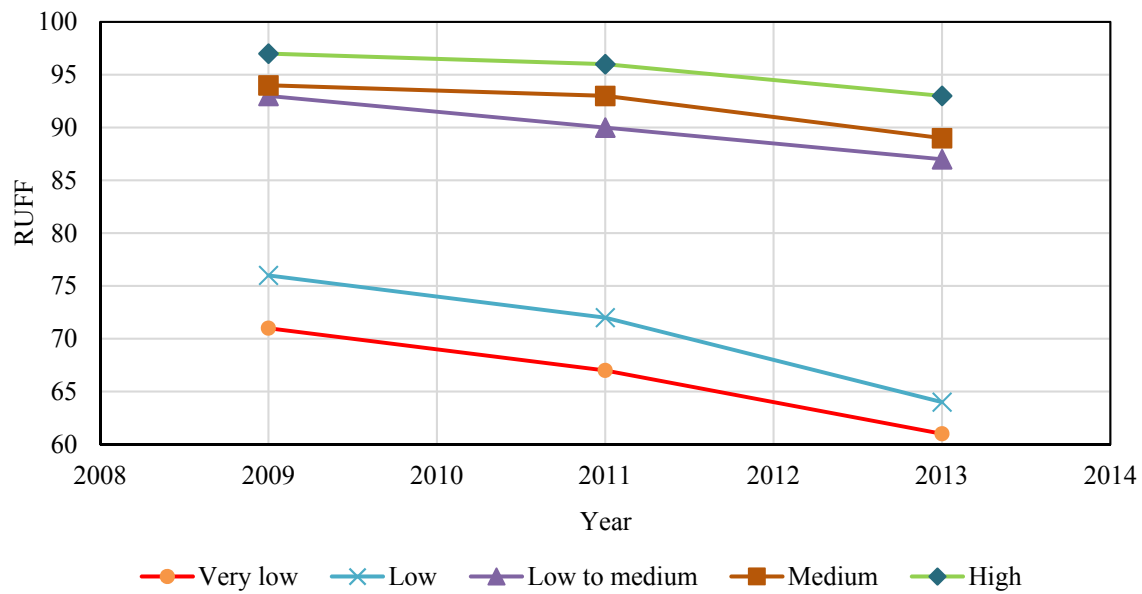


Figure 50
Roughness deterioration for major collectors

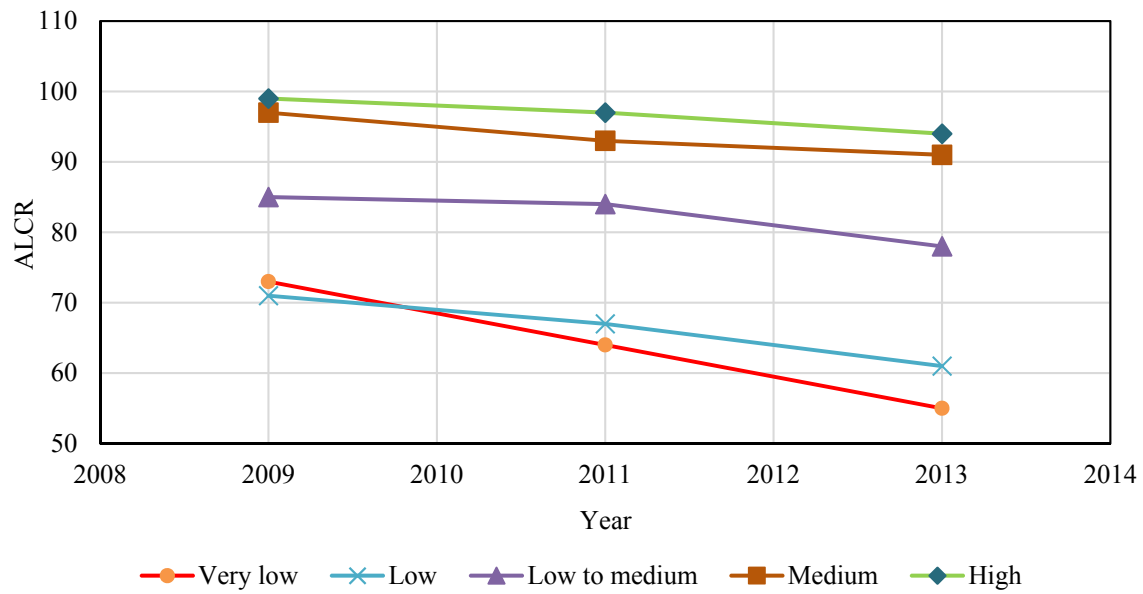


Figure 51
Alligator cracking deterioration for arterials

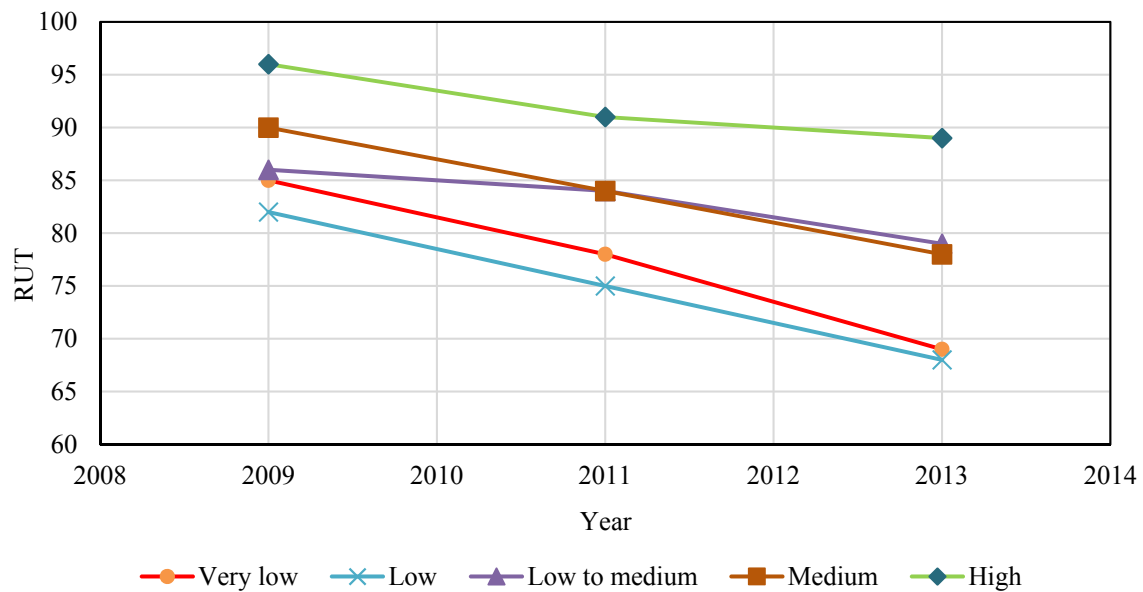


Figure 52
Rutting deterioration for arterials

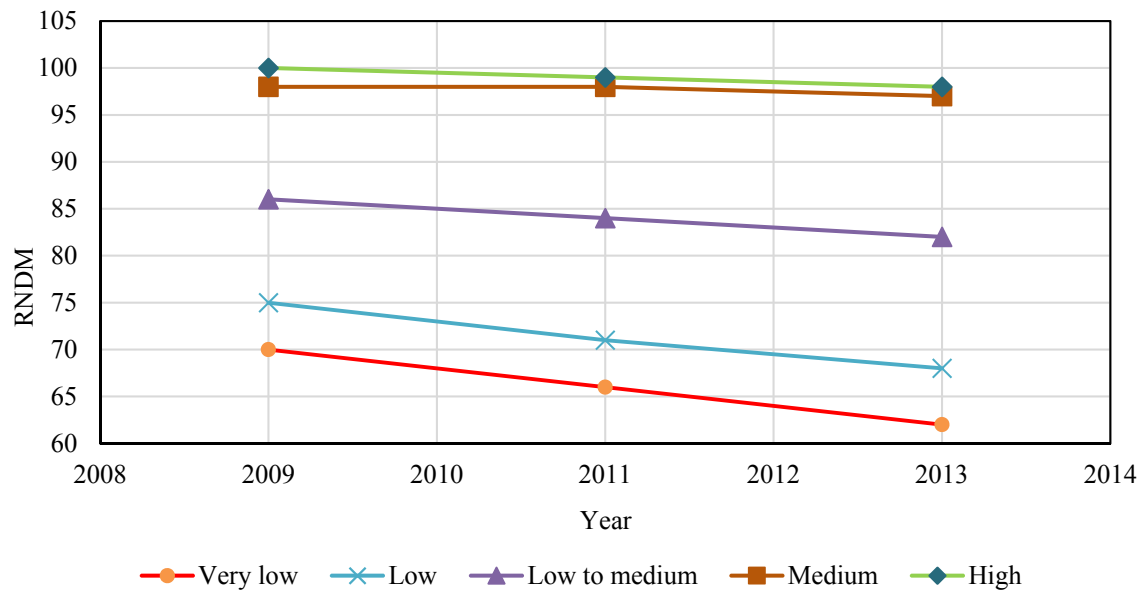


Figure 53
Random cracking deterioration for arterials

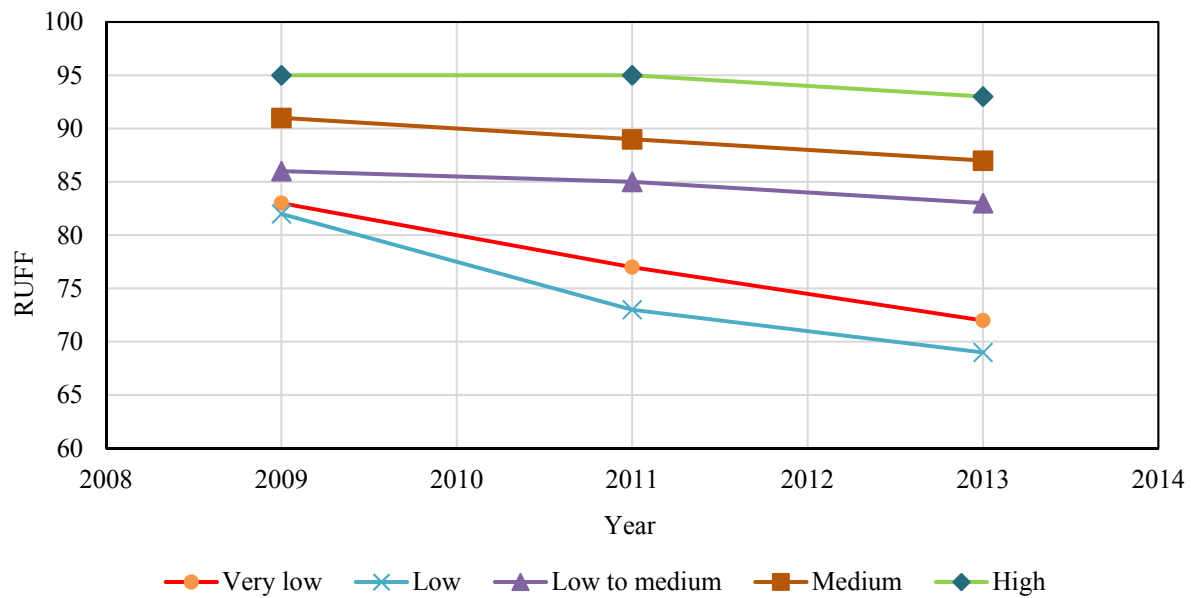


Figure 54
Roughness deterioration for arterials

Table 27
Linear fitting of deterioration rates for major collectors

Rank	ALCR Equation	RUT Equation	RNDM Equation	RUFF Equation
Very low	$y = -4.25x + 8636$	$y = -4.75x + 9632$	$y = -5.70x + 11556$	$y = -2.50x + 5093$
Low	$y = -2.79x + 5707$	$y = -1.40x + 2907$	$y = -3.63x + 7395$	$y = -3.00x + 6103$
Low - med.	$y = -2.37x + 4855$	$y = -1.01x + 2140$	$y = -2.35x + 4812$	$y = -1.50x + 3106$
Medium	$y = -0.25x + 602$	$y = -0.73x + 1569$	$y = -0.48x + 1063$	$y = -1.25x + 2605$
High	$y = -0.25x + 602$	$y = -0.40x + 903$	$y = -0.48x + 1071$	$y = -1.00x + 2106$

Table 28
Linear fitting of deterioration rates for arterials

Rank	ALCR Equation	RUT Equation	RNDM Equation	RUFF Equation
Very low	$y = -3.25x + 6598$	$y = -3.50x + 7113$	$y = -2.00x + 4088$	$y = -2.75x + 5607$
Low	$y = -2.50x + 5093$	$y = -3.50x + 7116$	$y = -1.75x + 3590$	$y = -3.25x + 6610$
Low - med.	$y = -1.75x + 3601$	$y = -1.75x + 3602$	$y = -1.00x + 2095$	$y = -0.75x + 1592$
Medium	$y = -1.50x + 3110$	$y = -3.00x + 6617$	$y = -0.25x + 600$	$y = -1.00x + 2100$
High	$y = -1.25x + 2610$	$y = -2.25x + 4616$	$y = -0.25x + 1104$	$y = -0.50x + 1099$

Overlay Design for Selected Pavement Sections

In this task, an overlay design was conducted for all sections that were included in the RWD testing program. Results of this analysis were used to assess the cost-efficiency of the RWD and to develop a methodology to incorporate structural capacity information into the PMS. Two approaches of overlay design were used, and their results were compared. First, the current approach adopted by the DOTD office of design, which does not incorporate structural capacity indicators based on NDT measurements. Second, a new approach was developed in which RWD measurements are incorporated into the design procedure.

Current Overlay Design Procedure

According to the DOTD office of design, the current overlay design procedure is presented. First, if the PMS maintenance decision for a road segment is “thin overlay,” the overlay is considered as a functional overlay with a thickness of 2 in., and no design is required. Second, if the PMS decision is “medium overlay” or “structural overlay,” the overlay thickness is estimated from the following equation:

$$\text{Overlay thickness} = \frac{SN_{req} - SN_{eff}}{a_1} \quad (33)$$

where,

SN_{req} = required structural number for a design life of 10 years;

SN_{eff} = effective structural number assuming 50% loss in structural capacity and 2 in. milling, as shown in equation (34); and

a_1 = asphalt layer structural coefficient (assumed 0.44).

$$SN_{eff} = \frac{a_1 * D_1 + a_2 * m_2 * D_2 + a_3 * m_3 * D_3}{2} - 2 * a_1 \quad (34)$$

The aforementioned assumption of 50% loss in structural capacity may lead to two types of error as shown in Figure 55. First, if the actual loss in structural capacity is less than 50%, the designed overlay using current design practice would be overestimated (Type I error). Second, if the actual loss in structural capacity is more than 50%, the designed overlay using the current practice would be underestimated (Type II error). Both types of error will lead to loss of funds. The proposed design approach is aimed at avoiding both Type I and Type II errors by taking into consideration the in-service pavement structural capacity.

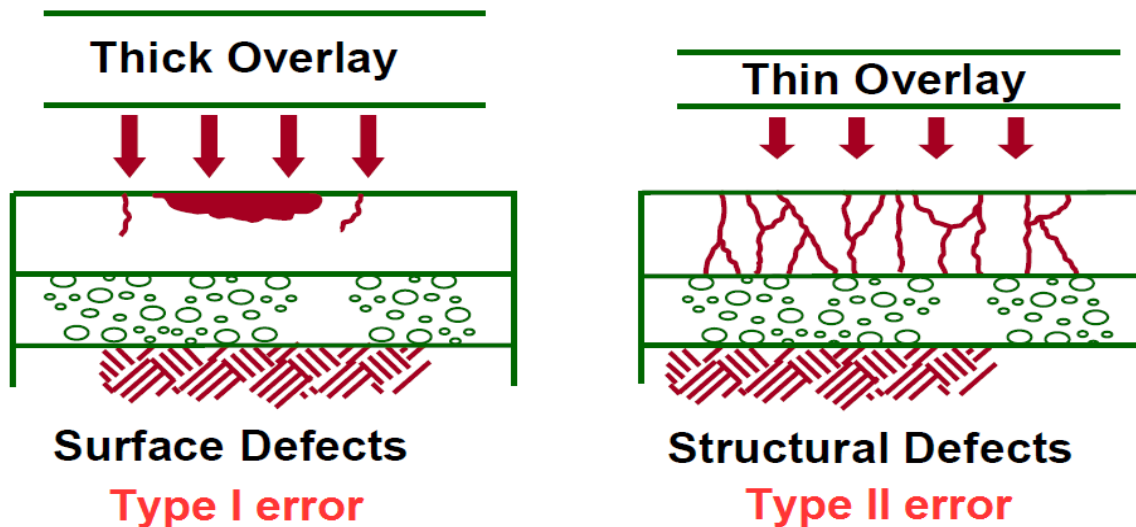


Figure 55
Type of errors in the current design procedure

Improved Overlay Design Procedure

The research team developed a procedure to incorporate RWD measurements in the overlay design. Such a procedure would allow taking into consideration in-service pavement structural conditions instead of assuming 50% loss in structural capacity. Furthermore, in the proposed procedure, road segments with PMS decisions of “thin overlay,” “medium overlay,” and “structural overlay” are all considered for overlay design. Figure 56 shows a comparison between the two overlay design procedures. Equation (32) is used to calculate SN_{req} , and equation (33) is used for calculating the overlay thickness; however, $SN_{RWD0.1}$ is used to estimate the effective structural number, which is termed SN_{RWDeff} .

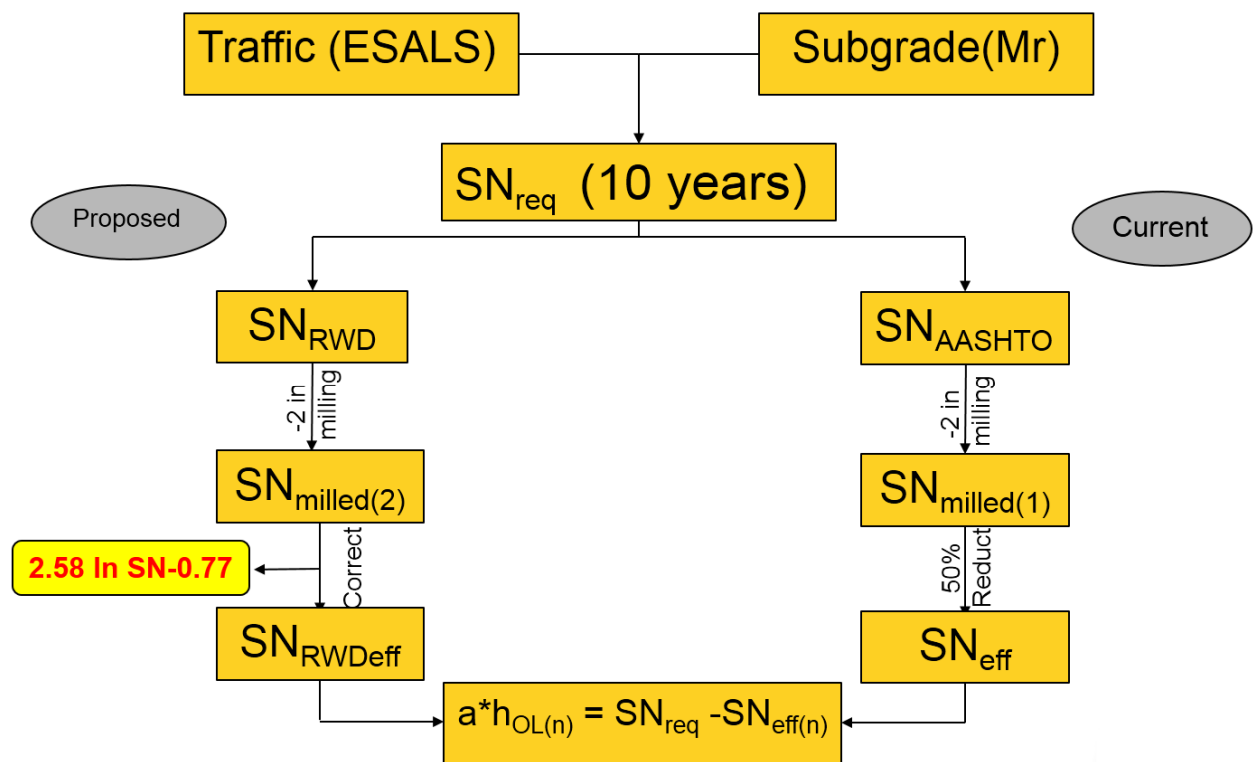


Figure 56
Current and proposed overlay design procedures

According to LTRC study FHWA/LA.08/454 conducted by Wu and Gaspard, the SN calculated from FWD measurements (SN_{FWD}) needs to be calibrated for Louisiana’s conditions when used for overlay design purposes [41, 42]. The researchers developed a model to estimate the SN_{eff} from the SN_{FWD} as shown in equation (35). Since the model proposed for $SN_{RWD0.1}$ was developed and validated based on SN_{FWD} , SN_{RWD} was subjected to the same calibration procedure as shown in equation (36):

$$SN_{eff} = 2.58 \ln (SN_{FWD}) - 0.77 \quad (35)$$

$$SN_{RWD_{eff}} = 2.58 \ln (SN_{RWD0.1}) - 0.77 \quad (36)$$

Comparing Results of Both Procedures

Overlay design was conducted for all road segments tested with RWD and with PMS decisions of thin, medium, or thick overlay using the current DOTD and the proposed design procedures. It is noted that a minimum overlay thickness of 2 in. was assigned for the aforementioned road segments. Findings of this analysis are shown in Figure 57; current design practice generally resulted in thicker overlay thicknesses (conservative design) especially in the urban principal arterial category. Comparison of the two design approaches is further evaluated in the following sections.

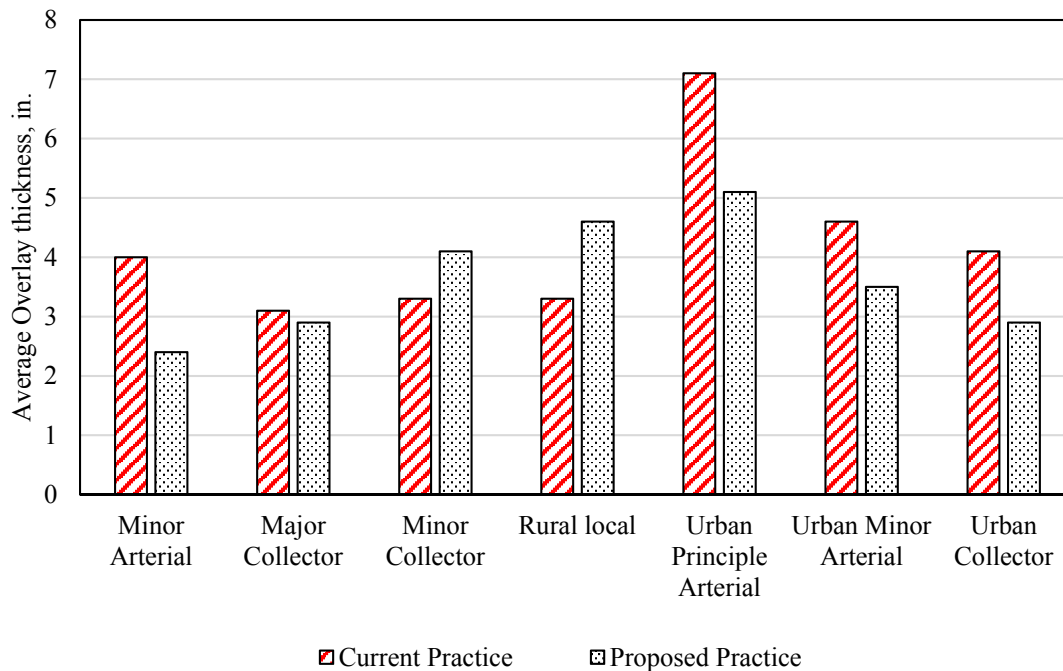


Figure 57
Average overlay thicknesses using current and proposed design procedures

Validation of the proposed approach

The objective of this analysis was to check the reliability and the effectiveness of the proposed overlay design approach. Sections with noteworthy differences in the overlay thickness designed using the proposed approach in comparison to the current approach and

that had available backcalculated layer moduli were considered for further analysis. A multi-layer elastic software (KenPave) was used to calculate the critical pavement responses (tensile strain at the bottom of the AC layer and vertical strain on top of the subgrade) for the two design approaches, i.e., current and proposed overlay design procedures. Pavement responses were calculated for a load application of 9,000 lbs. on a dual tire assembly with a radius of 5.9 in. The numbers of cycles for fatigue and subgrade rutting failure were estimated according to the Asphalt Institute (AI) methodology using equations (9) and (10).

The number of cycles for fatigue failure and subgrade rutting failure (N_d and N_f) calculated from equations (9) and (10) was compared to the actual traffic (ESALs) to determine the design life. Table 29 presents the results of the analysis. As shown in Table 29, the modified design procedure was more precise in satisfying the required 10-year design life for the different pavement sections.

Table 29
Comparison between overlay design procedures using a mechanistic-empirical approach

Section#	Current overlay design procedure				Proposed overlay design procedure			
	Overlay thickness	ϵ_t	ϵ_c	Design life (years)	Overlay thickness	ϵ_t	ϵ_c	Design life (years)
837-15	4.0	6.6E-6	1.7E-4	16	2.0	4.8E-6	2.1E-6	12
831-07	4.5	2.2E-4	2.5E-4	14	2.5	3.1E-4	3.5E-4	10
167-04	4.5	2.7E-4	1.1E-3	4	7.5	8.4E-5	7.6E-4	13
68-02	4.0	3.3E-5	7.2E-4	7	5.0	2.3E-5	6.1E-4	12

Figure 58 presents the correlations between pavement SN calculated based on FWD measurements and both the $SN_{RWD0.1}$ and the 50% loss of the original structural capacity assumption. It is clear from these results that $SN_{RWD0.1}$ correlates much better with the SN calculated based on FWD than the 50% loss of SN assumption.

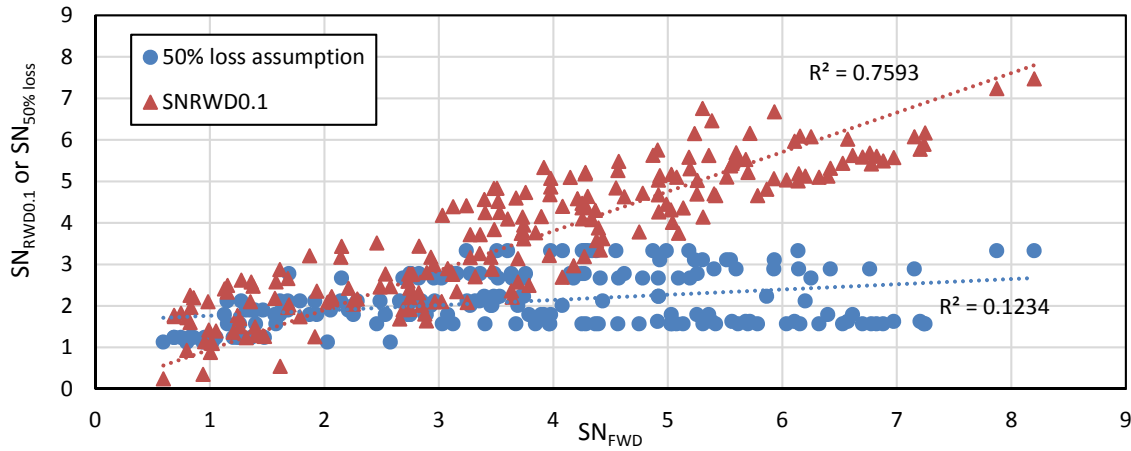


Figure 58
Comparison of $SN_{RWD0.1}$ and 50% structural capacity loss assumption to SN_{FWD}

Investigate the Feasibility of Determining the Subgrade Modulus from RWD Data

In this task, the development of a model that utilizes RWD deflection measurements to predict the subgrade resilient modulus for flexible pavements at the network-level is described. For model development, RWD and FWD measurements obtained from the testing program conducted in Louisiana were used to train an ANN-based model. After the learning process, the ANN model was validated using RWD and FWD data obtained from the testing program independently conducted at the MnROAD test facility in Minnesota.

To develop the proposed ANN model, the FWD sensor D₇ (60 in. from the center of the plate) measurements were used in equation (3) to calculate the subgrade resilient modulus for the tested pavement sections, Step 1. No temperature correction was applied for the D₇ measurements as they are only affected by the subgrade properties [30.] Second, statistical correlations were investigated between RWD measurements and the subgrade resilient modulus calculated from Step 1. The RWD measurements were corrected to a reference temperature of 20°C using BELLS equation and the AASHTO 1993 procedure [18, 43]. Finally, the RWD measurements and the subgrade resilient modulus values calculated from FWD were utilized to develop and validate the ANN model.

Correlation between the RWD and the Subgrade Resilient Modulus

As described earlier, the RWD reports the average deflections on 0.1-mile intervals along with the standard deviations. Therefore, four readings can be obtained from the device; the average deflection at the rear axle (D₀) and its standard deviation (σ_{D0}), and the average

deflection at 18 in. (D_1) and its standard deviation (σ_{D1}). The statistical correlations between these four parameters and the subgrade resilient modulus were investigated for the measurements obtained from the Louisiana testing program.

An analysis of variance (ANOVA) was conducted between the subgrade resilient modulus and the four RWD measurements using the SAS 9.4 software. Table 30 summarizes the results of the statistical analyses. As shown in this table, Parameters D_0 , σ_{D0} , and D_1 were found to be significantly correlated to the subgrade resilient modulus. On the other hand, σ_{D1} was not statistically correlated to the subgrade resilient modulus. The coefficient of determination (R^2) between each parameter and the subgrade resilient modulus was also calculated. Figure 59 presents the correlations between the D_1 and D_0 with the M_r . As shown in Figure 59, there is a downward trend between the decrease in subgrade resilient modulus and the measured RWD deflections; yet, considering only one deflection measurement is not sufficient to accurately predict the subgrade resilient modulus as evident by the low R^2 shown in this figure.

Based on these findings, the three RWD measurements (D_0 , σ_{D0} , and D_1) were considered in the ANN model for prediction of the subgrade resilient modulus. As previously noted, the RWD prototype used in MnROAD measured the secondary deflection (D_1) at 15 in. instead of 18 in. To develop a model that is compatible with measurements of both prototypes, “ $D1/r$ ” was used in the model instead of D_1 ; where, r is the radial distance from the RWD rear axle. A multi-linear regression model was developed using SAS 9.4 and resulted in an R^2 of 0.6 and an RMSE of 15%; therefore, ANN was utilized in the present study to develop a model with better accuracy than the multi-linear regression model. Comparing linear regression with ANN is out of the scope of this study as recent studies concluded that comparison between linear regression models and ANN-based models is not adequate [44].

Table 30
Correlation between RWD measurements and the FWD subgrade resilient modulus

Parameter	P-Value	R^2
D_0	<0.0001	0.2950
σ_{D0}	<0.0001	0.4023
D_1	<0.0005	0.1933
σ_{D1}	0.9087	0.1679

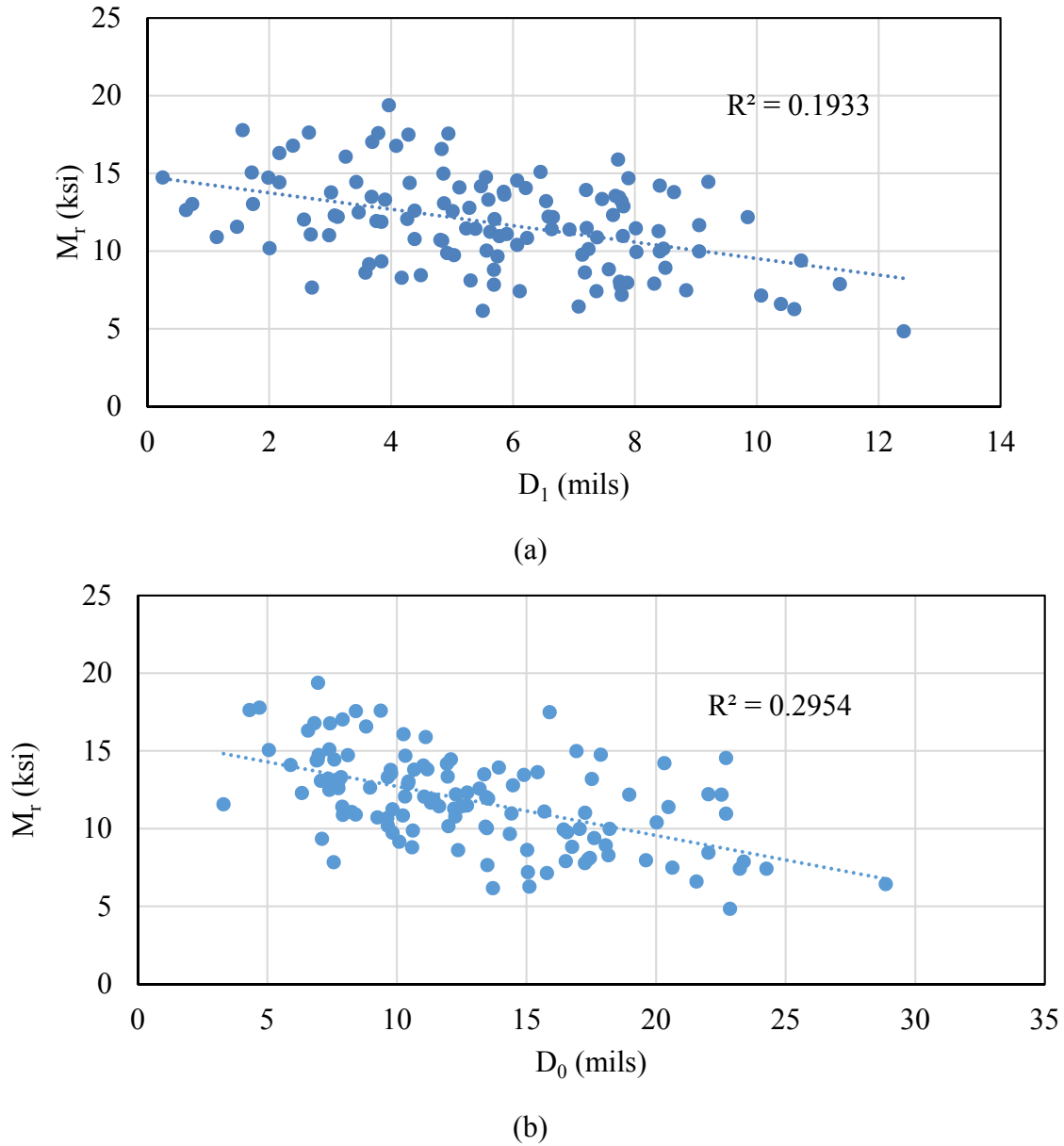


Figure 59
Correlation between the subgrade resilient modulus and (a) D_1 and (b) D_0

ANN-Model Development

A multilayered feed-forward ANN using a back-propagation error algorithm was developed with a tan-sigmoid transfer function and a linear activation function. The simplest network topology that produces acceptable prediction accuracy was selected to avoid overfitting of the model [31, 32]. The network topology consisted of three layers of neurons and two layers of weights; an input layer (i) of 3 neurons; a hidden layer (j) of 2 neurons; a target output layer (k) of 1 neuron, layer of weights between neuron layers i and j (ij), and layer of

weights between neuron layers j and k (jk). Weights in layers ij and jk were named “ W ” and “ W' ,” respectively. In addition, biases values were added to the sums calculated at each neuron (except layer i). Biases in layers j and k were named “ b ” and “ B ,” respectively [32]. To train the network, such that the proper weights and biases are calculated, the input layer was fed with the three selected RWD measurements (D_0 , σ_{D0} , and D_1), and the target layer was fed with the subgrade resilient modulus values (M_r). The network structure is shown in Figure 60.

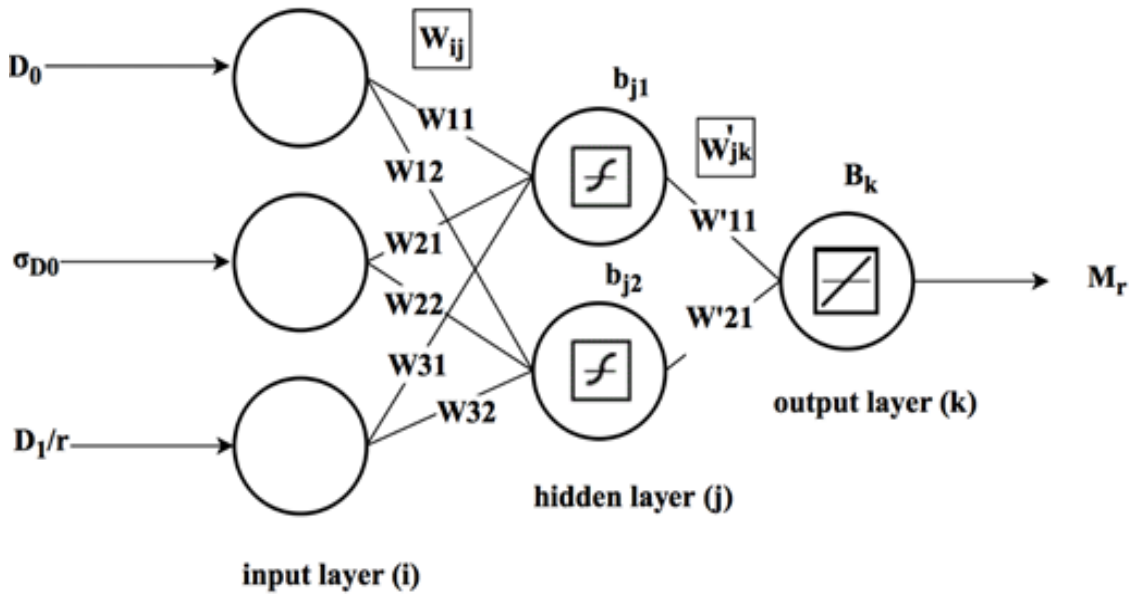


Figure 60
Structure of the ANN model

Data from the Louisiana testing program were utilized in the model development phase (124 road segments). The data were divided into 70% for training, 15% for validation, and 15% for testing. To avoid overfitting and to increase the network generalization ability, training was halted when the validation set error stopped decreasing, as shown in Figure 61. Since the testing data set had no effect on the training phase, it was used to provide an independent measure of the network performance.

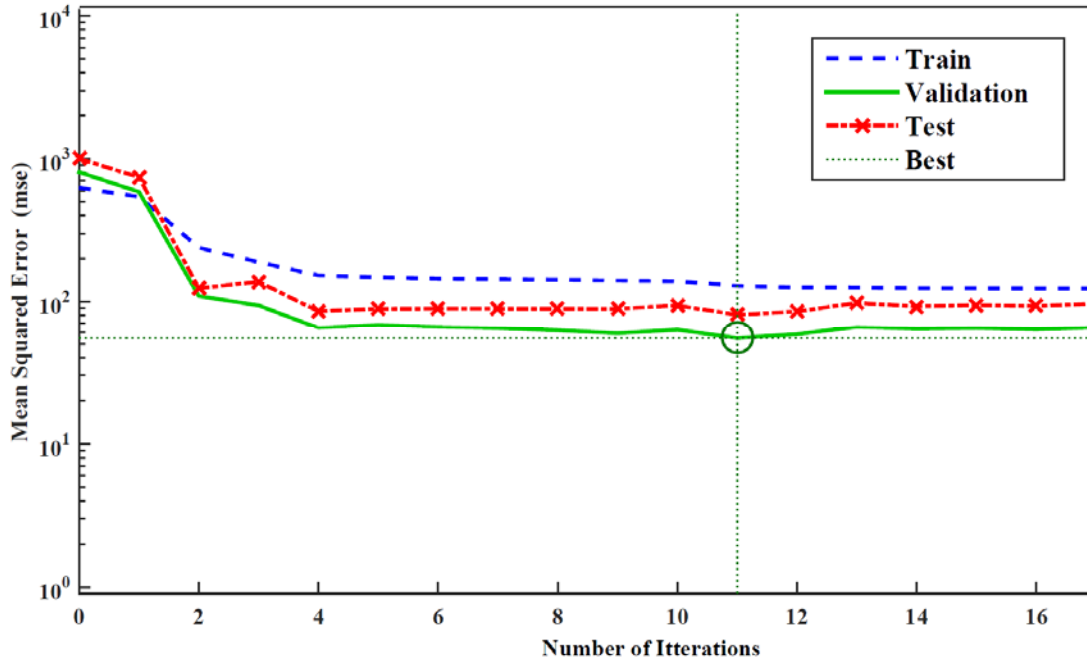


Figure 61
ANN model performance

Model Prediction

The regression plots of the ANN model for the training, validating, testing, and overall sets are shown in Figure 62. All data processing was performed off-line using a commercial software package (MATLAB R2013a, The MathWorks Inc.). As shown in this figure, the model had acceptable prediction accuracy with an R^2 of 0.73. In addition, the RMSE (%) was calculated at 12%. The RMSE (%) was calculated as follows:

$$RMSE\% = 100 * \sqrt{\frac{\sum_1^n [\text{Predicted } M_r(\text{RWD}) - \text{Calculated } M_r(\text{FWD})]^2}{n}} / \frac{\sum_1^n \text{calculated } M_r}{n} \quad (37)$$

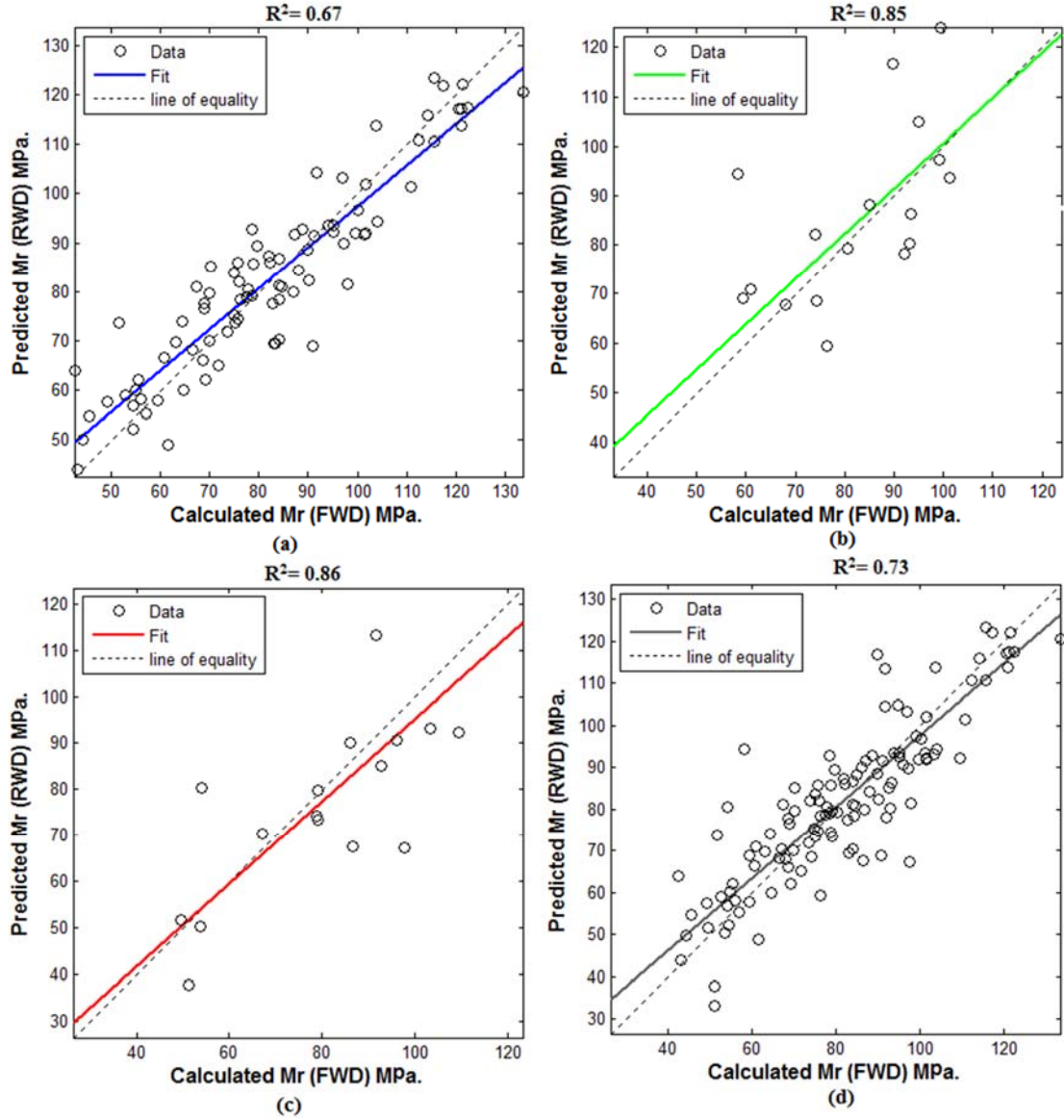


Figure 62
Regression plots of the developed ANN model for (a) the training data set, (b) the validation data set, (c) the testing data set, and (d) all data

Network Description

At the end of the learning phase, proper weights were assigned to every connection, and proper biases were assigned to each neuron as follows:

$$W_{ij} = \begin{bmatrix} -37.4 & -42.8 & -0.03 \\ -0.2 & -0.35 & -0.17 \end{bmatrix}$$

$$b_j = \begin{bmatrix} 22.49 \\ -0.47 \end{bmatrix}$$

$$W'_{jk} = [0.027 \quad 1.80]$$

$$B_k = 0.415$$

Forward Calculations

Artificial neural network models are considered by many researchers as "black-boxes" [45-47]. With a complex network structure, it is difficult to explicitly describe the learned relationship between the input and the output variables. However, the simplicity of the model presented in this study (only one hidden layer with only 2 neurons) allows to describe the network in a form of a simple equation. The general equation of a backpropagation algorithm-based neural network with one hidden layer, one output variable, and a tan-sigmoid (tansig) transfer function can be described as follows [32]:

$$k = (B_k + \sum_1^{n_j} \text{tansig}(b_j + \sum_1^{n_i} a_i W_{ij}) W_{jk}) \quad (38)$$

where,

k= the model output at layer k;

n_j = number of neurons in the hidden layer;

n_i = number of neurons in the input layer;

a_i = the input variables; and

The tansig function can be described as follows:

$$\text{tansig}(x) = \frac{e^x - e^{-x}}{e^x + e^{-x}} \quad (39)$$

A linear activation function was then utilized to transfer the output in layer k to the final output (M_r). The following expression describes the model developed utilizing ANN to predict the subgrade resilient modulus based on RWD measurements:

$$M_r = 119.7 * \left[0.415 + 0.027 * \text{tansig} \left(22.49 - 37.4D_0 - 42.8\sigma_{D_0} - 0.03 \frac{D_1}{r} \right) + 1.80 * \text{tansig} \left(-0.47 - 0.2D_0 - 0.35\sigma_{D_0} - 0.17 \frac{D_1}{r} \right) \right] + 195.2 \quad (40)$$

Model Evaluation and Analysis

The limits of agreement (LoA) methodology, developed by Bland and Altman, is a simple and powerful methodology for assessing agreements between two devices or procedures [48]. The methodology was successful to the extent that the reference that introduced this method has become one of the most cited statistical papers [49]. Bland and Altman

concluded that using only regular regression could be misleading when comparing two devices or methodologies for two reasons. First, correlation depends on the range and distribution of the variables. Second, correlation ignores any systematic bias between the two variables [50]. A recent study concluded the usefulness of the LoA methodology for comparing TSD and the FWD measurements [51].

The procedure of the LoA methodology consists of the following steps: (1) plot a chart with the differences between measurements by two methods on the Y-axis, and the mean of the two measurements on the X-axis, (2) calculate the mean and the standard deviation (σ) of the differences, and (3) calculate the mean $\pm 1.96 \sigma$. One would then expect 95% of differences between measurements by the two methods to lie within these limits. Figure 63 shows the LoA between the subgrade resilient modulus values calculated based on FWD and RWD measurements; the chart is also known as the Bland and Altman chart.

As shown in Figure 63, 95% of the differences between the M_r values calculated based on the FWD and the RWD measurements did not exceed the range of ± 3 ksi, which is reasonable especially at the network level. The figure provides a better understanding of the model accuracy in predicting M_r based on RWD data. The figure also shows that the error in the predicted subgrade resilient modulus is independent of the M_r value.

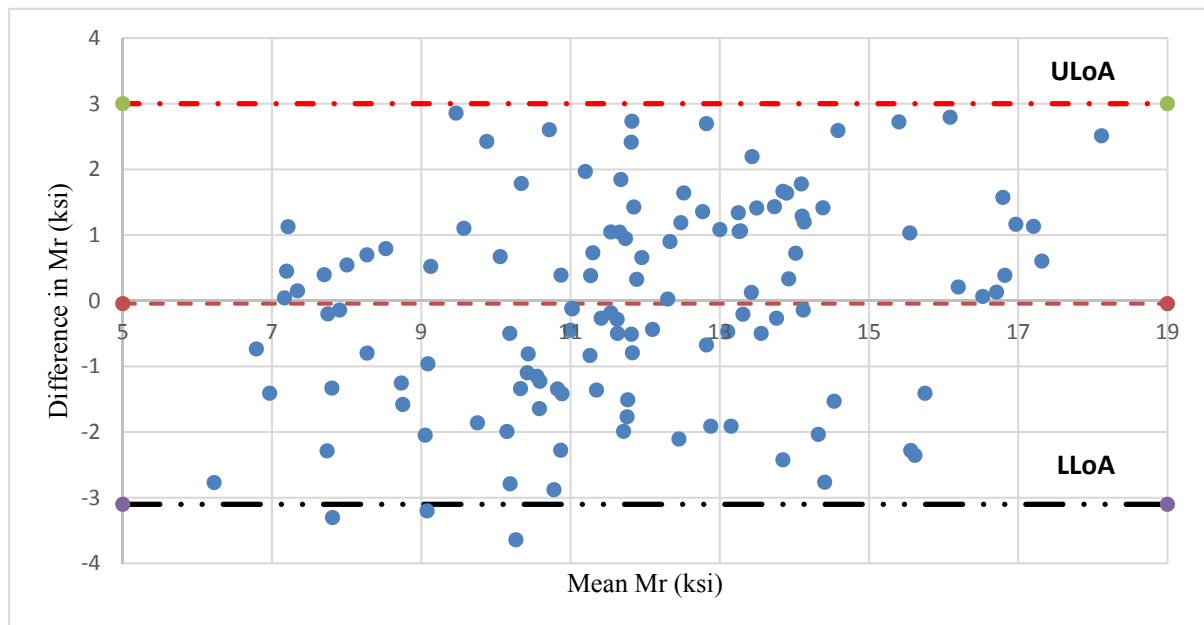


Figure 63
Bland and Altman Chart for the subgrade resilient modulus calculated based on FWD and RWD measurements

Model Validation

The generalization ability of the presented ANN model was tested using measurements obtained from the testing program conducted at MnROAD. RWD data from 16 flexible pavement testing cells were used as inputs in the ANN model to predict the subgrade resilient modulus. The M_r predicted values were then compared with those calculated based on FWD measurements, see equation (24). The model showed acceptable accuracy with an R^2 of 0.72 and a RMSE of 8% as shown in Figure 64.

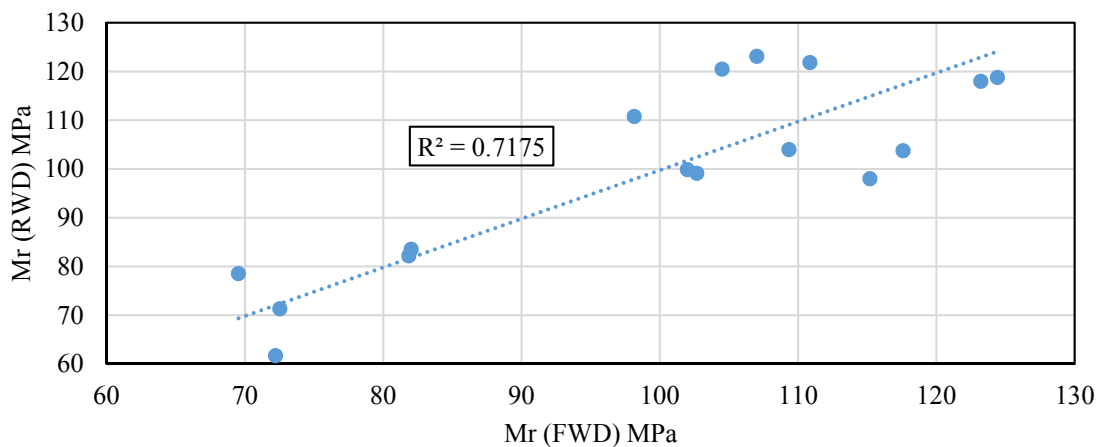


Figure 64
Model validation using data from the MnROAD testing program

Cost Efficiency and Added Values of RWD Testing

Two approaches were developed to implement RWD measurements into the DOTD current practices. In the first approach, the SCI was converted to a scaled index from 0 to 100 and was added to the State PMS treatment selection matrix. In the second approach, the calculated $SN_{RWD0.1}$ was added to the State overlay design procedure (see Figure 56). Figure 65 presents the general layout of the two developed approaches. Description of the two approaches is presented in the following sections.

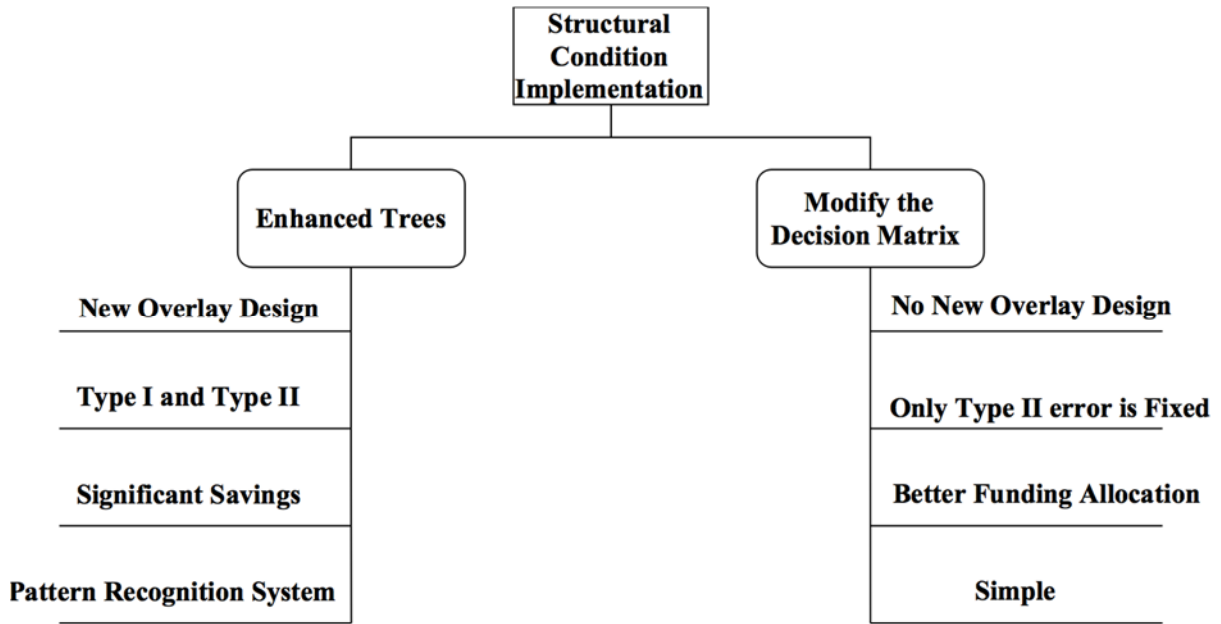


Figure 65
General layout of the proposed implementation approaches

Approach 1: Modify the Treatment Selection Decision Matrix Procedure

In the first approach, the SCI was converted to a scaled index from 0 to 100, where a value of 100 indicates excellent structural condition, and was added to the state treatment selection matrix. The SCI was converted to a scale from 0 to 100 (SSCI) to follow the same scale adopted by the other PMS indices using a sigmodal function as presented in equation (41):

$$SSCI = \frac{100}{1 + e^{-4.346(SCI - 0.768)}} \quad (41)$$

where,

SCI= Structural Condition Index; and

SSCI= Scaled Structural Condition Index.

Figure 66 shows the correlation between the SCI and the SSCI. Modified treatment selection matrices were developed with the implementation of the SSCI and are presented in Tables 31 to 32.

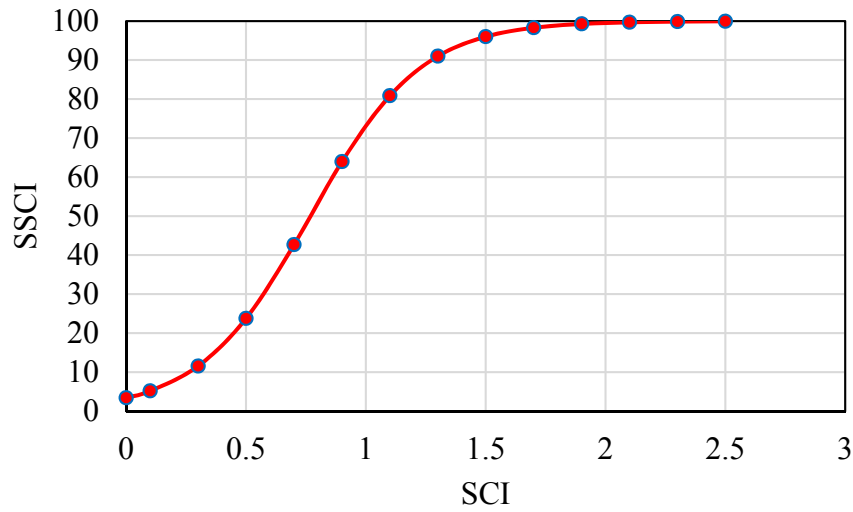


Figure 66
Correlation between the SCI and the SSCI

Table 31
Modified decision matrix for arterials

	ALCR	RNDM	PTCH	RUT	RUFF	SSCI
Micro-surfacing	≥ 95	≥ 95	≥ 95	$\geq 65 - < 80$	≥ 80	≥ 95
Thin overlay (2in.)	≥ 90	$\geq 80 - < 95$	≥ 80	< 65	$\geq 70 - < 80$	$\geq 75 - < 95$
Medium overlay	$\geq 50 - < 90$	< 80	$\geq 60 - < 80$	----	< 70	$\geq 60 - < 75$
Structural overlay	< 50	----	< 60	----	----	< 60

Table 32
Modified decision matrix for collectors

	ALCR	RNDM	PTCH	RUT	RUFF	SSCI
Polymers S. treat.	$\geq 85 - < 95$	$\geq 80 - < 95$	≥ 85	≥ 65	≥ 80	≥ 95
Microsurfacing	≥ 95	≥ 95	≥ 95	$\geq 65 - < 80$	≥ 80	≥ 95
Thin overlay (2 in.)	----	----	----	----	----	$\geq 75 - < 95$
Medium overlay	$\geq 60 - < 85$	< 80	$\geq 65 - < 85$	< 65	$\geq 60 - < 80$	$\geq 60 - < 75$
In-place stabilization	< 60	----	< 65	----	< 60	< 60

The impacts of the proposed modifications presented in Tables 31 and 32 were investigated. The effects were analyzed using two levels of decisions: treatment selections are assigned to every 0.1 mile road segment and treatment selections are assigned to every control section, which assumes that only one treatment decision is assigned to every homogenous pavement section. Table 33 presents the effects of applying the modified decision matrix if decisions are made to every 0.1 mile road segment. Similarly, Table 34 presents the effects of applying the modified decision matrix if decisions are made to every homogeneous control section. It is noted that by applying the modified decision matrix procedure, the M&R cost would increase by 14% as the recommended modifications only address Type II error (i.e., applying a functional treatment to a structurally deficient pavement). Since the functional indices were not changed, Type I error was not addressed by adding the proposed structural condition index. To address both Type I and II errors, Approach 2 should be used, which is recommended.

Table 33
Change in treatment selection by applying proposed modification to decision matrix

Modified Matrix Decision									
Current Decision		DN	MS	PST	TO	MO	SO	IPS	Change
	DN*	4195	0	0	512	132	0	206	16.8%
	MS*	0	145	0	31	3	0	2	19.9%
	PST*	0	0	491	159	49	0	90	37.8%
	TO*	0	0	0	1529	159	0	384	26.2%
	MO*	0	0	0	0	1751	8	578	25.1%
	SO*	0	0	0	0	0	10	0	0.0%
	IPS*	0	0	0	0	0	0	1281	0.0 %

Where, DN*= Do Nothing, MS*= Microsurfacing, PST*= Polymer Surface Treatment, TO*= Thin Overlay, MO*= Medium Overlay, SO*= Structural Overlay, and IPS* = in place Stabilization

Table 34
Change in projected cost of treatments based on modified decision matrix

Decision	Number of sections	
	Current Practice	Modified Practice
DN	39	30
MS	0	0
PST	0	0
TO	2	7
MO	91	83
SO	0	3
IPS	12	21
Total Cost	\$256,625,600	\$279,741,800

Approach 2: Modify Treatment Selection and Overlay Design Procedure

In the second approach, the calculated $SN_{RWD0.1}$ was added to the state overlay design procedure and SSCI was added to the State treatment selection matrix. The main advantage of this approach is that it uses $SN_{RWD0.1}$ to estimate in-service pavement structural conditions instead of assuming a 50% loss in structural capacity as it is currently assumed. Two enhanced decision trees were developed to implement the proposed changes to the overlay

design procedure. The enhanced decision trees were developed for arterials and collectors and are shown in Figures 67 and 68. The decision trees were constructed based on the following assumptions:

- Sections in poor structural conditions should receive rehabilitation treatments that increase pavement structural capacity.
- Sections in good structural conditions would receive the same (M&R) actions selected according to the current DOTD decision matrix, see Table 3.
- Medium and structural overlays would be designed utilizing the $SN_{RWD0.1}$ as described earlier.
- Minimum overlay thickness was set at 50.8 mm (2 in.).

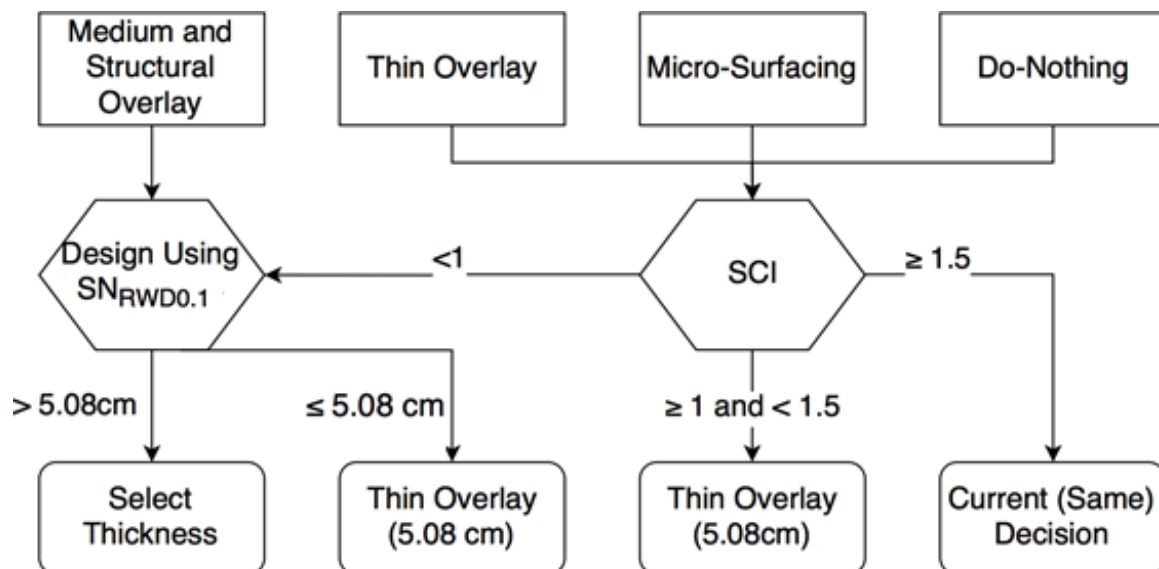


Figure 67
Enhanced decision tree for arterials

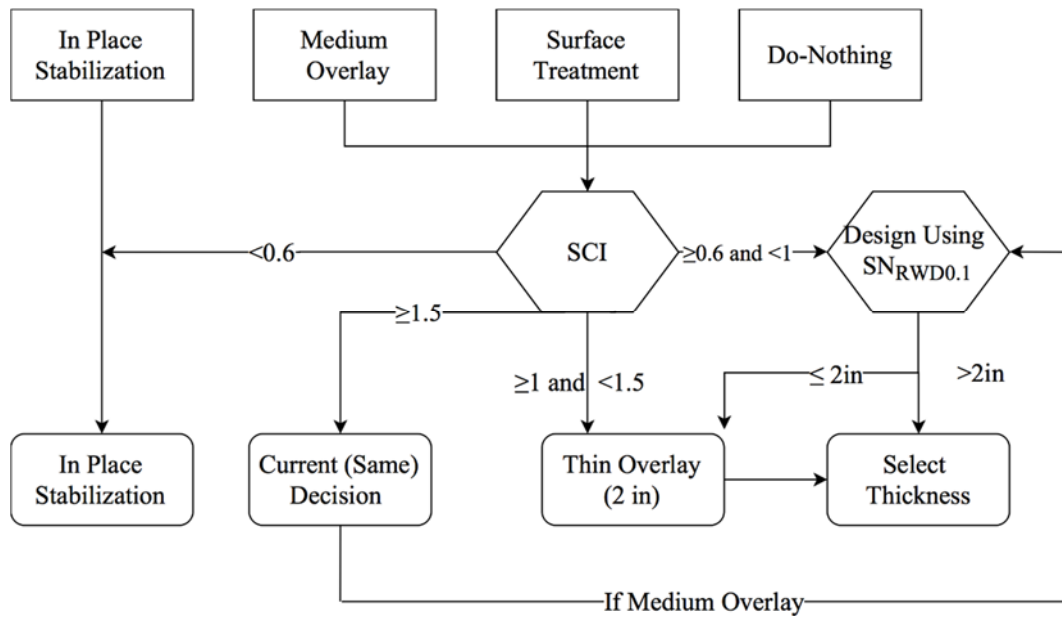


Figure 68
Enhanced decision tree for collectors

To assess the cost-efficiency and added value of the second approach, the enhanced decision trees were applied to the road network in District 05, which was tested using RWD. Comparisons were made between the PMS decisions using the current decision matrix, see Table 3, and the enhanced decision trees. Table 35 and 36 present the change in treatment selection of the current DOTD PMS practice and the proposed enhanced decision procedure for the functional classes of rural minor arterials and the rural major collectors, at the segments level. As shown in these tables, the second approach can address both Type I and II errors in treatment selection. It also provides a more accurate overlay design by using $SN_{RWD0.1}$ to estimate in-service pavement structural conditions instead of assuming a 50% loss in structural capacity as it is currently assumed.

Table 35
Transition matrix for the current and the enhanced trees procedure for the rural minor arterials

Current decision/ New decision	DN*	MS*	TO*	MO*	SO*	Type I error %	Type II error %	Total error %
DN*	260	0	68	0	0	0	20.7	20.7
MS*	0	3	6	0	0	0	66.7	66.7
TO*	0	0	72	0	1	0	1.4	1.4
MO*	0	0	196	66	39	65.1	13.0	78.1
SO*	0	0	0	0	1	0	0.0	0.0

Table 36
Transition matrix for the current and the enhanced trees procedure for the rural major collectors

Current decision/ New decision	DN*	PST*	MS*	MO*	TO*	IPS*	Type I error %	Type II error %	Total error %
DN*	1601	0	0	218	0	56	0.0	14.6	14.6
MS*	0	0	18	2	0	1	0.0	15.0	15.0
PST*	0	210	0	44	0	9	0.0	20.2	20.2
MO*	0	0	0	567	1265	142	64.1	7.2	71.3
IPS*	0	0	0	0	0	359	0.0	0.0	0.0

The cost associated with each treatment is presented in Table 37 from PMS sources.

Table 37
Construction cost for each treatment strategy per mile

Treatment Type	Construction cost/ mile 2 lanes (2014)
Microsurfacing	\$67,000
Polymer Surface treatment	\$72,000
Thin Overlay	\$184,000
Medium Overlay	\$334,000
Structural Overlay	\$360,000
In place Stabilization	\$496,000

Tables 38 to 42 present the comparison between the current decision matrix and the enhanced decision trees for rural minor arterials, rural major collectors, urban minor arterials, rural minor collectors, and rural locals, at the segment level, while Table 43 presents the same comparison at the control section level. To compare the difference in cost between the two decision-making processes, the cost of performing each treatment was obtained from the PMS database. Construction and RWD testing costs were considered in this analysis; however, other sources of cost, such as user cost, were not considered.

Table 38
Current and enhanced decision comparison for rural minor arterials

Current Decision	# Segments	Enhanced Decision	# Segments
Do Nothing	328	Do Nothing	260
Microsurfacing	9	Microsurfacing	3
Thin Overlay	73	Thin Overlay	342
Medium Overlay	301	Medium Overlay	66
Structural Overlay	1	Structural Overlay	41
Total # segments	712	Total # segments	712
Treatment cost	\$11,492,900	Treatment cost	\$9,998,025
RWD testing cost	\$0.00	RWD testing cost	\$4,725

Table 39
Current and enhanced decision comparison for rural major collectors

Current Decision	# Segments	Enhanced Decision	# Segments
Do Nothing	1,875	Do Nothing	1601
Microsurfacing	21	Microsurfacing	18
Polymer Surface treatment	268	Polymer Surface treatment	210
Thin Overlay	0	Thin Overlay	1,265
Medium Overlay	1969	Medium Overlay	831
In place Stabilization	359	In place Stabilization	567
Total # segments	4,492	Total # segments	4,492
Treatment cost	\$85,641,300	Treatment cost	\$80,818,700
RWD testing cost	\$0.00	RWD testing cost	\$31,500

Table 40
Current and enhanced decision comparison for urban minor arterials

Current Decision	# Segments	Enhanced Decision	# Segments
Do Nothing	260	Do Nothing	217
Microsurfacing	10	Microsurfacing	7
Thin Overlay	121	Thin Overlay	238
Medium Overlay	161	Medium Overlay	52
Structural Overlay	10	Structural Overlay	48
Total # segments	562	Total # segments	562
Treatment cost	\$8,030,800	Treatment cost	\$7,897,500
RWD testing cost	\$0.00	RWD testing cost	\$6,600

Table 41
Current and enhanced decision comparison for rural locals

Current Decision	# Segments	Enhanced Decision	# Segments
Do Nothing	239	Do Nothing	163
Microsurfacing	3	Microsurfacing	3
Polymer Surface treatment	79	Polymer Surface treatment	24
Thin Overlay	0	Thin Overlay	172
Medium Overlay	591	Medium Overlay	286
In place Stabilization	610	In place Stabilization	874
Total # segments	1,522	Total # segments	1,522
Treatment cost	\$50,584,300	Treatment cost`	\$56,277,300
RWD testing cost	\$0.00	RWD testing cost	\$16,800

Table 42
Current and enhanced decision comparison for rural minor collectors

Current Decision	# Segments	Enhanced Decision	# Segments
Do Nothing	551	Do Nothing	367
Microsurfacing	11	Microsurfacing	10
Polymer Surface treatment	340	Polymer Surface treatment	240
Thin Overlay	0	Thin Overlay	561
Medium Overlay	1476	Medium Overlay	843
In place Stabilization	837	In place Stabilization	1,194
Total # segments	3,215	Total # segments	3,215
Treatment cost	\$93,335,300	Treatment cost	\$99,534,400
RWD testing cost	\$0.00	RWD testing cost	\$38,400

Table 43
Current and enhanced decision comparison at the control sections level

Decision	Number of sections	
	Current Practice	Modified Decision Trees (Approach 2)
DN	39	26
MS	0	0
PST	0	27
TO	2	46
MO	91	106
SO	0	0
IPS	12	15
Cost	\$256,625,600	\$182,974,600

The cost and productivity of RWD testing were based on the data obtained from ARA, Inc. as shown in Table 44 [14].

Table 44
Cost and productivity of RWD testing

Functional Class	Productivity lane-mile/ day	Cost \$ per lane-mile
Interstate	250	\$42
Secondary roads	150	\$70
Local Roads	100	\$105

Monetary savings were calculated as follows:

$$\text{Savings} = \text{current decision cost} - (\text{enhanced decision cost} + \text{RWD testing cost}) \quad (42)$$

In lights of the results presented in Tables 37 to 41, it was observed that there is a correlation between the savings that could be achieved through the second approach and the roadway functional class. Applying the second approach on major collectors and arterials resulted on positive saving values; however, applying the enhanced decision procedure on local roads and minor collectors resulted in negative saving values as shown in Figure 69. In addition, it is noted from Table 44 that there is a significant reduction in RWD productivity when operated in local roads, which results in increasing the cost of testing. The correlation between the dollar saving amount and the AADT is shown in Figure 70. As shown in this figure, RWD testing would provide significant savings at an AADT of 5,000 or greater.

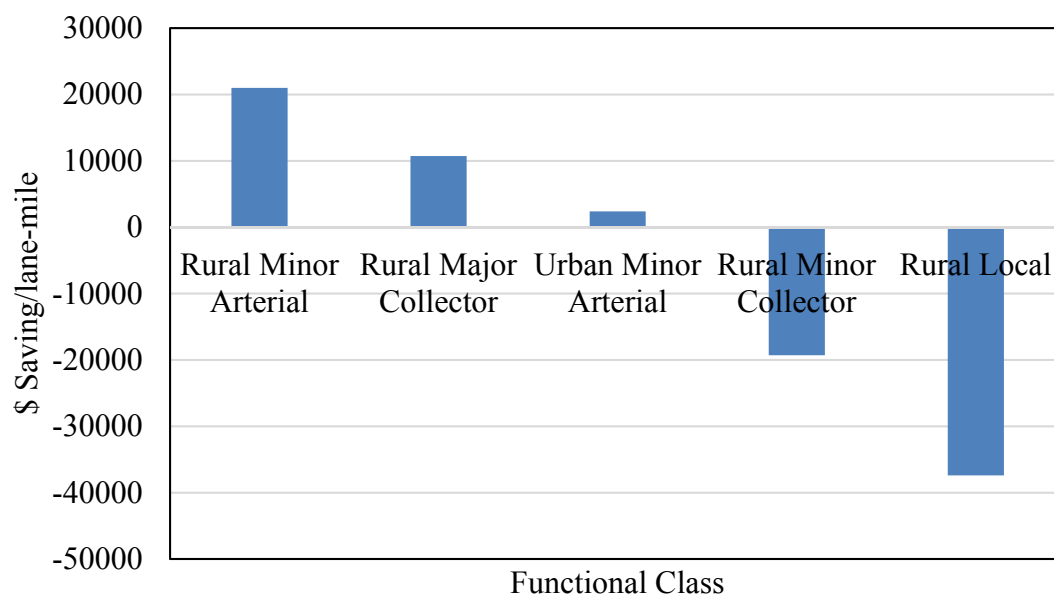


Figure 69
Monetary saving for each roadway functional class

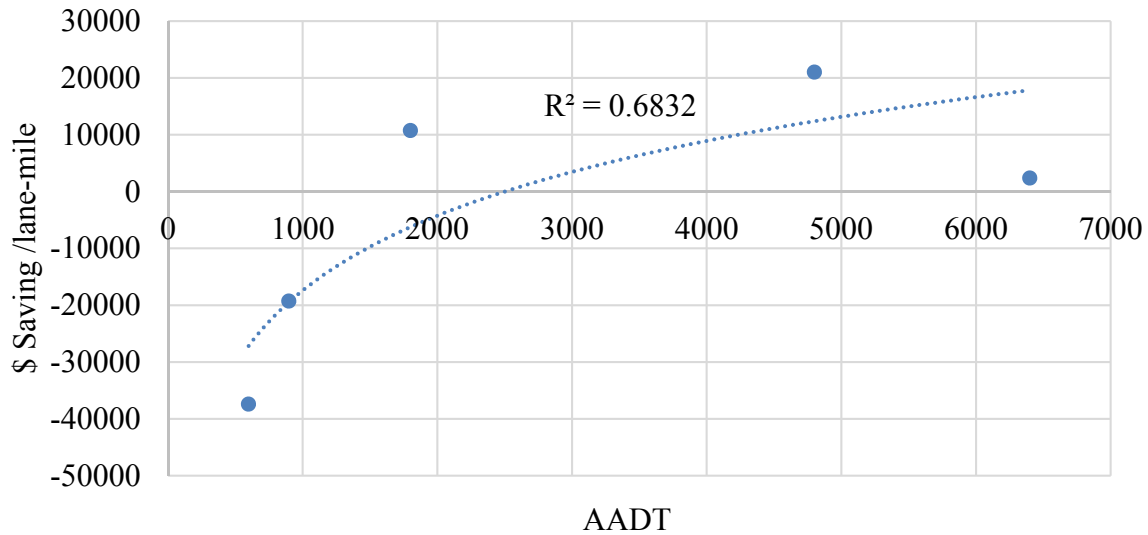


Figure 70
Correlation between the saving amount and traffic volume

Develop a One-Step Enhanced Decision Making Tool

The objective of this task was to develop a one-step enhanced decision-making tool that would consider both structural and functional pavement conditions in treatment selection as well as the modified overlay design procedure. To achieve this objective, an ANN-based pattern recognition system was trained and validated using pavement condition data and RWD measurements-based SN ($SN_{RWD0.1}$) to arrive at the most optimum maintenance and rehabilitation (M&R) decisions. The developed tool is time-efficient since it allows PMS engineers to determine the final enhanced M&R decisions (which requires several analysis steps) in only one step.

Pattern recognition is one of the most important applications of Artificial Intelligence (AI). Through pattern recognition, machines can observe information, learn to distinguish patterns of interest, and make sound and reasonable decisions about the classifications of patterns [52]. Machine recognition of patterns has been successfully applied to solve problems in a variety of engineering and scientific disciplines. A pattern can be a fingerprint image, a handwritten cursive word, a human face, or a speech signal [52]. In pavement and transportation engineering, pattern recognition algorithms have been utilized in many applications such as crack detection through image processing, estimation of asphalt mix properties, traffic simulation, and monitoring travel behavior [53-56].

Pattern recognition was applied by using a feed forward ANN with a back-propagation optimization algorithm. The network prediction accuracy is expressed in the form of “confusion matrices” instead of the common regression plots. A confusion matrix encloses information about actual and predicted patterns. The matrix has two dimensions, one with the actual pattern or “class” of an object, and the other with the pattern as predicted from the ANN. A basic confusion matrix with patterns P_1 , P_2 , and P_n is presented in Figure 71, where N_{ij} indicates the number of samples actually belonging to class P_i but classified by the ANN as class P_j [57].

		Predicted		
		P_1	$\dots P_j \dots$	P_n
Actual	P_1	N_{11}	N_{1j}	N_{1n}
	\vdots		\vdots	
	P_i	N_{i1}	$\dots N_{ij} \dots$	N_{in}
	\vdots		\vdots	
	P_n	N_{n1}	N_{nj}	N_{nn}

Figure 71
Pattern Recognition Confusion Matrix

Two main performance indicators can be calculated from the confusion matrix; accuracy and precision. Accuracy is the proportion of total predictions that were correct, and precision is a measure of the accuracy for a specific class [57]:

$$\text{Accuracy} = \sum_{i=1}^n N_{ii} / \sum_{i=1}^n \sum_{j=1}^n N_{ij} \quad (42)$$

$$\text{Precision}_i = N_{ii} / \sum_{k=1}^n N_{ki} \quad (43)$$

Procedure Overview

To develop the enhanced decision-making tool, the following steps were conducted:

- **Step 1:** Initial rehabilitation decisions were selected based on the Louisiana current decision matrix; see Table 3.
- **Step 2:** The SCI was calculated using $SN_{RWD0.1}$ as the SN_{eff} and the required SN for a design life of 10 years as the SN_{req} .
- **Step 3:** Enhanced decision were determined by utilizing the aforementioned enhanced decision trees, see Figures 67 and 68.

- **Step 4:** Overlays were designed by utilizing the $SN_{RWD0.1}$ instead of the 50% loss in the structural capacity assumption.
- **Step 5:** An ANN was trained by feeding the input layer with the PMS data and $SN_{RWD0.1}$, and the output (target) layer was fed with the final enhanced decisions obtained from Steps 3 and 4. Figure 72 shows an overview of the developed procedure.

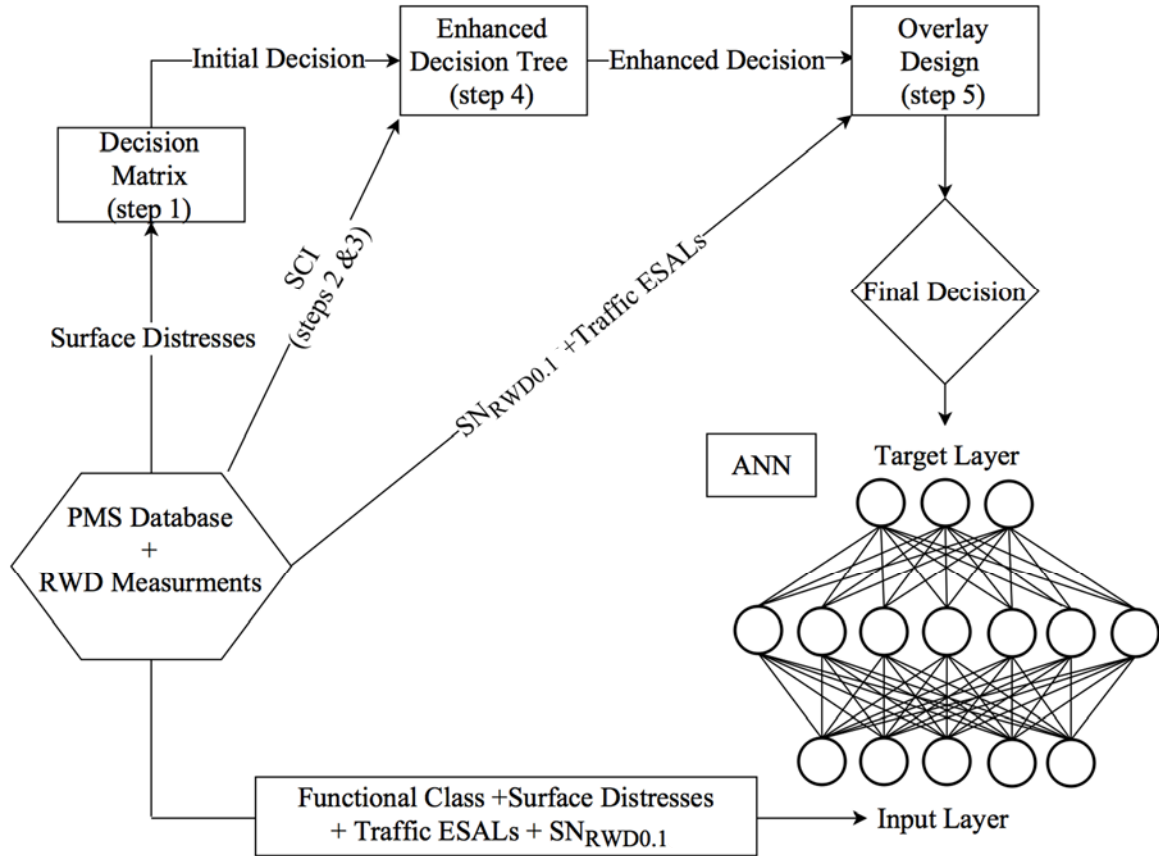


Figure 72
Overview of the system developing procedure

Develop the Pattern Recognition System

An ANN-based pattern recognition system was developed to provide decision makers with a quick and accurate tool to apply the enhanced decision matrix and the proposed overlay design methodology. A multilayered feed-forward ANN was selected with a hard-lim transfer function, which develops outputs in the form of “0” or “1” as illustrated in Figure 17. The network utilizes a scaled conjugate gradient backpropagation training algorithm (trainscg), and the errors are represented in the form of the mean square error (MSE). The

network architecture consisted of three layers; an input layer of 8 neurons; a hidden layer of 20 neurons; and a target (output) layer of 7 neurons. The number of neurons in the hidden layer was selected based on an iterative process. The criterion was to select the least number of hidden neurons without affecting the network performance to avoid overfitting.

Network Inputs. The simplest set of inputs that correlated with the enhanced decision process and that required no optimization analysis to be conducted by the PMS engineers were selected and were fed to the ANN input layer. Calculation of the SCI required the SN_{req} to be optimized based on the AASHTO 1993 flexible pavement design equation; therefore, it was not implemented in the ANN model. Based on equation (31) and the AASHTO overlay design model, the SCI is a function of the $SN_{RWD0.1}$, the traffic ESALs, the subgrade modulus of resilience (M_r), allowable loss in pavement serviceability index (ΔPSI), and the design reliability. The design reliability and ΔPSI are commonly assigned the values of 90% and 2.5, respectively. The M_r values for the tested road segments were assumed to be 9,000 psi according to the DOTD soil maps for District 05; however, this assumption may be changed as needed. Based on these assumptions, the SCI would be a function of the $SN_{RWD0.1}$ and the traffic ESALs. Therefore, the ANN input layer was fed with the $SN_{RWD0.1}$, the traffic ESALs, and the pavement surface distresses utilized in the decision matrix shown in Table 3. In addition, a neuron in the input layer was assigned to define the segment functional class (arterials or collector). In the case of arterials, an input of “1” was defined, and in the case of collectors, an input of “2” was defined.

Network Targets. The final decisions obtained from the enhanced decision flowchart (Step 4) and the proposed overlay design procedure (Step 5) were used to feed the network output (target) layer. An overview of the steps followed to develop the ANN network is shown in Figure 72. Surface distresses obtained from the PMS database were first used to determine the initial M&R decisions through the current decision matrix, see Table 3. The initial decisions along with the corresponding SCI values were then used into the enhanced decision flowcharts (see Figures 67 and 68) to determine the enhanced decisions. The modified overlay design procedure was used to design the overlay, if applicable, and to reach the final treatment selection. The final decisions were then defined as targets (outputs) to the ANN-based pattern recognition system. On the other hand, the pavement surface distresses data, the road segment functional class, the traffic data, and the $SN_{RWD0.1}$ were defined as independent inputs to the ANN-based pattern recognition system. Finally, the system was trained to correlate between the inputs and the targets.

More details about the ANN structure are shown in Figure 73. As shown in this figure, pavement surface distresses data (ALCR, RUT, RNDM, PTCH, and RUFF), the road

segment functional class (arterial or collector), the traffic loads (ESALs), and the $SN_{RWD0.1}$ were incorporated into the ANN with eight neurons in the input layer. On the other hand, the corresponding final M&R decisions were incorporated into the ANN with seven neurons in the target layer. A hidden (processing) layer of 20 neurons, all connected to each neuron in the input and the target layers, were used to establish adequate correlations between the network inputs and targets.

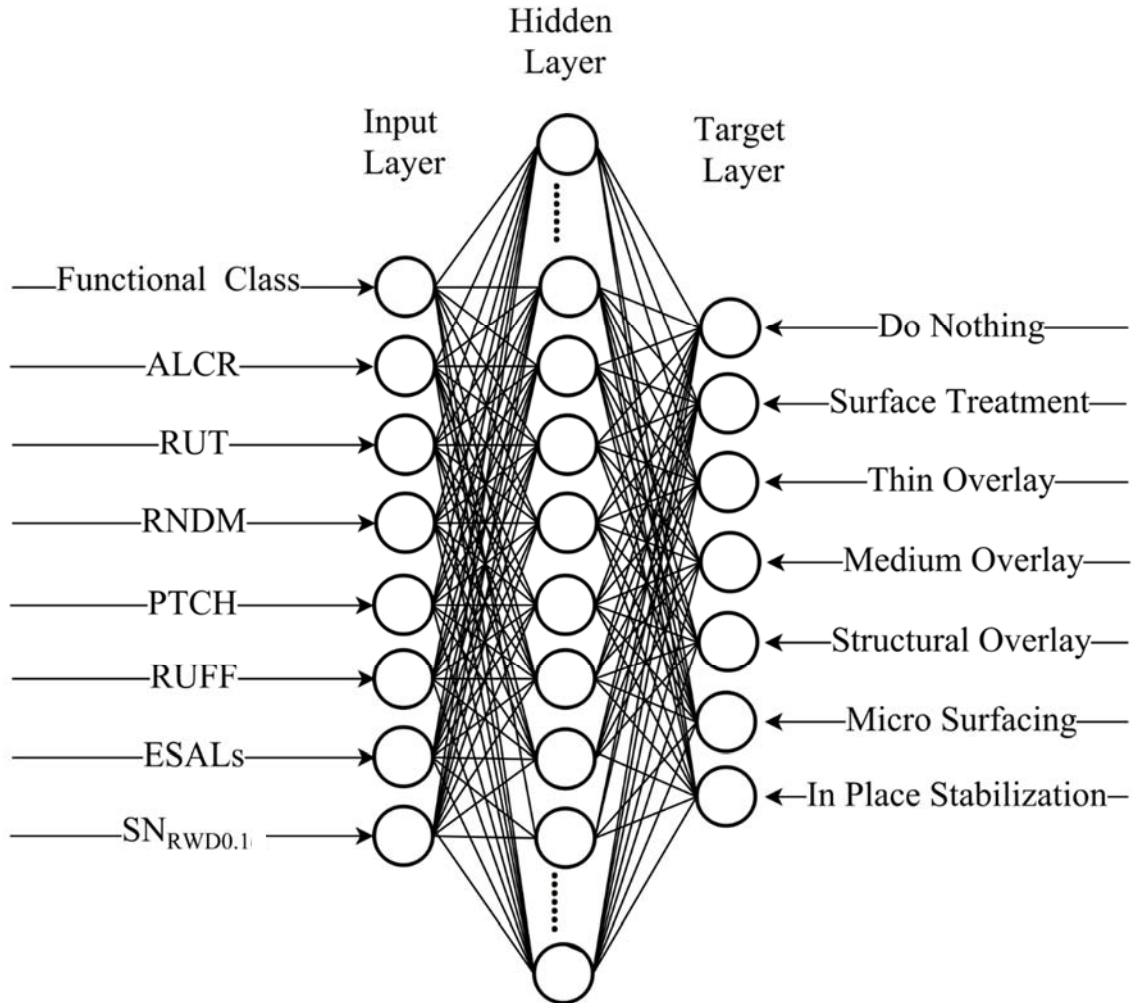


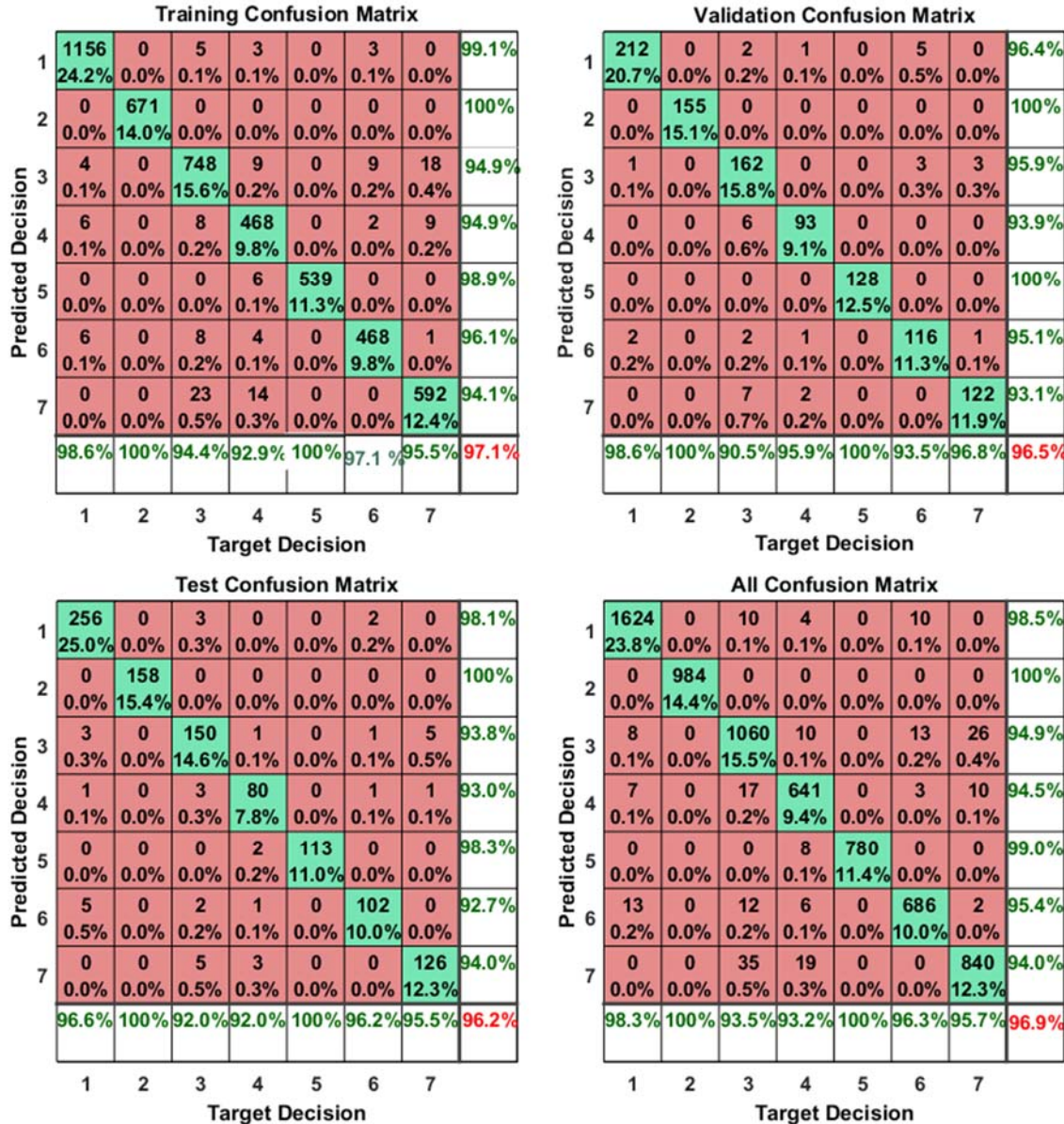
Figure 73
The ANN-based pattern recognition model structure

Network Training and Performance

Data from 5,174 road segments were used to build the ANN model, where each segment represents one data point. An oversampling technique was utilized so that the dataset is balanced, and each treatment decision is satisfactorily represented. The oversampling process

results in an increase in the dataset size to reach 6,828 data points. In the DOTD database, the performance indices are reported on intervals of 0.1 mile, so that all segments have the same length (0.1 mile), so that no weighting was needed. The data were divided into 70% for training, 15% for validation, and 15% for testing. Training was halted when the validation set error stopped decreasing to avoid overfitting and to increase the generalization ability of the network. The network training time was found to be 3.68 seconds. The testing data set had no effect on the training, so it was used to provide an independent measure of the network performance.

The confusion matrices showed an overall pattern prediction accuracy of 96.9%, which indicates the effectiveness of this method to predict maintenance and rehabilitation decisions. Figure 74 shows the confusion matrices for the training, testing, validation, and overall step for the pattern recognition system. The matrices present N_{ij} with its percentage, precision of every decision, and the overall accuracy as discussed earlier, see equations (42) and (43). All data processing was performed off-line using a commercial software package (MATLAB R2013a, The MathWorks Inc.).



Where, 1= Do nothing, 2= Micro-surfacing, 3= Thin Overlay, 4= Medium Overlay, 5= Structural Overlay, 6= Surface Treatment, and 7= In-Place Stabilization.

Figure 74
Confusion matrices of the pattern recognition system for (a) the training data set (b) the validation data set (c) the testing data set (d) all data

Forward Calculations

Once the training phase is complete and the desired accuracy is achieved, the ANN model can be saved as a MATLAB file, which can be utilized to perform forward calculations, and predict maintenance and rehabilitation decisions. The processing time of the forward

calculation for the 5,174 decisions was found to be 0.045 seconds. The output of the forward calculation analysis would consist of a table in which the selected maintenance and rehabilitation decision assigned for each road segment is presented by a “1,” and the other non-selected rehabilitation decisions would have an output of “0.” Table 45 presents an illustration of the forward calculations outputs. In addition to the MATLAB file, a MATLAB code for the trained system was generated. Such a code can be utilized to develop a program with a user-friendly interface, which can be used by PMS engineers in the state.

Table 45
Forward calculations output form

Model Output							Final Decision
1*	2*	3*	4*	5*	6*	7*	
1	0	0	0	0	0	0	Do Nothing
0	1	0	0	0	0	0	Micro-Surfacing
0	0	1	0	0	0	0	Thin Overlay
0	0	0	1	0	0	0	Medium Overlay
0	0	0	0	1	0	0	Structural Overlay
0	0	0	0	0	1	0	Surface Treatment
0	0	0	0	0	0	1	In Place Stabilization

Where, 1= Do nothing, 2*= Micro-surfacing, 3*= Thin Overlay, 4*= Medium Overlay, 5*= Structural Overlay, 6*= Surface Treatment, and 7*= In Place Stabilization.*

CONCLUSIONS

The objective of this study was twofold. First, the study evaluated previously-developed structural capacity indicators in predicting pavement structural deficiency based on RWD measurements. Based on this evaluation, the research team introduced modifications to improve prediction of pavement structural capacity. Second, in this study a methodology was developed to integrate the most promising indicator into the Louisiana PMS decision matrix. In addition, this project assessed the cost-efficiency of RWD testing in identifying and repairing structurally-deficient sections prior to reaching very poor conditions. Based on the results of the study and the conducted cost analysis, the following conclusions were drawn:

Structural Capacity Indicators

- The SN showed the most promising capability in identifying structurally-deficient and structurally-sound pavement sections. In addition, the SN model was found to have the highest uniformity coefficient (82%) among the different indices.
- In light of the ANOVA analysis, the SN was concluded to be the structural capacity indicator that is less affected by pavement surface conditions, while the ZRI was concluded to be the structural capacity indicator that is most affected by pavement surface conditions. Core samples investigation also supported this conclusion.
- Sections considered structurally-deficient according to the SN thresholds were found to be the same as those considered deficient according to the RI thresholds.
- The SN was selected as the most promising structural capacity indicator.

Modifications to the SN Model

- The modified SN model ($SN_{RWD0.1}$) was developed to predict structural capacity from RWD measurements every 0.1 mile. The model showed an acceptable coefficient of determination (R^2) of 0.7677 and a RMSE of 0.8.
- Core samples showed that sections that were predicted to be structurally-deficient suffered from asphalt stripping and material deterioration problems.
- Results support that the developed model provides additional information that complements the existing functional indices in PMS and that could be used to predict pavement structural conditions with an acceptable level of accuracy.

Structural Health Index

- The Structural Health Index (SHI), on a scale from zero to 100, was developed to describe the structural integrity of pavement sections based on the backcalculated layer moduli of in-service pavements as predicted from FWD testing.
- Evaluation and validation of the SHI was successful and indicated that the new index responded realistically to sections in poor and in good structural conditions.
- It was shown that the new index provides additional information that complements the existing functional indices in PMS by successfully identifying structurally-deficient sections.

Rates of Deterioration

- A structural condition index (SCI) was developed based on $SN_{RWD0.1}$ to categorize pavement sections according to structural conditions (e.g., very low, low, medium, etc.).
- Based on the analysis of PMS data, sections with very low SCI values were observed to deteriorate significantly faster than those with high SCI values.
- The rates of deterioration were found to be independent of the initial values of the performance indices for collectors; however, for the arterials, the rate of deterioration was found to be affected by both the SCI value and the initial values of the performance indices.

Overlay Design

- An approach was developed to implement RWD measurements in AC overlay design procedure. The proposed procedure implements the $SN_{RWD0.1}$ in the AASHTO 1993 design method instead of assuming a 50% loss in structural capacity.
- The new overlay design procedure would allow for optimum funding allocation and would assist the designer avoid both type I error (False Positive) and type II error (False Negative).
- The proposed and the current design approaches were compared using a mechanistic AC overlay design method (Asphalt-Institute); the new design approach was more effective in avoiding type I and type II errors.

Subgrade Resilient Modulus

- An ANN-based model was developed to estimate the subgrade resilient modulus based on RWD measurements. The model was developed based on data obtained from the testing program conducted in Louisiana's District 05 and was validated based on data obtained from a testing program conducted at the MnROAD facility in Minnesota.
- The limits of agreement methodology showed that 95% of the differences between the M_r values calculated based on FWD and RWD measurements will not exceed the range of ± 3 ksi, which is acceptable especially at the network level.
- The ANN model showed acceptable accuracy in both the development and validation phases with coefficients of determination of 0.73 and 0.72, respectively. The RMSE was found 12% and 8% in the development and the validation phase, respectively.

Cost Effectiveness Analysis of RWD Testing

- The SCI was converted into a scaled indicator from 0 to 100 (SSCI), and its incorporation into the PMS decision matrices was developed.
- Two enhanced decision trees for collectors and arterials were developed for demonstrating the incorporation of RWD measurements and the SSCI into the PMS decision making process.
- The implementation of RWD measurements into PMS decision making process as well as the State overlay design procedure would provide significant savings to the Department if applied on relatively high volume roads with an AADT of 5,000 or more (e.g., Interstates, Arterials, and Major Collectors).

Development of a One-Step Decision Making Tool

- An ANN-based pattern recognition system was trained and validated based on pavement condition data and RWD measurements-based SN to arrive at the most optimum M&R decisions.
- The developed model showed an acceptable overall maintenance and rehabilitation decision prediction accuracy of 96.9%.
- High model generalization ability was demonstrated as the prediction accuracy of the testing data set (which was not used in the model training) was 96.2%.

RECOMMENDATIONS

Based on the findings and the results of this project, it is recommended to regularly test the road segments in the State trafficked with an AADT of 5,000 or more using RWD at a frequency of once every four years. In addition, continuous deflection data should be incorporated into the Louisiana PMS for treatments' selection as well as the State overlay design procedure. The effective pavement structural number is recommended to be used in the overlay design procedure instead of the current practice of assuming 50% loss in the original structural capacity. The proposed modification to the overlay design procedure is implementation-ready and should be utilized by the Department to maximize savings to the State from using RWD. The following future research activities are also recommended:

- Additional RWD and FWD comparison testing is recommended to be conducted throughout the state of Louisiana to validate and fine-tune the models and procedures presented in this report.
- Continuous pavement deflection testing such as RWD is recommended to be performed at least every 4 years to monitor pavement structural conditions at the network level.
- Pavement deterioration rates at different SCI intervals should be monitored before and after applying treatments to update the enhanced decision trees.

ACRONYMS, ABBREVIATIONS, AND SYMBOLS

AADT	Annual Average Daily Traffic
AASHTO	American Association of State Highway and Transportation Officials
AC	Asphalt Concrete
ADT	Average Daily Traffic
ALCR	Alligator Cracking Index
ANOVA	Analysis of Variance
ARAN	Automatic Road Analyzer
CM	Corrective Maintenance
D ₀	Maximum Surface Deflection
DN	Do Nothing
DOTD	Department of Transportation and Development
ESAL	Equivalent Single Axle Load
FHWA	Federal Highway Administration
ft.	foot (feet)
FWD	Falling Weight Deflectometer
GPR	Ground Penetrating Radar
HMA	Hot Mix Asphalt
IHS	Interstate Highway Significance
IRI	International Roughness Index
in.	inch(es)
ksi	Kilo pounds per square inch
lb.	pound(s)
LTRC	Louisiana Transportation Research Center
MATT	Materials Testing System
NHS	National Highway of Significance
PCC	Portland Cement Concrete
PCI	Pavement Condition Index
PM	Preventive Maintenance
PMS	Pavement Management System
psi	Pounds per square inch
PTCH	Patching Index
RC	Rehabilitation/Reconstruction
RHS	Rural Highway of Significance
RI	Rolling Wheel Deflectometer Index

RM	Restorative Maintenance
RNDM	Random Cracking Index
RUFF	Roughness Index
RUT	Rutting Index
RWD	Rolling Wheel Deflectometer
SCI	Structural Condition Index
SHI	Structural Health Index
SHRP	Strategic Highway Research Program
SN	Structural Number
SQL	Structure Query Language
SSCI	Scaled Structural Condition Index
SHS	State Highway of Significance
TAND	Highway Need System
TOPS	Tracking of Projects System
TSD	Traffic Speed Deflectometer
USDOT	United States Department of Transportation
ZRI	Zone Rolling Wheel Deflectometer Index

REFERENCES

1. Rada, G.R., Visintine, B.A., Hicks, R.G., Cheng, D., and Van T.P. "Use of Emerging Technologies in support of Pavement Preservation Decision Making," 9th International Conference on Managing Pavement Assets, 2015.
2. Bryce, J., Flintsch, G., Katicha, S., and Diefenderfer, B. "Developing a network-level structural capacity index for structural evaluation of pavements," Report No. VCTIR 13-R9, 2013, available at http://www.viriniadot.org/vtrc/main/online_reports/pdf/13-r9.pdf.
3. Kumlai, A., Sangpetngam, B. and Chalempong, S. "Development of equations for determining layer elastic moduli using pavement deflection characteristics," In Transportation Research Board 91st Annual Meeting, 2013, pp.14-0976.
4. Alavi, S., LeCates, J.F., and Tavares, M.P. "Falling weight deflectometer usage," A Synthesis of Highway Practice. NCHRP 381. Final Report, Washington, D.C., 2008.
5. Vavrik, W.R., Douglas, S., and Jeff, B. "Rolling Wheel Deflectometer-Based Pavement Management System: Champaign County, Illinois," In Transportation Research Board 87th Annual Meeting, No. 08-2728, 2008.
6. Roberts, J., U. Ai, T. Toole, and T. Martin. "Traffic speed deflectometer: data review and lessons learnt," No. AP-T279/14, 2014.
7. Khattak, M.J., Baladi, G.Y., and Sun, X. "Development of index based pavement performance models for pavement management system (PMS) of LADOTD," No. FHWA/LA. 08/460, 2009.
8. Manuel, L., Ivan, D., and Zheng, L. "Development of a new methodology for characterizing pavement structural condition for network-level applications," Center for Transportation Research, Bureau of Engineering Research, the University of Texas at Austin, No. FHWA/TX-04/0-4322-1, 2003.
9. Khattak, M.J., Baladi, G.Y., Zhang, Z., and Ismail, S. "A review of the pavement management system of the state of Louisiana-phase," *Transportation Research Record: Journal of the Transportation Research Board*, 2008, pp. 18-27.
10. "LADOTD Pavement Management System Guide," 2006.

11. Khattak, M.J., Gilbert, Y.B., Xiaoduan, S., Jared, V., and Corey, L. "Development of uniform sections for PMS inventory and application," No. FHWA/LA. 08/430. 2007.
12. Wu, Z., and Yang, X. "Evaluation of current Louisiana flexible pavement structures using PMS data and new mechanistic-empirical pavement design guide," Louisiana Transportation Research Center No. FHWA/LA. 11/482, 2012.
13. Flintsch, G., Katicha, S., Bryce, J., Ferne, B., Nell, S., and Diefenderfer, B. "Assessment of continuous pavement deflection measuring technologies," No. SHRP 2 Report S2-R06F-RW-1, 2013.
14. Briggs, R.C., Johnson, R.F., Stubstad, R.N., and Pierce, L.A. "Comparison of the rolling wheel deflectometer with the falling weight deflectometer." Nondestructive testing of pavements and backcalculation of moduli, third volume, ASTM STP 1375, S.D. Tayabji and E.O. Lukanen, Eds., American Society for Testing and Materials, West Conshohocken, PA, pp. 444-456, 2000.
15. Elseifi, M., Abdel-Khalek, A.M. and Dasari, K. "Implementation of rolling wheel deflectometer (RWD) in PMS and pavement preservation," Louisiana Department of Transportation and Development, FHWA/11.492, 2012.
16. Elseifi, M.A., Abdel-Khalek, A.M., Gaspard, K., Zhang, Z. and Ismail, S. "Evaluation of continuous deflection testing using the rolling wheel deflectometer in Louisiana," *Journal of Transportation Engineering*, 138(4), pp.414-422, 2011.
17. Zhang, Z., Gaspard, K. and Elseifi, M.A. "Evaluation of PMS recommendations for flexible pavement rehabilitation using RWD deflection data," *Transportation Research Record: Journal of the Transportation Research Board*. 01506444, 2014.
18. Gaspard, K., Zhang Z., and Elseifi, M.A. "Integration of Rolling Wheel Deflectometer Deflection Measurements into Pavement Management Systems: Use of Multivariate Statistical Methods and Fuzzy Logic," *Transportation Research Record: Journal of the Transportation Research Board* 2366, pp. 25-33, 2013.
19. Elseifi, M.A., Gaspard, K., Wilke, P.W., Engineer, P.P., Zhang, Z., Hegab, A. and Planner, I.V. "Evaluation and Validation of a Model to Predict Pavement Structural Number Using Rolling Wheel Deflectometer (RWD) Data," Transportation Research Board 94th Annual Meeting, No. 15-4276, 2015.
20. "Investigation of Structural Capacity of PennDOT Roads," *ARA inc.*, 2013.

21. Gedafa, D.S., Hossain, M., Miller, R. W., and Steele, D. "Network level pavement structural evaluation using rolling wheel deflectometer," Transportation Research Board 87th Annual Meeting, No. 08-2648, 2008.
22. Gedafa, D.S., Steele, D.A., Hossain, M., and Miller, R. "Network level testing for pavement structural evaluation using a rolling wheel deflectometer," *Journal of Testing and Evaluation*, 2010, pp 1-10.
23. Sivaneswaran N. "Network level pavement structural evaluation – a way forward," National Pavement Evaluation Conference 2014 Blacksburg, Virginia, 2014.
24. Flora, W.F., Ong, G.P.R., and Sinha, K.C. "Development of a structural index as an integral part of the overall pavement quality in the INDOT PMS," 2010.
25. Murphy, M., and Zhang, Z. "Validation and implementation of the structural condition index (SCI) for network-level pavement evaluation," No. FHWA/TX-11/5-4322-01-1), 2011.
26. Tutumluer, E., and Sarker, P. "Development of improved overlay thickness design alternatives for local roads," Illinois Center for Transportation/Illinois Department of Transportation, 2015.
27. Ceylan, H., Bayrak, M.B., and Gopalakrishnan K. "Neural networks applications in pavement engineering: A recent survey," *International Journal of Pavement Research and Technology*, 7(6), pp.434, 2014.
28. Ye, Z., Xu, Y., Veneziano, D., and Shi, X. "Evaluation of winter maintenance chemicals and crashes with an artificial neural network," *Transportation Research Record: Journal of the Transportation Research Board*, Vol. 2440, pp. 43–50, 2014.
29. Plati, C., Georgiou, P., and Papavasiliou, V. "Simulating pavement structural condition using artificial neural networks," *Structure and Infrastructure Engineering*, pp. 1–10, 2015.
30. Kim, M.Y., Burton, M., Prozzi, J.A., and Murphy, M. "Maintenance and rehabilitation project selection using artificial neural networks," Transportation Research Board 93rd Annual Meeting (No. 14-3620), 2014.
31. Lawrence, S., Giles, C.L., and Tsoi, A.C. "Lessons in neural network training: Overfitting may be harder than expected," AAAI/IAAI (pp. 540-545), 1997.

32. Leverington, D. "A basic introduction to feedforward backpropagation neural networks," Neural Network Basics, 2012.
33. Nasimifar, M., Senthimurugan, T., Siddarthan, R.V., and Sivanesarwan, N. "Robust deflection indices from traffic-speed deflectometer measurements to predict critical pavement responses for network-level pavement management system application," ASCE, *Journal of Transportation Engineering*, Vol. 142, No. 3, 2016.
34. Elbagalati, O., Elseifi, M.A., Gaspard, K., and Zhang, Z. "Prediction of in-service pavement structural capacity based on traffic-speed deflection measurements," ASCE, *Journal of Transportation Engineering*, 2016, 04016058.
35. NCHRP synthesis 381 "Falling weight deflectometer usage," Transportation Research Board Annual Meeting, Washington, D.C., 2008.
36. Fernando, E.G., Liu, W., and Ryu, D. "Development of a procedure for temperature correction of backcalculated AC modulus," Texas Transportation Institute, Texas A&M University System, No. FHWA/TX-02/1863-1, 2001.
37. Taha, M.R., Hardwiyono, S., Md Yusoff, N. I., Mohd Nayan, K.A., and Hainin, M.R. "The effect of temperature changes on elastic modulus of flexible pavements," *Journal Kejuruteraan (Journal of Engineering)*, 24, 7-14, 2013.
38. Elbagalati, O., Elseifi, M.A., Gaspard, K., and Zhang, Z. "Development of the pavement structural health index based on falling weight deflectometer testing," *International Journal of Pavement Engineering*, pp.1-8, 2016.
39. Southgate, H.F. "Sensitivity study of 1986 AASHTO guide for design of pavement structures," 1991.
40. Richardson, D.N. "Determination of AASHTO layer coefficients for granular materials by use of resilient modulus," The 37th Annual UMR Asphalt Conference, 1994.
41. Wu, Z. and Gaspard, K. "Mechanistic flexible pavement overlay design program," No. FHWA/LA. 08/454, 2009.
42. Wu, Z., Zhang, Z. and Abadie, C. "Determining structural strength of existing asphalt layer using condition survey data," *International Journal of Pavement Engineering*, 14(7), pp.603-611, 2013.

43. Kim, Y. Richard, H., and Park, G. "Use of falling weight deflectometer multi-load data for pavement strength estimation," No. FHWA/NC/2002-006, 2002.
44. Karlaftis, M., and Vlahogianni, E. "Statistical methods versus neural networks in transportation research: Differences, similarities and some insights," *Transportation Research Part C: Emerging Technologies*, Vol. 19, No. 3, 2011, pp. 387–399.
45. Benítez, J.M., Castro, J. L., and Requena, I. "Are artificial neural networks black boxes?" *IEEE Transactions on neural networks*, 8(5), 1156-1164, 1997.
46. Attoh-Okine, N.O., Cooger, K., and Mensah, S. "Multivariate adaptive regression (MARS) and hinged hyperplanes (HHP) for doweled pavement performance modeling," *Construction and Building Materials*, 23(9), 3020-3023, 2009.
47. Hsie, M., Ho, Y.F., Lin, C.T., and Yeh, I.C. "Modeling asphalt pavement overlay transverse cracks using the genetic operation tree and Levenberg–Marquardt Method," *Expert Systems with Applications*, 39(5), 4874-4881, 2012.
48. Bland, J.M., and Altman, D. "Statistical methods for assessing agreement between two methods of clinical measurement," *The lancet*, 327(8476), 307-310, 1986.
49. Ryan, T.P., and Woodall, W.H. "The most-cited statistical papers," *Journal of Applied Statistics*, 32(5), 461-474, 2005.
50. Bland, J. M., and Altman, D.G. "Applying the right statistics: analyses of measurement studies," *Ultrasound in obstetrics & gynecology*, 22(1), 85-93, 2003.
51. Katicha, S. W., Flintsch, G.W., Ferne, B., Bryce, J. Limits of agreement method for comparing TSD and FWD measurements," *International Journal of Pavement Engineering*, 15(6), 532-541, 2014.
52. Basu, J.K., Bhattacharyya, D., and Kim, T. "Use of artificial neural network in pattern recognition," *International Journal of Software Engineering and its Applications* 4, No. 2, 2010.
53. Li, Q., Zou, Q., Zhang, Z., and Mao, D. "Seed-growing approach for crack-line detection from pavement images," *Image and Vision Computing*, Vol. 29, No. 12, 2011, pp. 861–872.

54. Shangguan, P., Al-Qadi, I.L., and Lahouar, S. "Pattern recognition algorithms for density estimation of asphalt pavement during compaction: a simulation study," *Journal of Applied Geophysics*, Vol. 107, 2014, pp. 8–15.
55. Chen, Y., Kim, J., and Mahmassani, H.S. "Pattern recognition using clustering algorithm for scenario definition in traffic simulation-based decision support systems," 17th International IEEE Conference on Intelligent Transportation Systems (ITSC), 2014.
56. Allahviranloo, M. "Pattern Recognition and Personal Travel Behavior," Transportation Research Board 95th Annual Meeting, No. 16-3970. 2016.
57. Deng, X., Q. Liu, Y. Deng, and Mahadevan, S. "An improved method to construct basic probability assignment based on the confusion matrix for classification problem," *Information Sciences*, Vol. 340-341, 2016, pp. 250–261.

APPENDIX

Structurally Deficient Sections According to Each Indicator

Table 46
List of structural deficient section based on SN

Control Section	SN	AVG Ruff	AVG ALC	AVG RUT	AVG PCI	AVG PTCH	RNDM AVG
167-04	2.3	73.8	85.6	95.7	76.4	86.2	88.5
172-30	2.4	62.8	82.7	91.2	70.5	84.6	89.8
328-03	2.2	58.6	75.1	93.2	66.6	88.0	78.3
331-01	2.0	49.0	76.1	85.8	55.3	65.5	88.1
332-02	1.5	56.1	68.4	91.6	51.7	46.1	71.7
818-03	2.4	67.9	98.3	86.8	78.4	94.6	99.2
160-02	1.9	60.8	70.9	82.0	62.9	84.9	75.7
161-06	2.1	75.7	97.6	92.2	82.6	97.0	89.5
164-04	2.6	80.0	75.9	88.7	73.1	89.1	79.8
166-04	2.4	67.3	77.4	92.0	63.2	58.1	83.1
184-01	1.8	76.9	95.2	96.6	84.0	98.8	90.1
319-05	2.5	75.3	99.5	97.6	82.8	89.8	98.3
328-02	1.0	65.6	74.2	95.0	66.3	75.0	81.3
51-08	3.0	79.0	71.0	82.8	72.0	96.9	74.6
161-03	2.2	71.0	100.0	79.5	79.1	98.6	99.6
161-08	2.8	76.4	98.8	74.8	79.6	100.0	99.9
333-03	3.1	75.6	99.6	68.9	73.3	85.2	99.9
818-01	2.6	64.6	82.3	89.4	70.4	80.7	86.8
818-08	2.4	64.1	68.3	79.7	62.1	71.2	77.2

Table 47
List of structural deficient section based on RI

Control Section	RI	AVG Ruff	AVG ALC	AVG RUT	AVG PCI	AVG PTCH	RNDM AVG
167-04	142.2	73.8	85.6	95.7	76.4	86.2	88.5
172-30	150.2	62.8	82.7	91.2	70.5	84.6	89.8
328-03	161.4	58.6	75.1	93.2	66.6	88.0	78.3
331-01	170.1	49.0	76.1	85.8	55.3	65.5	88.1
332-02	226.2	56.1	68.4	91.6	51.7	46.1	71.7
818-03	130.4	67.9	98.3	86.8	78.4	94.6	99.2
157-02	111.6	73.3	98.6	95.2	84.1	97.5	99.1
160-02	153.7	60.8	70.9	82.0	62.9	84.9	75.7
161-06	157.0	75.7	97.6	92.2	82.6	97.0	89.5
164-04	128.2	79.8	75.9	88.7	73.1	89.1	79.8
166-04	149.6	67.3	77.4	92.0	63.2	58.1	83.1
171-03	119.0	75.4	82.0	93.2	79.0	99.3	85.7
184-01	193.5	76.9	95.2	96.6	84.0	98.8	90.1
51-08	97.4	79.0	71.0	82.8	72.0	96.9	74.6
161-03	145.3	71.0	100.0	79.5	79.1	98.6	99.6
161-08	110.8	76.4	98.8	74.8	79.6	100.0	99.9
318-02	99.6	67.5	76.7	94.8	66.4	71.2	84.2
325-01	88.4	72.8	92.4	97.3	79.6	90.8	91.3
333-02	100.7	80.3	91.8	83.9	75.5	78.3	88.9
333-03	106.2	75.6	99.6	68.9	73.3	85.2	99.9
818-01	108.3	64.6	82.3	89.4	70.4	80.7	86.8
818-08	126.5	64.1	68.3	79.7	62.1	71.2	77.2

Table 48
List of structural deficient section based on ZRI

Control Section	ZRI	AVG Ruff	AVG ALC	AVG RUT	AVG PCI	AVG PTCH	RNDM AVG
296-02	234.3	51.6	65.7	93.2	42.7	24.0	82.2
318-01	200.9	75.4	100.0	88.4	77.8	73.6	100.0
328-03	250.9	53.8	65.3	87.6	61.6	82.0	70.5
332-02	238.4	64.2	67.9	98.0	56.3	50.5	67.0
818-03	307.6	70.0	100.0	83.6	80.4	100.0	100.0
834-08	212.9	62.0	100.0	90.8	78.0	100.0	100.0
862-04	230.9	75.0	49.5	91.6	60.8	66.7	82.4
68-01	222.6	83.8	73.4	93.2	79.2	97.6	83.7
68-02	297.0	76.6	95.4	91.6	85.2	100.0	97.4
164-04	185.6	55.0	70.2	66.8	61.5	100.0	79.4
166-04	228.5	78.4	94.2	91.6	85.4	98.0	93.5
171-03	197.4	76.0	77.0	80.4	76.9	100.0	89.3
184-01	345.5	77.4	96.8	98.0	85.2	100.0	89.0
161-03	270.0	43.8	100.0	81.2	66.4	100.0	100.0
161-08	206.9	71.6	100.0	72.4	77.1	100.0	97.9
185-03	282.4	78.6	91.7	94.8	83.2	100.0	83.7
325-01	205.7	54.6	98.0	98.0	72.3	100.0	83.7
333-01	157.3	85.8	100.0	94.8	91.4	100.0	100.0
333-03	223.3	78.2	100.0	68.4	77.9	100.0	100.0
818-01	201.6	70.4	69.0	85.2	71.2	77.4	79.2

This public document is published at a total cost of \$250. 42 copies of this public document were published in this first printing at a cost of \$250. The total cost of all printings of this document including reprints is \$250. This document was published by Louisiana Transportation Research Center to report and publish research findings as required in R.S. 48:105. This material was duplicated in accordance with standards for printing by state agencies established pursuant to R.S. 43:31. Printing of this material was purchased in accordance with the provisions of Title 43 of the Louisiana Revised Statutes.